

# THE PROCEEDINGS OF THE PHYSICAL SOCIETY

## Section A

VOL. 64, PART 2

1 February 1951

No. 374 A

## CONTENTS

	PAGE
Mr. H. N. V. TEMPERLEY. The Theory of the Propagation in Liquid Helium II of 'Temperature-Waves' of Finite Amplitude . . . . .	105
Mr. D. V. OSBORNE. Second Sound in Liquid Helium II . . . . .	114
Dr. R. J. BENZIE and Dr. A. H. COOKE. The Magnetic Susceptibility of Copper Sulphate . . . . .	124
Prof. H. FRÖHLICH. Theory of the Superconducting State: II—Magnetic Properties at the Absolute Zero of Temperature . . . . .	129
Dr. R. E. B. MAKINSON and Mr. M. J. BUCKINGHAM. The Second Order Photoelectric Effect at a Metal Surface . . . . .	135
Miss DORIS KUHLMANN (now Mrs. WILSDORF). On the Theory of Plastic Deformation . . . . .	140
Mr. A. J. FOREMAN, Dr. M. A. JASWON and Mr. J. K. WOOD. Factors Controlling Dislocation Widths . . . . .	156
Mr. T. H. BRAID and Dr. H. O. W. RICHARDSON. Further Studies—Experimental and Theoretical—of a Wide-Angle $\beta$ -Spectrometer which uses a Prolate Spheroidal Magnetic Field . . . . .	163
Dr. J. C. BARTON, Dr. E. P. GEORGE and Dr. A. C. JASON. Observations of Slow Mesons and Nuclear Disintegrations in Photographic Plates exposed under Carbon Absorbers . . . . .	175
Dr. E. P. GEORGE and Mr. J. EVANS. Disintegrations produced by the Nuclear Capture of Slow Negative $\mu$ -Mesons . . . . .	193
Mr. J. H. CARVER and Dr. D. H. WILKINSON. Some Gamma-Rays from Light Elements under Proton Bombardment . . . . .	199
Letters to the Editor:	
Mr. J. J. WILKINS and Mr. F. K. GOWARD. Fall and Re-increase of the $^{12}\text{C}(\gamma, 3^4\text{He})$ Cross Section . . . . .	201
Dr. A. P. FRENCH and Mr. D. M. THOMSON. The Reaction $^{23}\text{Na}(d, \alpha)^{21}\text{Ne}$ . . . . .	203
Dr. B. BLEANEY and Mr. H. E. D. SCOVIL. Nuclear Spin of Erbium-167 . . . . .	204
Mr. R. J. ELLIOTT and Dr. K. W. H. STEVENS. A Preliminary Survey of the Paramagnetic Resonance Phenomena observed in Rare Earth Ethyl Sulphates . . . . .	205
Mr. R. G. MOORHOUSE. Scattering of Neutrons by Ferromagnetic Crystals . . . . .	207
Dr. D. GEIST. A Note on the Radially Symmetrical Phase Growth Controlled by Heat Conduction . . . . .	208
Dr. G. STEPHENSON. Calculation of Relative Transition Probabilities for First Negative Bands of $\text{N}_2^+$ . . . . .	209
Mr. G. K. MEHTA and Miss V. RAJESWARI. $\text{C}_2$ (Swan) Bands in Krypton . . . . .	210
Mr. J. SHARPE and Dr. G. H. STAFFORD. The $^{12}\text{C}(n, 2n)^{11}\text{C}$ Reaction in an Anthracene Crystal . . . . .	211
Dr. E. W. TITTERTON and Mr. T. A. BRINKLEY. The Reaction $^6\text{Li}(\gamma n)^5\text{Li}$ and Energy Levels of the $^5\text{Li}$ Nucleus. . . . .	212
Contents for Section B . . . . .	214
Abstracts for Section B . . . . .	215

Price to non-members 10s. net, by post 6d. extra. Annual subscription: £5 5s.

Composite subscription for both Sections A and B: £9 9s.

Published by

THE PHYSICAL SOCIETY

1 Lowther Gardens, Prince Consort Road, London S.W.7



# PROCEEDINGS OF THE PHYSICAL SOCIETY

The *Proceedings* is now published monthly in two Sections.

## ADVISORY BOARD

*Chairman*: The President of the Physical Society (L. F. BATES, D.Sc., Ph.D., F.R.S.)

E. N. DA C. ANDRADE, Ph.D., D.Sc., F.R.S.  
 Sir EDWARD APPLETON, G.B.E., K.C.B.,  
 D.Sc., F.R.S.  
 P. M. S. BLACKETT, M.A., F.R.S.  
 Sir LAWRENCE BRAGG, O.B.E., M.C., M.A.,  
 Sc.D., D.Sc., F.R.S.  
 Sir JAMES CHADWICK, D.Sc., Ph.D., F.R.S.  
 Lord CHERWELL OF OXFORD, M.A., Ph.D.,  
 F.R.S.  
 Sir JOHN COCKCROFT, C.B.E., M.A., Ph.D.,  
 F.R.S.

Sir CHARLES DARWIN, K.B.E., M.C., M.A.,  
 Sc.D., F.R.S.  
 N. FEATHER, Ph.D., F.R.S.  
 G. I. FINCH, M.B.E., D.Sc., F.R.S.  
 D. R. HARTREE, M.A., Ph.D., F.R.S.  
 N. F. MOTT, M.A., D.Sc., F.R.S.  
 M. L. OLIPHANT, Ph.D., D.Sc., F.R.S.  
 F. E. SIMON, C.B.E., M.A., D.Phil., F.R.S.  
 T. SMITH, M.A., F.R.S.  
 Sir GEORGE THOMSON, M.A., D.Sc., F.R.S.

Papers for publication in the *Proceedings* should be addressed to the Hon. Papers Secretary,  
 Dr. H. H. HOPKINS, at the Office of the Physical Society, 1 Lowther Gardens, Prince  
 Consort Road, London S.W. 7. Telephone: KENSington 0048, 0049.

Detailed Instructions to Authors were included in the February 1948 issue of  
 the *Proceedings*; separate copies can be obtained from the Secretary-Editor.

## BULLETIN ANALYTIQUE

Publication of the Centre National de la Recherche Scientifique, France

The *Bulletin Analytique* is an abstracting journal which appears in three parts, Part I covering scientific and technical papers in the mathematical, chemical and physical sciences and their applications, Part 2 the biological sciences and Part 3 philosophy.

The *Bulletin*, which started on a modest scale in 1940 with an average of 10,000 abstracts per part, now averages 35 to 45,000 abstracts per part. The abstracts summarize briefly papers in scientific and technical periodicals received in Paris from all over the world and cover the majority of the more important journals in the world scientific press. The scope of the *Bulletin* is constantly being enlarged to include a wider selection of periodicals.

The *Bulletin* thus provides a valuable reference book both for the laboratory and for the individual research worker who wishes to keep in touch with advances in subjects bordering on his own.

A specially interesting feature of the *Bulletin* is the microfilm service. A microfilm is made of each article as it is abstracted and negative microfilm copies or prints from microfilm can be purchased from the editors.

The subscription rates per annum for Great Britain are 4,000 frs. (£4) each for Parts 1 and 2, and 2,000 frs. (£2) for Part 3. Subscriptions can also be taken out to individual sections of the *Bulletin* as follows:

	frs.	
Pure and Applied Mathematics—Mathematics—Mechanics	550	14/6
Astronomy—Astrophysics—Geophysics .. ..	700	18/-
General Physics—Thermodynamics—Heat—Optics—Elec- tricity and Magnetism .. ..	900	22/6
Atomic Physics—Structure of Matter .. ..	325	8/6
General Chemistry—Physical Chemistry .. ..	325	8/6
Inorganic Chemistry—Organic Chemistry—Applied Chemistry—Metallurgy .. ..	1,800	45/-
Engineering Sciences .. ..	1,200	30/-
Mineralogy—Petrography—Geology—Palaeontology ..	550	14/6
Biochemistry—Biophysics—Pharmacology .. ..	900	22/6
Microbiology—Virus and Phages .. ..	600	15/6
Animal Biology—Genetics—Plant Biology .. ..	1,800	45/-
Agriculture—Nutrition and the Food Industries .. ..	550	14/6

Subscriptions can be paid directly to the editors: Centre National de la Recherche Scientifique,  
 18, rue Pierre-Curie, Paris 5ème (Compte-chèque-postal 2,500-42, Paris), or through Messrs. H. K.  
 Lewis & Co. Ltd., 136, Gower Street, London W.C. 1.



## THE PHYSICAL SOCIETY

### MEMBERSHIP

Membership of the Society is open to all who are interested in Physics:

**FELLOWSHIP.** A candidate for election to Fellowship must as a rule be recommended by three Fellows, to two of whom he is known personally. Fellows may attend all meetings of the Society, are entitled to receive Publications 1 (either Section A or Section B), 4 and 5 below, and may obtain the other publications at much reduced rates.

**STUDENT MEMBERSHIP.** A candidate for election to Student Membership must be between 18 and 26 years of age and must be recommended from personal knowledge by a Fellow. Student Members may attend all meetings of the Society, are entitled to receive Publications 1 (either Section A or Section B) and 4, and may obtain the other publications at much reduced rates.

Books and periodicals may be read in the Society's Library, and a limited number of books may be borrowed by Fellows and Student Members on application to the Honorary Librarian.

Fellows and Student Members may become members of the *Colour Group*, the *Optical Group*, the *Low Temperature Group* and the *Acoustics Group* (specialist Groups formed in the Society) without payment of additional annual subscription.

### PUBLICATIONS

1. *The Proceedings of the Physical Society*, published monthly in two Sections, contains original papers, lectures by specialists, reports of discussions and of demonstrations, and book reviews. Section A contains papers mainly on atomic and sub-atomic subjects; Section B contains papers on macroscopic physics.

2. *Reports on Progress in Physics*, published annually, is a comprehensive review by qualified physicists.

3. *The Handbook of the Physical Society's Annual Exhibition of Scientific Instruments and Apparatus*. This Exhibition is recognized as the most important function of its kind, and the Handbook is a valuable book of reference.

4. *The Bulletin*, issued at frequent intervals during the session, informs members of programmes of future meetings and of the business of the Society generally.

5. *Physics Abstracts (Science Abstracts A)*, published monthly in association with the Institution of Electrical Engineers, covers the whole field of contemporary physical research.

6. *Electrical Engineering Abstracts (Science Abstracts B)*, published monthly in association with the Institution of Electrical Engineers, covers the whole field of contemporary research in electrical engineering.

7. *Special Publications*, critical monographs and reports on special subjects prepared by experts or committees, are issued from time to time.

### MEETINGS

At approximately monthly intervals throughout each annual session, meetings are held for the reading and discussion of papers, for lectures, and for experimental demonstrations. Special lectures include: the *Guthrie Lecture*, in memory of the founder of the Society, given annually by a physicist of international reputation; the *Thomas Young Oration*, given biennially on an optical subject; the *Charles Chree Address*, given biennially on Geomagnetism, Atmospheric Electricity, or a cognate subject; and the biennial *Rutherford Memorial Lecture*. Meetings are generally held each year at provincial centres, and from time to time meetings are arranged jointly with other Societies for the discussion of subjects of common interest.

Each of the four specialist Groups holds about five meetings in each session.

### SUBSCRIPTIONS

Fellows pay an Entrance Fee of £1 1s. and an Annual Subscription of £3 3s. Student Members pay only an Annual Subscription of 15s. Second Section of *Proceedings* 30s. No entrance fee is payable by a Student Member on transfer to Fellowship.

*Further information may be obtained from the Secretary-Editor  
at the Offices of the Society:*

1 LOWTHER GARDENS, PRINCE CONSORT ROAD, LONDON S.W. 7  
Telephone: KENsington 0048, 0049



PROCEEDINGS OF THE PHYSICAL SOCIETY  
in  
MICROFILM

The Physical Society has agreed with University Microfilms, Ann Arbor, Michigan, for the reproduction of the *Proceedings of the Physical Society* in Microfilm form.

This service is available only to subscribers to the paper edition of the Journal, and is intended to be of assistance to libraries both in saving accessible space and in improving borrowing facilities.

The microfilm is produced as a 'positive', i.e. black printing on white background, and is supplied on metal reels suitably labelled, distribution being made at the end of the year.

*Inquiries to be addressed to*  
**THE UNIVERSITY MICROFILMS**  
313 N. First Street, Ann Arbor, Michigan, U.S.A.

An essential  
component unique  
in this country

Seamless, one-piece, metal bellows combining the properties of a compression spring capable of repeated flexing, a packless gland, and a container which can be hermetically sealed. Hydraulically formed by a process unique in this country, they are tough, resilient, with a uniformity of life, performance and reliability unobtainable by any other method.



**FOR:** Automatic coolant regulation. Movement for pressure change. Packless gland to seal spindle in high vacua. Reservoir to accept liquid expansion. Dashpot or delay device. Barometric measurement or control. Pressurised couplings where vibration or movement is present. Dust seal to prevent ingress of dirt. Pressure reducing valves. Hydraulic transmission. Distance thermostatic control. Low torque flexible coupling. Pressure sealed rocking movement. Pressurised rotating shaft seals. Aircraft pressurised cabin control. Refrigeration expansion valves. Thermostatic Steam Traps. Pressure amplifiers. Differential pressure measurements. Thermostatic operation of louvre or damper.

*Write for List No. V 800-1.*

**Drayton 'Hydroflex' METAL BELLOWS**

Drayton Regulator & Instrument Co. Ltd., West Drayton, Mdx. - W. Drayton 26lf

HANDBOOK  
OF THE  
PHYSICAL SOCIETY'S  
35th EXHIBITION  
OF  
SCIENTIFIC INSTRUMENTS  
AND APPARATUS  
1951

5s.; by post 6s.

To be published at the  
beginning of March

*Orders, with remittances, to*  
**THE PHYSICAL SOCIETY**  
1 Lowther Gardens, Prince Consort Road,  
London S.W.7

THE HANDBOOK OF THE  
PHYSICAL SOCIETY'S 34th EXHIBITION  
OF SCIENTIFIC INSTRUMENTS  
AND APPARATUS,  
1950

5s.; by post 6s.

*Orders, with remittances, should be sent to*  
**THE PHYSICAL SOCIETY**  
1 Lowther Gardens, Prince Consort Rd., London S.W.7

BINDING CASES  
for the  
PROCEEDINGS OF THE  
PHYSICAL SOCIETY

Binding cases for Sections A and B (separate) for Volume 63 (1950) may be obtained for 7s. each, post free, from the Offices of the Society.

The *Proceedings* may be bound in the Society's green cloth for 13s. 6d. each. Journals for binding should be sent direct to Messrs. Taylor and Francis, Ltd., Red Lion Court, Fleet Street, London E.C.4. Remittances should be sent to the Physical Society.



## PROCEEDINGS OF THE PHYSICAL SOCIETY

### ADVERTISEMENT RATES

The *Proceedings* are divided into two parts, A and B. The charge for insertion is £18 for a full page in either Section A or Section B, £30 for a full page for insertion of the same advertisement in both Sections. The corresponding charges for part pages are:

$\frac{1}{2}$ page	£9 5 0	£15 10 0
$\frac{1}{4}$ page	£4 15 0	£8 0 0
$\frac{1}{8}$ page	£2 10 0	£4 5 0

Discount is 20% for a series of six similar insertions and 10% for a series of three.

The printed area of the page is  $8\frac{1}{2}'' \times 5\frac{1}{2}''$ , and the screen number is 120.

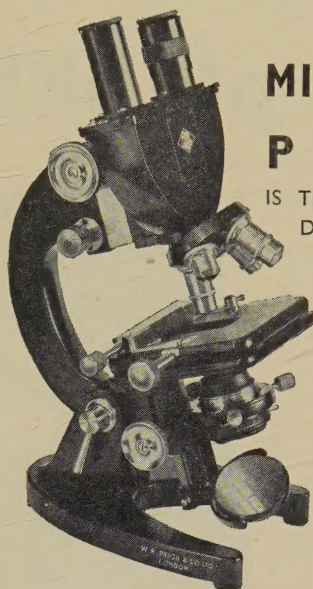
Copy should be received at the Offices of the Physical Society six weeks before the date of publication of the *Proceedings*.

THE HALL MARK OF A  
PRECISION BUILT MICROSCOPE



## MICROSCOPES BY P R I O R

IS THE ORDER OF THE  
DAY FROM AN EVER  
INCREASING CIRCLE  
OF DISCERNING  
MICROSCOPE USERS.



Literature  
on  
request

## W. R. PRIOR & CO. LTD.

28A, DEVONSHIRE STREET, LONDON, W.1.  
WELbeck 4695

## RESONANT ABSORBERS AND REVERBERATION

*Report of the*

1947 SUMMER SYMPOSIUM

OF THE  
ACOUSTICS GROUP  
OF THE  
PHYSICAL SOCIETY

together with the Inaugural Address  
of the Group:

### ACOUSTICS AND SOME ALLIED STUDIES

by ALEXANDER WOOD

57 pages. 7s. 6d.; by post 8s.

*Orders, with remittances, to be sent to*

THE PHYSICAL SOCIETY  
1 Lowther Gardens, Prince Consort Road,  
London S.W.7

## SYMPOSIUM ON NOISE AND SOUND TRANSMISSION

*Report of the*

1948 SUMMER SYMPOSIUM

OF THE  
ACOUSTICS GROUP  
OF THE  
PHYSICAL SOCIETY

200 pages. 17s. 6d.; by post 18s.

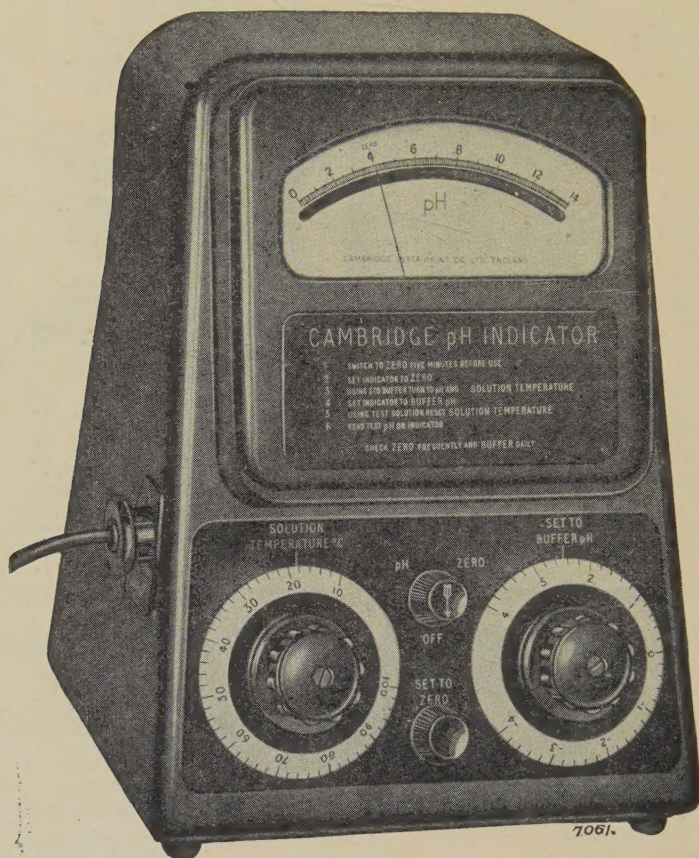
(Price 10s. 6d., by post 11s., to Fellows of  
the Society and Members of the Acoustics  
Group)

*Orders, with remittances, to be sent to*

THE PHYSICAL SOCIETY  
1 Lowther Gardens, Prince Consort Road,  
London S.W.7



# CAMBRIDGE DIRECT READING pH INDICATOR



A NEW pH INDICATOR CHARACTERISED BY PORTABILITY, ROBUSTNESS AND GREAT STABILITY; COVERING THE FULL RANGE OF 0 TO 14 pH. DIRECTLY READABLE TO 0.1 pH AND BY ESTIMATION EASILY TO 0.05. ALL MAINS OPERATED

*Details are given in SHEET 294-L. May we send a copy?*

**CAMBRIDGE INSTRUMENT COMPANY LTD.**

13, GROSVENOR PLACE, LONDON, S.W.1.  
WORKS: LONDON & CAMBRIDGE.



# THE PROCEEDINGS OF THE PHYSICAL SOCIETY

## Section A

VOL. 64, PART 2

1 February 1951

No. 374 A

### The Theory of the Propagation in Liquid Helium II of 'Temperature-Waves' of Finite Amplitude

By H. N. V. TEMPERLEY

King's College, Cambridge

*Communicated by D. Shoenberg; MS. received 26th June 1950*

**ABSTRACT.** The two-fluid model of liquid helium II is applied to the problem of predicting the behaviour of waves and pulses of second sound of finite amplitude. It is found that equations quite analogous to the Riemann and Rankine-Hugoniot equations for ordinary sound waves and shock fronts can be established. These equations predict the 'overtaking effect' with the establishment of a 'temperature-shock' for pulses of second sound of finite amplitude. The temperature-shocks should be of 'front-edge' type (propagation of an abrupt rise in temperature) if the liquid helium is at a temperature below  $1.96^{\circ}\text{K.}$ , but should become 'back-edge', corresponding to an abrupt fall in temperature, between  $1.96^{\circ}\text{K.}$  and the  $\lambda$ -point. There is experimental evidence in support of both these predictions. It is shown that, just as for ordinary shock fronts, the irreversible effects due to the passage of a temperature shock should be proportional to the cube of the height of the shock.

#### § 1. INTRODUCTION

RECENT measurements on the propagation of temperature differences in liquid helium II (Pellam 1949, Osborne 1951) have provided evidence, first that a pulse of finite amplitude changes its shape as it travels forward, and secondly that the front of such a pulse may become effectively vertical when it has travelled far enough. This suggests that this phenomenon of 'second sound', the propagation of temperature differences without appreciable attenuation or dispersion over a wide range of frequencies, may have other properties similar to those of ordinary sound. In particular, one is tempted to look for something analogous to the Riemann theory of the propagation of sound of finite amplitude, and to the Rankine-Hugoniot theory of the propagation of pressure discontinuities or 'shock fronts'. In this paper such results will be derived on the basis of the 'two-fluid' model of liquid helium II—that is, on the postulate that liquid helium II can be represented as consisting of two mutually interpenetrating liquids each having its own density and velocity-field and being capable of relative motion without appreciable friction, at all events as long as the relative velocity is not too great. This model has been shown (Gorter and Mellink 1949) to give a reasonable quantitative account of many of the experimental facts, but its relationship with the 'surface creep' phenomena that are known to occur with liquid helium II has still to be worked out.



## § 2. THE EQUATIONS OF MOTION

Various attempts have been made to derive the equations of motion in such a way as to include second and higher order terms in the velocities (for example, Landau 1941, Zilsel 1949, Gorter and Mellink 1949). Unfortunately, the higher order terms obtained by different workers do not agree, and the matter is therefore re-investigated in the Appendix, the equations derived being closely similar to those of Zilsel (1949), but differing slightly from them.

We obtain the following two equations, where  $\rho_n$  and  $\rho_s$  are respectively the masses of normal and superfluid components per unit volume, and  $u_n$ ,  $u_s$  the corresponding hydrodynamic velocities:

$$\frac{\partial}{\partial t}(\rho_n u_n + \rho_s u_s) + \frac{\partial}{\partial x}(\rho_n u_n^2 + \rho_s u_s^2) + \frac{\partial P}{\partial x} = 0, \quad \dots\dots(1)$$

$$g \frac{\partial \rho}{\partial t} + \frac{\partial}{\partial x} \left[ \left( g + \frac{\rho}{\rho_n} TS \right) \rho_n u_n + g \rho_s u_s \right] + T \frac{\partial(\rho S)}{\partial t} + \frac{1}{2} \frac{\partial}{\partial t}(\rho_n u_n^2 + \rho_s u_s^2) + \frac{1}{2} \frac{\partial}{\partial x}(\rho_n u_n^3 + \rho_s u_s^3) = 0. \quad \dots\dots(2)$$

In addition we have the equation of continuity,

$$\frac{\partial \rho}{\partial t} + \frac{\partial}{\partial x}(\rho_n u_n + \rho_s u_s) = 0, \quad \dots\dots(3)$$

and the postulate that entropy is transported by one of the fluids only, the normal component, the superfluid component being unable to carry entropy:

$$\frac{\partial(\rho S)}{\partial t} + \frac{\partial}{\partial x}(\rho u_n S) = 0. \quad \dots\dots(4)$$

Equation (4) also states that entropy is conserved, which means that the effect of irreversible processes is neglected. Such neglect seems justified by the experimental fact that both absorption and dispersion of second sound are small over a wide range of frequencies, except possibly in the neighbourhood of the transition temperature.

We introduce the two velocities  $V$  and  $W$ , which we may call the 'stream velocities', associated respectively with ordinary sound and second sound, defined as follows:

$$\rho V = \rho_n u_n + \rho_s u_s, \quad W = u_n - u_s. \quad \dots\dots(5)$$

$V$  is a measure of the translation of the liquid as a whole, and  $W$  is the relative velocity of the two components. In terms of these velocities, equations (1) to (4) may be rewritten

$$\frac{\partial}{\partial t}(\rho V) + \frac{\partial}{\partial x} \left( \rho V^2 + \frac{\rho_n \rho_s}{\rho} W^2 \right) + \frac{\partial P}{\partial x} = 0, \quad \dots\dots(6)$$

$$\rho_s S W \frac{\partial T}{\partial x} + \frac{1}{2} \frac{\partial}{\partial t} \left( \frac{\rho_n \rho_s}{\rho} W^2 \right) + \frac{1}{2} \frac{\partial}{\partial x} \left[ \frac{3 \rho_n \rho_s V W^2}{\rho} + \frac{\rho_n \rho_s (\rho_s - \rho_n) W^3}{\rho^2} \right] - V \frac{\partial}{\partial x} \left[ \frac{\rho_n \rho_s W^2}{\rho} \right] = 0, \quad \dots\dots(7)$$

$$\frac{\partial \rho}{\partial t} + \frac{\partial}{\partial x}(\rho V) = 0, \quad \dots\dots(8)$$

$$\frac{\partial(\rho S)}{\partial t} + \frac{\partial}{\partial x}(\rho V S + \rho_s S W) = 0. \quad \dots\dots(9)$$



In deriving equation (7) from equation (2) use has been made of equations (6) and (8) to eliminate terms involving  $V$  and the pressure. Equations (6) and (8) show us that, if thermal expansion can be neglected, ordinary sound is excited by second sound only through the third term in equation (6), which is of order  $W^2$ , so that, if we have a purely thermal source, the ordinary sound will have an amplitude proportional to  $W^2$ , and we can consistently neglect the third term in equation (9), of order  $W^3$ , and the terms involving  $VW^2$  in equation (7), of order  $W^4$ . If the effect of thermal expansion becomes important, as it may near the transition temperature, we can no longer neglect these terms with consistency, as the amplitude of  $V$  is then proportional to that of  $W$ , and the third term in equation (9) is then only of order  $W^2$ , so that we cannot then consistently consider the non-linear theory of second sound while neglecting the first sound that it excites.

### § 3. THE RIEMANN THEORY OF SECOND SOUND

Assuming a zero coefficient of expansion and neglecting  $V$ , equations (7) and (9) may be written in the form

$$\rho_s S \frac{\partial T}{\partial x} + \frac{\rho_n \rho_s}{\rho} \frac{\partial W}{\partial t} + \frac{1}{2} \frac{W(\rho_s - \rho_n)}{\rho} \frac{\partial \rho_n}{\partial t} + \frac{3}{2} W \frac{\rho_n \rho_s (\rho_s - \rho_n)}{\rho^2} \frac{\partial W}{\partial x} = O(W^3) \dots\dots (10)$$

$$\rho_s S \frac{\partial W}{\partial x} - WS \frac{\partial \rho_n}{\partial x} + W \rho_s \frac{\partial S}{\partial x} + \rho \frac{\partial S}{\partial t} = 0. \dots\dots (11)$$

We now make an assumption, originally due to Tisza (1940), that the entropy per unit mass of normal fluid is constant, that is  $\rho S = \rho_n S_n$ , where  $S_n$  is a constant. Taken together with equation (4), this would imply that the total masses of normal and superfluid are separately conserved, and thus neglects the possibility of transitions between the two fluids, so that it cannot be more than an approximation. However, our experimental knowledge of the behaviour of  $\rho_n$  and  $S$  as functions of temperature indicate that the accuracy of the assumption is probably reasonable down to about  $1^\circ \text{K.}$ , so that we put the consequences of the assumption on record, until the behaviour of  $S_n$  as a function of temperature is accurately known, when the terms involving  $S_n$  can easily be calculated. Making this assumption, and introducing the velocity  $C_2$  of second sound, defined by the equation

$$C_2^2 = \frac{\rho_s}{\rho_n} \frac{S^2}{\partial S / \partial T} = \frac{\rho_s S_n}{\partial \rho_n / \partial T}, \dots\dots (12)$$

and a function  $\sigma$ , analogous to the Riemann function, defined by

$$d\sigma = \frac{\rho C_2}{\rho_n \rho_s} d\rho_n, \dots\dots (13)$$

we may write equations (10) and (11) in the form

$$C_2 \frac{\partial \sigma}{\partial x} + \frac{W(\rho_s - \rho_n)}{\rho} \frac{\partial W}{\partial x} + \frac{\partial W}{\partial t} = 0, \dots\dots (14)$$

$$C_2 \frac{\partial W}{\partial x} + \frac{W(\rho_s - \rho_n)}{\rho} \frac{\partial \sigma}{\partial x} + \frac{\partial \sigma}{\partial t} = 0, \dots\dots (15)$$

which imply that the quantity  $\sigma + W$  is propagated with a velocity  $C_2 + W(\rho_s - \rho_n)/\rho$ , while the quantity  $\sigma - W$  is propagated in the opposite direction with a velocity  $C_2 - W(\rho_s - \rho_n)/\rho$ . (To see this, add and subtract equations (14) and (15).)

We have thus arrived at a theory quite analogous to the Riemann theory of ordinary sound in one dimension, but there are some very important differences: The Riemann theory of first sound is exact, whereas we have neglected terms of the



order  $W^3$  in addition to those involving  $S_n$  in deriving equations (14) and (15). There is no particular difficulty in taking these terms into account, but, as we have seen, we ought then logically to consider also the first sound excited by the second sound. Secondly, the presence of the term  $W(\rho_s - \rho_n)/\rho$  in the propagation velocity is, in general, much more important than the fact that  $C_2$  itself varies with temperature, whereas, with ordinary sound, the particle velocity is usually small compared with the change of sound velocity with pressure. Thirdly, the theory predicts that the front edge of a temperature pulse should progressively become steeper only if  $\rho_s > \rho_n$ , that is, if  $T < 1.96^\circ \text{K}$ . For temperatures between this and the transition temperature, the theoretical prediction is that the steepening should occur at the rear edge of the pulse. However, the coefficient of expansion is becoming appreciable in this region of temperatures, and the excitation of first sound and the consequent cross terms can probably be no longer neglected.

#### § 4. SHOCK-FRONT THEORY

We attempt to find a solution of equations (6) to (9), representing a disturbance of constant form travelling forwards with a constant velocity  $U$ , by imposing a backward velocity  $U$  upon everything and then setting all time derivatives equal to zero. Equation (8) then becomes  $(\partial/\partial x)[\rho(U - V)] = 0$  or  $\rho(U - V)$  is a constant, which constant we may put equal to  $\rho_0 U$ , where the suffix zero always refers to conditions in the undisturbed liquid, so that  $V_0$  and  $W_0$  are always zero. Thus we may write equation (6) in the form

$$P_0 + \rho_0 U^2 = P + \rho(U - V)^2 + \frac{\rho_n \rho_s}{\rho} W^2. \quad \dots\dots (16)$$

Equations (8) and (9) may also be handled in this way, but equation (7) is not quite so simple, because, when we put all time derivatives equal to zero, the remaining terms do not form an exact differential in the variable  $x$ . However, equation (2), from which equation (7) was derived, does have this property, and so we may use it instead. Equations (7) to (9) are thus replaced by

$$(g_0 + T_0 S_0) \rho_0 U + \frac{1}{2} \rho_0 U^3 = g[\rho_n(U - u_n) + \rho_s(U - u_s)] + T \rho S(U - u_n) + \frac{1}{2} \rho_n (U - u_n)^3 + \frac{1}{2} \rho_s (U - u_s)^3, \quad \dots\dots (17)$$

$$\rho_0 U = \rho(U - V) \quad \dots\dots (18)$$

$$\rho_0 U S_0 = \rho S(U - V) - \rho_s S W. \quad \dots\dots (19)$$

We now suppose that, just as in ordinary shock-front theory, these equations can be applied when the differences of temperature and pressure are finite but steady, so that the only effect of viscosity, thermal conduction and mutual friction between the fluids is to prevent the shock front from becoming completely abrupt. Since, in our model, a reversible mechanism exists by which temperature differences can give rise to relative motion of the two fluids, there may not always be the irreversible transformation of potential or kinetic energy into heat that occurs at shocks in other fluids. The interesting question therefore arises whether a sudden *drop in temperature* can ever be propagated as a shock. A negative pressure shock is excluded because the compressibility decreases and, therefore, the velocity of ordinary sound increases with pressure. The Riemann theory shows us that, above  $1.96^\circ \text{K}$ ., the front edge of a positive temperature pulse should be spreading out and the back edge sharpening up, so that this region of temperature seems to be a possible one for 'back-edge' or negative shocks, and this will be



confirmed by a calculation of possible shock-front velocities. This effect was confirmed experimentally by Osborne (1951), but there are disturbing effects, such as the thermal expansion and the possible attenuation of second sound in this region of temperature (Pellam 1949), which may prevent a quantitative verification. The exact causes of this attenuation are not known, but one of them may well be a conversion of second sound into ordinary sound by one of the two mechanisms already mentioned, both of which should theoretically become more and more effective as we approach the  $\lambda$ -point.

From equation (17), written in terms of the velocities  $V$  and  $W$ , by expanding  $g - g_0$  in ascending powers of  $P - P_0$  and  $T - T_0$ , using equation (16) to eliminate the term in  $P - P_0$ , and neglecting the thermal expansion, we get

$$\rho_0 U \left[ \frac{1}{2} \frac{(P - P_0)^2}{\rho_0^2} \frac{\partial \rho}{\partial P} + \frac{1}{2} (T - T_0)^2 \frac{\partial S}{\partial T} \right] + \dots = \frac{1}{2} U \left( \rho V^2 + \frac{\rho_n \rho_s}{\rho} W^2 \right) - \frac{1}{2} \left[ \rho V^3 + 3 \frac{\rho_n \rho_s}{\rho} V W^2 + \frac{\rho_n \rho_s}{\rho^2} (\rho_s - \rho_n) W^3 \right]. \quad \dots (20)$$

From equations (18) and (19) we get

$$V = \frac{U(\rho - \rho_0)}{\rho}, \quad W = \frac{U \rho_0 (S - S_0)}{\rho_s S}. \quad \dots (21)$$

In the absence of any source of first sound, equation (16) shows that  $P - P_0$  and therefore  $V$  and  $\rho - \rho_0$  are all of the order  $W^2$ .

If in equation (20) we neglect all terms of order  $W^4$ , we obtain for the velocity of a 'temperature shock' the possible values

$$U^2 = S^2 \left( \frac{T - T_0}{S - S_0} \right)^2 \frac{\rho_s}{\rho_n} \frac{\rho}{\rho_0} \frac{\partial S}{\partial T} \left( 1 - \frac{(\rho_s - \rho_n)(S - S_0)}{\rho_s S} \right)^{-1} \quad \text{or} \quad U \simeq \frac{1}{2} \frac{(\rho_s - \rho_n) W}{\rho} \pm C_2.$$

For a front-edge shock to maintain itself, its velocity must be numerically greater than  $C_2$ , the velocity of propagation of a disturbance of very small amplitude, so that we are led to expect front-edge shocks for  $\rho_s$  greater than  $\rho_n$ , but otherwise back-edge shocks. The velocity of propagation for a shock of height  $T - T_0$  is thus equal to the Riemann velocity associated with a wave of height  $\frac{1}{2}(T - T_0)$ .

In deriving the velocity of propagation of a shock we have not had to use Tisza's assumption. Indeed, by a process of successive approximation, we could derive, from the above equations, the velocity of propagation of a shock to any desired degree of accuracy, even if we did not neglect thermal expansion.

As a check on these equations we may notice that if we put  $u_n = u_s$  or  $W = 0$  in equations (16) to (18) they become precisely the same as the shock-front equations in an ordinary fluid, equation (18) being the equation of continuity, equation (16) that of conservation of momentum, and equation (17), after the use of equation (18), becoming just the conservation of enthalpy plus kinetic energy. Equation (19) is inapplicable, except for very weak shocks, in an ordinary fluid, and for a shock to be physically possible there must be an increase of entropy in the fluid after the shock has passed. In this way it is possible to rule out the possibility of negative pressure shocks (subject to reasonable assumptions about the equation of state).

Equation (19) when applied to liquid helium apparently indicates that any 'spare' heat can be taken up by a change in  $W$ , the relative velocity of the two fluids, instead of being dissipated as in an ordinary fluid. The experimental fact that second sound can be propagated without appreciable attenuation if the pulses are not steeply sloped indicates that this thermodynamically reversible mechanism



predominates for waves and gently sloped pulses, and one would expect the minimum possible thickness of a shock front to be determined by the condition that the rate of transfer of energy by conduction or viscous damping becomes comparable with the rate of transfer by the reversible conversion of temperature difference into relative motion of the fluids.

Consider a pulse of height  $\Delta T$  and maximum mutual velocity  $W$ , and suppose that it rises to its peak in a distance  $\Delta x$ . The rate of transfer of thermal energy per unit area is of the order of magnitude  $C_2 \rho S \Delta T \simeq \rho C_2^2 W$ . If heat conductivity were present alone, the rate of transfer of heat across the shock front would be of the order of magnitude  $K \Delta T / \Delta x$  per unit area. Taking  $K$  as of the same order as for helium I, that is  $6 \times 10^{-5}$  cal/deg/cm/sec.,  $\rho$  as  $0.15$  gm/cm<sup>3</sup>,  $C_2$  as  $2 \times 10^3$  cm/sec. and  $S$  as  $10^7$  ergs/gm/degree, we obtain  $\Delta x \sim 10^{-6}$  cm. If viscosity were present alone, the rate of loss of kinetic energy would be of the order of magnitude  $\eta W C_2 / \Delta x$  per unit area. Taking  $\eta = 30 \times 10^{-6}$  poise, we obtain as an estimate for the thickness of the shock front  $\Delta x \sim 10^{-7}$  cm. These estimates are of the same order of magnitude as those for the thickness of an ordinary shock.

Another way in which we might expect a lower limit to be set on the thickness of a shock front is through the mutual friction between the two liquids (proportional to  $W^3$ ) inferred by Gorter and Mellink (1949) from flow experiments in slits and tubes. By itself this mechanism does not seem to constitute a dissipative process, even if, as is not at all certain, the  $W^3$  form applicable to processes of steady flow can be applied to second sound. For mutual friction between the fluids indeed provides a mechanism by which kinetic energy can be converted into heat, but since this heat will nearly all appear in the places where the amplitude of the mutual motion is a maximum, it can again be converted into kinetic energy unless heat conductivity or the viscosity of the normal fluid come into play. It therefore seems that this mutual friction does not, by itself, limit the thickness of a shock.

There is one point which needs discussion in connection with the existence of shock fronts associated with a sudden drop in temperature. At first sight they might appear to contradict thermodynamics, in that the passage of such a shock leaves the liquid behind it at a reduced temperature and, therefore, with a smaller entropy (since the density is practically unaltered). We consider the conditions that would have to be satisfied by a source capable of maintaining such a shock at a steady amplitude as it travels down a tube. (This is analogous to the problem of maintaining a steady pressure shock in a gas by means of the motion of a piston behind it.) If the shock is travelling in the positive direction with a velocity  $U$ , and the source is supposed to be at the origin,  $u_n$  will be in the negative direction while  $u_s$  will be in the positive direction. If these conditions are to persist right up to the source, it can only mean that there is a continual conversion of normal fluid into superfluid at the source, that is to say, that the source must contain some mechanism for withdrawing entropy from the liquid. (It would be possible to do this, for instance, by means of a paramagnetic salt in a magnetic field that was steadily diminished with time.) The necessary rate of withdrawal of entropy would be  $\rho_n u_n S_n$ , which, by equation (19), exactly balances the rate of change of entropy content of the system  $U(\rho_0 S_0 - \rho S)$  due to the advance of the shock. However, even in 'ideal' circumstances, this balance between the rate of withdrawal of entropy at the source and the rate of loss of entropy by the liquid holds only in the limit of very small shocks. For shocks of finite amplitude we have also to take account of the changes in kinetic energy that must occur at the source. The



rate at which kinetic energy is brought up to the source by the normal fluid is  $-\frac{1}{2}\rho_n u_n^3$ , while it is being withdrawn from the source by the superfluid at the rate  $\frac{1}{2}\rho_s u_s^3$ . If no ordinary sound is present  $\rho_n u_n + \rho_s u_s$  vanishes. The rate at which kinetic energy is having to be created is thus proportional to  $u_s(u_s^2 - u_n^2)$ , which is positive if  $|u_s| > |u_n|$ , that is, if  $\rho_s < \rho_n$ . In these conditions we have the following state of affairs. Work has to be done at the source (e.g. by pulling the magnetized salt into a region of weaker field) in order to withdraw entropy at the rate  $\rho_n u_n S_n$ . Work has also to be done to create the extra kinetic energy. Thus, if  $\rho_s < \rho_n$ , the work done at the source is greater than that corresponding to the entropy removed from the liquid even if nothing but reversible processes occur at the source, and the regime is therefore thermodynamically possible, whereas a negative shock is not thermodynamically possible for  $\rho_s$  greater than  $\rho_n$ . An exactly similar argument shows that steady positive shocks are impossible for  $\rho_s$  less than  $\rho_n$ . The 'dissipative' terms which arise through the existence of the two velocities  $u_n$  and  $u_s$  are thus of the order  $(\Delta T)^3$  or  $W^3$ , just as the dissipation in pressure shocks is of the order  $(\Delta P)^3$  or  $V^3$ .

In practice, *steady* negative shocks have not yet been observed, but positive pulses of temperature have been produced, and negative shocks have appeared at their trailing edges when  $\rho_s < \rho_n$  (Osborne 1950). It seems that we could calculate their attenuation by an argument exactly analogous to that used to calculate the dissipation of energy in explosion pulses, where we have a shock followed by a Riemann wave of decreasing amplitude. The Riemann wave travels faster than the shock and is 'eaten up' by it, the energy in the portion of the wave thus destroyed corresponding just to the energy dissipated by viscosity and thermal conduction in the limiting case when these are very small but the shock front very steep. In our case the shock at the trailing edge travels *faster* than the Riemann wave (at a velocity of approximately  $C_2 - \frac{1}{2}(\rho_n - \rho_s)W$  compared with  $C_2 - (\rho_n - \rho_s)W$ , and the latter is again gradually 'eaten up'. Physically this means that the heat originally contained in the positive pulse is eventually dissipated into the whole region traversed by it. When  $\rho_s > \rho_n$  dissipation occurs via a front-edge shock, the analogy with an ordinary pressure pulse then being almost exact.

The assumption implicit in equation (19), that the rate of creation of entropy at the shock front is negligible, is thus seen to lead to thermodynamically consistent results. This arises because of the existence of two velocity fields.

#### ACKNOWLEDGMENTS

The author wishes to thank Mr. D. V. Osborne for many helpful discussions during the preparation of this paper, and also to put on record that he was the first to derive equations practically equivalent to equations (14) and (15) of this paper. The author also wishes to thank him for access to his experimental results before publication.

#### REFERENCES

- GORTER, C. J., 1949, *Physica*, **15**, 523.  
 GORTER, C. J., and MELLINK, J. H., 1949, *Physica*, **15**, 285.  
 LANDAU, L., 1941, *J. Phys. U.S.S.R.*, **5**, 71.  
 OSBORNE, D. V., 1951, *Proc. Phys. Soc. A*, **64**, 114.  
 PELLAM, J. R., 1949, *Phys. Rev.*, **75**, 1183.  
 TISZA, L., 1940, *J. Phys. Radium*, ser. 8, **1**, 350.  
 ZILSEL, P. R., 1949, International Conference on Very Low Temperatures at Massachusetts Institute of Technology.



## APPENDIX

*Derivation of Equations (1) and (2) of the Text*

We apply the principles of conservation of energy and momentum to a small volume fixed in space, enclosed between parallel planes at distances  $x$  and  $x + dx$  from the origin, of unit cross section. The extension to three dimensions is obvious. Applying first the principle of conservation of momentum, the net force on the volume is  $-(\partial P/\partial x)dx$ , which must be equal to the total change of momentum within the volume. This change arises from the changes in both density and velocity of both normal and superfluid within the volume, together with the net momentum carried into the volume by the motion of the two fluids. Since the rate of transport of momentum by a fluid of velocity  $u$  and density  $\rho$  is  $\rho u^2$  per unit area, we have

$$\frac{\partial}{\partial t}(\rho_n u_n + \rho_s u_s) + \frac{\partial}{\partial x}(\rho_n u_n^2 + \rho_s u_s^2) + \frac{\partial P}{\partial x} = 0, \quad \dots\dots (A1)$$

which is equation (1) of the text.

We apply the principle of conservation of energy in the following form. Since we are supposing that no heat enters the volume by conduction or radiation, the sum of the rates of change of internal energy and kinetic energy due to the changes of densities and velocities within the volume and the net rates at which these energies are being brought into the volume by convection must be zero, that is

$$\begin{aligned} \left(\frac{\partial \rho_n}{\partial t}\right)\left(\frac{\partial E}{\partial N}\right)_n + \rho_n T \frac{\partial S_n}{\partial t} + \left(\frac{\partial \rho_s}{\partial t}\right)\left(\frac{\partial E}{\partial N}\right)_s + \frac{\partial}{\partial x} \left[ \rho_n u_n \left(\frac{\partial E}{\partial N}\right)_n + \rho_s u_s \left(\frac{\partial E}{\partial N}\right)_s \right] \\ + \frac{1}{2} \frac{\partial}{\partial t}(\rho_n u_n^2 + \rho_s u_s^2) + \frac{1}{2} \frac{\partial}{\partial x}(\rho_n u_n^3 + \rho_s u_s^3) = 0. \quad \dots\dots (A2) \end{aligned}$$

The first and third terms in equation (A2) represent the respective changes in internal energy due to variations in the masses of normal and superfluid within the volume, while the second term allows for a possible specific heat of the normal fluid,  $S_n$  being the entropy per unit mass of the normal fluid, which may be a function of pressure and temperature. We assume that the entropy of the superfluid is always zero, so that there is no corresponding term for the superfluid.  $(\partial E/\partial N)_n$  and  $(\partial E/\partial N)_s$  represent respectively the changes in internal energy due to the transfer at constant volume of unit mass of normal fluid and superfluid respectively.

These quantities can be derived thermodynamically as follows. For a homogeneous one-component assembly

$$dE = g dN + T d\Sigma - P dV, \quad \dots\dots (A3)$$

where  $\Sigma$  is the entropy of the whole assembly and  $g$  is the Gibbs function per unit mass of liquid. Assuming that a transfer of superfluid involves a strictly zero change of entropy, we have for transfers at constant volume and entropy

$$\left(\frac{\partial E}{\partial N}\right)_s = g, \quad \dots\dots (A4)$$

while for transfers at constant temperature and volume

$$\left(\frac{\partial E}{\partial N}\right)_T = g + T \left(\frac{\partial \Sigma}{\partial N}\right)_{V,T}. \quad \dots\dots (A5)$$



In order to maintain the temperature constant it is necessary to maintain within the volume the same value of  $\rho_n/\rho_s$ , which quantity is a function of the temperature only provided that we neglect thermal expansion. Thus we have

$$\left(\frac{\partial E}{\partial N}\right)_T = \frac{\rho_s}{\rho} \left(\frac{\partial E}{\partial N}\right)_s + \frac{\rho_n}{\rho} \left(\frac{\partial E}{\partial N}\right)_n, \quad \dots\dots(A6)$$

so that 
$$\left(\frac{\partial E}{\partial N}\right)_n = g + \frac{\rho}{\rho_n} T \left(\frac{\partial \Sigma}{\partial N}\right)_{V,T}. \quad \dots\dots(A7)$$

Gorter (1949) has called attention to the fact that a definite assumption is involved, for instance in replacing  $(\partial \Sigma / \partial N)_V$  by  $S$ , the entropy of unit mass of the whole liquid. This assumption is not nearly so drastic as that made by Tisza (1940), in which  $S$  is assumed to be always proportional to  $\rho_n/\rho$ , so that the quantity  $S_n = \rho S / \rho_n$  is constant. Making Gorter's assumption, and substituting from equations (A6) and (A7) into (A2), we obtain equation (2) in the text, the term  $\rho_n T (\partial S_n / \partial t)$  already mentioned being a correction for the fact that  $S_n$  may not be entirely independent of  $\rho_n$ , in which case  $\partial \Sigma / \partial N$ , taken at constant volume, is not quite equal to  $S$ .

The equations of motion may also be written, after using the equations of continuity,

$$\frac{\partial u_n}{\partial t} + u_n \frac{\partial u_n}{\partial x} - \frac{(u_n - u_s)}{2S_n} \left( \frac{\partial S_n}{\partial t} + u_n \frac{\partial S_n}{\partial x} \right) + \frac{1}{\rho} \frac{\partial P}{\partial x} + \frac{\rho_s}{\rho_n} S \frac{\partial T}{\partial x} = 0, \quad \dots\dots(A8)$$

$$\frac{\partial u_s}{\partial t} + u_s \frac{\partial u_s}{\partial x} - \frac{\rho_n(u_n - u_s)}{\rho_s 2S_n} \left( \frac{\partial S}{\partial t} + u_n \frac{\partial S_n}{\partial x} \right) + \frac{1}{\rho} \frac{\partial P}{\partial x} - S \frac{\partial T}{\partial x} = 0. \quad \dots\dots(A9)$$

For comparison the equations obtained by Zilsel (1949) by a variation method are

$$\frac{\partial u_n}{\partial t} + u_n \frac{\partial u_n}{\partial x} - \frac{(u_n - u_s)}{2S_n} \left( \frac{\partial S_n}{\partial t} + u_n \frac{\partial S_n}{\partial x} \right) + \frac{1}{\rho} \frac{\partial P}{\partial x} + \frac{\rho_s}{\rho_n} S \frac{\partial T}{\partial x} = 0, \quad \dots\dots(A10)$$

$$\frac{\partial u_s}{\partial t} + u_s \frac{\partial u_s}{\partial x} + \frac{1}{\rho} \frac{\partial P}{\partial x} - S \frac{\partial T}{\partial x} = 0. \quad \dots\dots(A11)$$

If  $S_n$  is constant these become equivalent.

Landau (1941), in his equation of motion for the superfluid, obtains an extra term described as the "kinetic energy of mutual motion", which is, apparently, based on the idea that the Gibbs function has to be corrected if the two fluids are in relative motion. The investigation given above seems to show, however, that the kinetic energy of the fluids is already allowed for through the Bernoulli terms in equations such as (A8) and (A9), and that the Landau correction is not needed. In any case, the introduction of the kinetic energy of mutual motion would only be correct in a frame of reference at rest relative to one of the fluids, and the remaining equations would have to be referred to a similar frame.

It is quite easy to modify the Riemann and shock-front theories to take account of such a term, if it really exists.

*Note added in proof.* While this paper was in the press, Zilsel published a revised derivation of the equations of motion using his variation method (*Phys. Rev.*, 1950, 79, 309). He now obtains the term  $\frac{1}{2}x(v_n - v_s)^2$ , as was found by Landau, but otherwise his equations are the same as (A10) and (A11) above. In his notation  $x = \rho_n/\rho$  and  $U$  is the internal energy, while  $\Gamma$  measures the rate of transition between normal and superfluid, and the



terms involving  $S_n$  in equations (A8)–(A11) above can also be expressed in terms of  $\Gamma$ . His present paper is open to the following criticisms:

(a) It is not mathematically consistent. Zilsel's equation (2.12),  $\partial U/\partial x = \frac{1}{2}(v_n - v_s)^2$ , implies the presence of a term  $\frac{1}{2}x(v_n - v_s)^2$  in  $U$ , yet, in his equations (2.8) and (2.9), no terms arising from  $\partial U/\partial v_n$  or  $\partial U/\partial v_s$  appear.

(b) The term  $-\text{div} \{ \frac{1}{2}(\rho_s \rho_n / \rho) v^2 \mathbf{v} \}$  occurring in his energy equation (3.12) is difficult to interpret physically. The kinetic energies of the normal and superfluid components are already taken fully into account by the other terms in this equation.

(c) Zilsel introduces the very interesting idea that the 'mutual friction' introduced by Gorter and Mellink (1949) is a manifestation of the transition terms involving  $\Gamma$  or  $S_n$  together with the creation of entropy by the viscous motion of the normal component. Gorter and Mellink had to postulate a *mutual* force acting on both normal and superfluid, in order to account both for the departure of the fountain effect from the theoretical value and for the linear relationship between fountain effect and heat conductivity. Such an apparent *mutual* force can be obtained from my equations, in which  $\Gamma$  appears in *both* equations of motion, but it is hard to see how Zilsel's equations, where  $\Gamma$  appears only in the equation of motion of motion of the normal fluid, can give it.

## Second Sound in Liquid Helium II

By D. V. OSBORNE

Royal Society Mond Laboratory, Cambridge

*Communicated by D. Shoenberg; MS. received 26th June 1950 and in revised form 24th August 1950*

**ABSTRACT.** A pulse technique for the propagation of second sound is described and the expected shape of the received pulse is discussed. In this connection, experimental evidence has been obtained for a temperature discontinuity at the interface between liquid helium II and a solid medium at second sound frequencies. The pulse method has been used to study the attenuation of second sound with distance and the formation of shock waves. The observations on the latter are shown to be in agreement with the predictions of the equations of motion of liquid helium II if second order terms are not neglected.

### § 1. INTRODUCTION

IT is now well known that temperature variations in liquid helium II are propagated according to a wave equation, and these temperature waves have received the name of second sound. The two principal quantities characteristic of any wave motion, namely the velocity and the impedance, have already been measured for second sound and their values may be considered well known at temperatures between  $1.1^\circ \text{K.}$  and the  $\lambda$ -point ( $2.19^\circ \text{K.}$ ), (Peshkov 1944, 1946, Lane, Fairbank and Fairbank 1947, Pellam 1949, Osborne 1948). This being so, interest naturally begins to centre on secondary effects, and this paper describes measurements on the attenuation of second sound with distance and on the propagation of waves of large amplitude. The pulse technique, briefly mentioned in an earlier note (Osborne 1948) and developed also by Pellam (1948, 1949), has been used throughout and a short description of the method will first be given, followed by a discussion of the principles from which it is possible to predict the general shape of the received pulse.



## § 2. GENERAL DESCRIPTION OF THE TECHNIQUE

A general scheme is shown in Figure 1. The essential features are a heater, usually of fine wire, from which the second sound is radiated, some kind of tube filled with helium down which it is propagated, and a resistance thermometer at which it is received and converted into an electrical signal. The auxiliary equipment must include a means of supplying power to the heater and a means

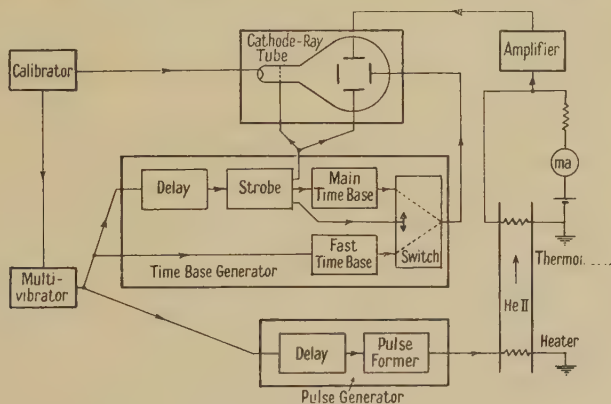


Figure 1. General scheme of pulse technique.

of amplifying and displaying the received electrical signal. In the case of the pulse technique, the requirements are very similar to those of a radar installation except that the pulse supplied to the heater is a pulse of direct current, not of alternating current, and it is the directly transmitted signal in which we are primarily interested, although echoes can readily be detected and do provide additional information.

At the heart of the pulse circuits is a multivibrator which has a natural recurrence frequency of 0.5 to 50 cycles per second. This device is loosely synchronized with a crystal oscillator which provides the standard of time in the form of calibrator pulses at intervals of  $20 \mu\text{sec}$ . The first duty of the multivibrator is to initiate a pulse for the heater, and this is accomplished by means of a conventional circuit incorporating a variable delay so that the pulse may occur at some convenient time shortly after the beginning of the multivibrator waveform.

The next requirement is that a time-base be started at the beginning of each cycle, and for this purpose the multivibrator drives a Miller time-base which is connected, through an electronic switch whose function will appear below, to the X plates of the cathode-ray tube.

There is also set in motion at the beginning of each cycle a mechanism for producing a short length of expanded time-base later on in the cycle. This is managed via a variable delay which provides a 'strobe' pulse after any desired time up to about 40 msec. This strobe drives a fast time-base and it also operates the electronic switch so that, during the period of the strobe pulse, the main time-base is replaced by the fast one. The strobe pulse fulfils one other function, namely the provision of a deflection voltage on the Y plate of the cathode-ray tube so that the fast trace shall appear below the main one.

For timing purposes the calibrator pulses from the crystal oscillator are supplied to the grid of the cathode-ray tube so that bright spots are seen on the

trace at intervals of 1 msec., together with fainter ones at intervals of  $\frac{1}{2}$  msec.,  $100\ \mu\text{sec.}$ , and  $20\ \mu\text{sec.}$

The phosphor bronze resistance thermometer which is used for detecting the signals carries a direct current of the order of a few milliamperes and the variations of resistance consequent upon the arrival of a second sound signal at the thermometer cause corresponding variations of the voltage across it. These variations are amplified by a three-valve amplifier of conventional design with an input transformer having a step-up ratio of 15 : 1, so that the overall voltage gain, including a small amplifier built into the oscilloscope, is about  $10^7$ , at frequencies from about 300 c/s. to 300 kc/s.

The temperature of the helium bath is obtained from the vapour pressure of the helium, using the 1949 scale (van Dijk and Shoenberg 1949).

### § 3. DISCUSSION OF THE EXPECTED SHAPE OF THE RECEIVED PULSE

Several authors (Dingle 1948, Osborne 1948, Pellam and Scott 1949) have commented on the analogy between the propagation of second sound and of electrical waves on wires, and Peshkov (1948a) has given a formally similar analysis although without actual reference to electrical waves. The analogy is a useful one, provided that all the relevant circuit elements are taken into account, but there is one important factor that has not been mentioned in previous treatments. This is the observation of Kapitza (1941) that heat transfer from a solid surface into liquid helium II is accompanied by a temperature discontinuity at the surface proportional to the heat flow per unit area. The constant of proportionality  $K$  is of the order of a few degrees per watt  $\text{cm}^{-2}$  and decreases towards the lambda point. Since in the analogy heat flow corresponds to current and temperature corresponds to voltage,  $K$  will appear as a resistance.

The liquid helium itself is equivalent to a transmission line of characteristic impedance  $\gamma$  given by

$$\gamma = (\rho c u_2)^{-1}, \quad \dots\dots(1)$$

where  $\rho c$  is the specific heat of helium II per unit volume, and  $u_2$  the velocity of second sound. This fact, which has been verified experimentally (Osborne 1948), may be deduced from the equations of motion which lead to the wave equation for second sound, but, as will now be shown, it is not in fact dependent upon this detailed theory. Let the assumption be made (say as an experimental fact) that in liquid helium II the propagation of temperature waves is possible without appreciable attenuation or dispersion. Then consider in one dimension the progress of a sudden step of temperature which in such a medium will travel without change of shape at a velocity  $u_2$ . Such a step will sweep out a volume  $u_2$  per unit time per unit area of wave-front and within this volume all the material will rise in temperature by the amplitude  $\Delta T$  of the step. The quantity of heat required to bring this about will be  $\rho c u_2 \Delta T$ . With the step, therefore, there must be associated a flow of heat per unit area  $W$  in the direction of propagation, where  $W = \rho c u_2 \Delta T$ . Therefore  $\gamma = \Delta T / W = (\rho c u_2)^{-1}$ , as stated above.

The behaviour of the solid media constituting the apparatus is to be obtained from the well-known equation of heat conduction

$$\nabla^2 \theta = \frac{s}{k} \frac{\partial \theta}{\partial t}, \quad \dots\dots(2)$$



where  $\theta(x, y, z, t)$  is the temperature at any point at time  $t$ ,  $s$  the specific heat per unit volume, and  $k$  the thermal conductivity. For a semi-infinite solid undergoing simple harmonic temperature variation at its plane surface, the solution is

$$\theta = \theta_1 \exp [-(s\omega/2k)^{1/2}x] \cos \{\omega t - x(s\omega/2k)^{1/2}\},$$

where  $\theta_1 \cos \omega t$  is the temperature at the surface  $x = 0$ . This is a wave attenuated to  $e^{-1}$  of its original amplitude in a distance

$$\delta = \lambda/2\pi = (2k/s\omega)^{1/2}. \quad \dots\dots(3)$$

The input impedance at the surface (i.e. temperature amplitude divided by the heat flow amplitude) is given by

$$Z = \frac{1}{2}(1-i)(ks\omega)^{-1/2}. \quad \dots\dots(4)$$

The representation of the propagation tube of Figure 2(a) by the equivalent circuit of Figure 2(b) can now be justified. The input power appears as a current  $I$  supplied to a capacity  $C_h$  representing the heater wire. Since the penetration depth for the heater wire is large compared with its radius, this is a sufficient approximation. Following Kapitza's observation, the heater is shown coupled to the helium through a resistance  $K_h$ . The heater is usually stretched across a solid backing, but is not in good thermal contact with it, and the backing is therefore shown coupled to the helium through a separate resistance  $K_1$ . The impedance  $Z_1$  of the backing is to be calculated from equation (4). The column of helium, in so far as wall effects may be neglected, is imagined as a transmission line of characteristic impedance  $\gamma$ . At the thermometer end we have circuit elements similar to those at the heater end, and the temperature amplitude which is finally detected is represented by the voltage across  $C_t$  the thermal capacity of the thermometer.

The conditions that a rectangular pulse of heat of duration  $\tau$  supplied to the heater shall be radiated and received without appreciable distortion are

$$|K_1 + Z_1| \quad \text{and} \quad |K_2 + Z_2| \gg \gamma$$

$$\text{and} \quad C_h(K_h + \gamma) \quad \text{and} \quad C_t(K_t + \gamma) \ll \tau.$$

At 1.7° K., with a heater and thermometer each consisting of 10 cm. of wire 80  $\mu$  in diameter stretched (zig-zag) across a tube of 1 cm<sup>2</sup> cross section,

$$\gamma \sim 10^{-3} \text{ deg. watt}^{-1}$$

$$K_1 \sim K_2 \sim 3 \text{ deg. watt}^{-1}$$

$$Z_1 \sim Z_2 \sim (1-i) 10 \text{ deg. watt}^{-1} \text{ at } 1 \text{ kc/s.}$$

$$K_h \sim K_t \sim 10 \text{ deg. watt}^{-1}$$

$$C_h \sim C_t \sim 10^{-7} \text{ joule deg}^{-1}.$$

$$\text{Therefore} \quad |K_1 + Z_1| \sim |K_2 + Z_2| \sim 1.6 \times 10^4 \gamma$$

$$\text{and} \quad C_h(K_h + \gamma) \sim C_t(K_t + \gamma) \sim 1 \mu\text{sec.}$$

Since the pulse lengths commonly used are in the range 0.1 msec.  $\leq \tau \leq$  1 msec., the above conditions for the absence of distortion are amply satisfied in practice. This fact has already been implicitly confirmed by the agreement between the measured and predicted values of  $\gamma$  (Osborne 1948). It will therefore be assumed in §§5 and 6 that the thermometer waveform is a true representation of the temperature variations being propagated through the liquid. With a thermometer mounted in front of a backing as illustrated in Figure 2(a), the

actual variation in temperature of the thermometer will be just twice the incident amplitude in the helium, i.e.  $2I\gamma$ , because of the reflection at the backing.

The above treatment has ignored attenuation in the helium and losses at the walls. The latter will be of the same order as the losses at the ends, i.e. negligible in the case considered. The former will be shown to be negligible except very near the lambda point (see Figure 5).

To show that circumstances can arise in which the thermometer does introduce distortion, a form of apparatus having a heater and thermometer of graphite deposited upon a backing (Fairbank and Lane 1947) is illustrated in Figure 3, together with the equivalent circuit. This design has been used by several workers, and the present author has employed it in circumstances where

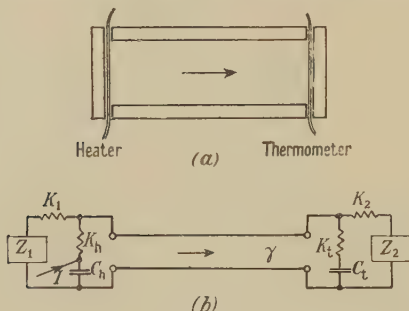


Figure 2. (a) Propagation tube with wire heater and thermometer. (b) Equivalent circuit.

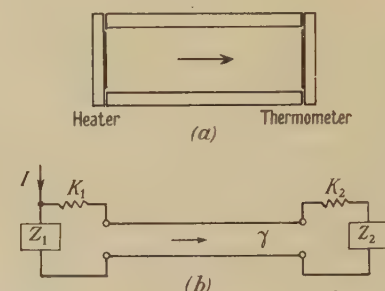


Figure 3. (a) Propagation tube with 'Aquadag' heater and thermometer. (b) Equivalent circuit.

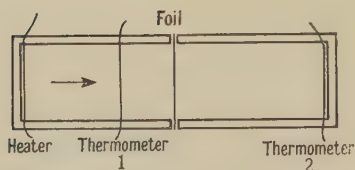


Figure 4. Propagation tube to measure transmission and reflection at a thin foil.

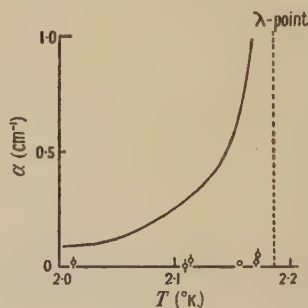


Figure 5. Attenuation of second sound with distance.  
Full line: Experimental curve (Pellam), pulse length 150  $\mu\text{sec}$ .  
Circles: Experimental points (Osborne), pulse length 600  $\mu\text{sec}$ .

the shape of the received pulse was unimportant. The essential difference between it and the previous design is that the heater and the backing are now coupled to the helium through the common impedance  $K_1$ . The current actually supplied to the line will therefore depend on the ratio of  $K_1$  to  $Z_1$  and, whilst the thermal data is very meagre, it suggests that  $K_1$  and  $|Z_1|$  are of the same order of magnitude. Similarly the pulse received at the thermometer will depend on the relative values of  $K_2$  and  $Z_2$ . It follows, since  $Z_1$  and  $Z_2$  are complex, that not only the amplitude but also the shape of the received pulse will depend on the relative values of  $K$  and  $Z$  at the temperature in question, and that if  $K$  is not much smaller than  $|Z|$ , the received pulse will be more or less severely



integrated. This in fact has been observed experimentally, the times of rise of the received pulse being of the order of 100–200  $\mu$ sec.

With a view to establishing the relevance of the impedance  $K$  to experiments on second sound, a propagation tube of the type shown in Figure 4 has been used. The first thermometer was an open wound one with a 'shadow area' of only 10% of the cross section of the tube. The copper foil had a thickness of 0.0025 cm., to be compared with a penetration depth  $\delta$  of the order of 1 cm. In the absence of a boundary impedance, therefore, the foil should have presented no appreciable obstacle to the transmission of second sound and there should have been no reflection from it. In fact there was no observable transmission and the reflection coefficient was very close to unity. A rough calculation on the basis of this result, taking into account the amplitude of the smallest transmitted signal which could have been detected, gives a lower limit of 0.1 deg.watt<sup>-1</sup> cm<sup>2</sup> for  $K$  at 1.2° K. This value is not inconsistent with Kapitza's measurements using a steady heat flow ( $K \sim 1$  deg.watt<sup>-1</sup> cm<sup>2</sup>).

#### § 4. SECOND SOUND WAVES OF FINITE AMPLITUDE

It was discovered fairly early in the investigation that, whereas a small pulse of second sound was propagated without change of shape, larger pulses became seriously distorted. Plate I shows the effect in question. It represents a series of oscillograms of the received temperature pulse for increasing amplitudes of the input pulse supplied to the heater. The upper trace is the main time-base going from left to right and the lower trace presents an expanded version of what occurs during the gap in the upper trace. A negative deflection on either trace represents a positive temperature excursion. In Plate I(a)\* the signal at small amplitudes is seen to have a flat top and sloping back and front edges. As the input is increased, the front edge becomes much steeper and actually occupies a shorter time, whereas the flat top and the back edge coalesce to form a long tail. At the same time the front edge not only becomes steeper but also occurs earlier.

Plate II shows that similar phenomena are observed at constant amplitude if the thermometer is progressively withdrawn from the heater, provided that the initial pulse be large enough. Near the heater the pulse is a fair reproduction of the input, whereas at greater distances the characteristic sharp rise and long tail appear.

This behaviour is familiar to students of ordinary sound as the generation of shock waves, and it is due to the non-linearity of the equations of motion of a compressible fluid. In the case of ordinary sound there are two contributory effects. In the first place the velocity of propagation increases with pressure so that, taking account of second order terms, the compressions will be propagated faster than the rarefactions; and in the second place any disturbance tends to be propagated at the velocity of sound relative to the local stream velocity, so that those points of the wave front where the stream velocity is in the same direction as the propagation will overtake the places where the stream velocity runs counter to the direction of propagation. Both of these effects are second order ones and are rarely observed for ordinary sound except in the very intense waves generated by explosions. Both effects cause the points of high pressure to overtake those of low pressure so that, for a positive pressure excursion, the leading edge becomes steeper and the trailing edge becomes a long tail. The

\* For Plates see end of issue.

process is limited when the leading edge becomes very steep by the dissipation due to the action of viscosity and thermal conductivity in the very steep pressure and temperature gradient at the wave front. This limiting condition is known as a shock wave or shock front, and the antecedent condition of a wave which is becoming progressively more distorted is referred to as the propagation of a wave of finite amplitude.

It is possible to obtain some idea of the physical meaning of the processes occurring in second sound if it is assumed that

$$\rho_n \mathbf{v}_n + \rho_s \mathbf{v}_s = 0 \quad \dots\dots(5)$$

and that the equation of motion is to be written down including the necessary second order term in the acceleration. The conventional

$$\frac{\partial \mathbf{v}_s}{\partial t} + \text{grad } G = 0 \quad \dots\dots(6)$$

then becomes

$$\frac{\partial \mathbf{v}_s}{\partial t} + (\mathbf{v}_s \cdot \text{grad}) \mathbf{v}_s + \text{grad } G = 0,$$

where  $G$  is the thermodynamic potential per unit mass of helium. A conventional Riemann treatment for plane waves leads to the expression

$$u' = u_2 + v_s, \quad \dots\dots(7)$$

where  $u'$  is the velocity of propagation of any plane in the wave front for which the superfluid velocity is  $v_s$ , and  $u_2$ , the velocity of propagation for very small amplitudes, is given by

$$u_2^2 = \frac{TS^2}{c} \frac{\rho_s}{\rho_n} \quad \dots\dots(8)$$

$c$  is the specific heat of helium per unit mass,  $S$  the entropy per unit mass,  $\rho_s$  and  $\rho_n$  the superfluid and normal parts of the density respectively, and  $T$  the absolute temperature.

As far as second sound is concerned, however, and probably in some other applications, the motion of the normal fluid is as reversible as that of the superfluid component and a gradient of  $G$  (which may be written  $(1/\rho) \text{grad } p - S \text{grad } T$ ) acts as a force upon both components. Equation (6), therefore, must be replaced by a form more symmetrical in  $v_n$  and  $v_s$ , and a convenient starting point is found in the formulation by Gorter and Mellink (1949), originally used in connection with their theory of mutual friction between the two components. If the friction and viscosity terms are omitted, there remain

$$\left. \begin{aligned} -\frac{\rho_s}{\rho} \text{grad } p + \frac{\rho_n \rho_s}{\rho} S_\lambda \text{grad } T &= \rho_s \frac{\partial \mathbf{v}_s}{\partial t} \\ -\frac{\rho_n}{\rho} \text{grad } p - \frac{\rho_n \rho_s}{\rho} S_\lambda \text{grad } T &= \rho_n \frac{\partial \mathbf{v}_n}{\partial t} \end{aligned} \right\}, \quad \dots\dots(9)$$

where  $S_\lambda$  is the value of  $S$  at the  $\lambda$ -point. As these equations stand, the use of equation (5) will lead straight to equation (6), but, if the second order terms  $(\mathbf{v}_s \cdot \text{grad}) \mathbf{v}_s$  and  $(\mathbf{v}_n \cdot \text{grad}) \mathbf{v}_n$  are included, an equation different from (6) is obtained. If the Riemann derivation is now carried through we arrive at

$$u' = u_2 + v_n + v_s, \quad \dots\dots(10)$$

This is the result given by Temperley (1951) in his rigorous derivation in which he proves that equation (5) is in fact sufficiently accurate for the purpose in hand provided that thermal expansion is negligible.



The first experimental results were obtained at a temperature of  $1.2^\circ\text{K.}$ , where  $\rho_s \gg \rho_n$ , and therefore, by equation (5),  $v_n \gg v_s$ . In this region,  $u' \simeq u_2 + v_n$ , and it should be possible to verify this formula by studying the rate at which the top of the leading edge of a pulse overtakes the foot.  $v_n$  can be calculated from the measured power input  $W$  using the relation

$$W = \rho S T v_n. \quad \dots\dots(11)$$

Data taken from Plate II give a value of  $u' - u_2$  equal to  $+140\text{ cm. sec}^{-1}$ , whereas  $v_n$  calculated from  $W$  is about  $+155\text{ cm. sec}^{-1}$ . In view of the uncertainty of the thermal data and the difficulty of measuring the rates of rise of the pulse, this agreement is satisfactory and confirms the theory quite well. It shows clearly the inadequacy of equation (7) which would predict a value of  $u' - u_2$  equal to  $-5\text{ cm. sec}^{-1}$ .

A further test is provided by the predictions at temperatures near the  $\lambda$ -point for which  $\rho_n > \rho_s$ . For a positive temperature excursion  $v_s$  is always in the opposite direction to  $u_2$  so that, for  $\rho_n > \rho_s$ ,  $v_n + v_s < 0$ , i.e.  $u' < u_2$ . In these circumstances the front edge of a positive pulse will be stretched out and it will be the back edge that is steepened to form a shock wave. At the temperature where  $\rho_n = \rho_s$ , about  $1.96^\circ\text{K.}$ ,  $u'$  is equal to  $u_2$  so far as second order terms are concerned, and any distortions can only be calculated by taking into account third and higher order terms.

These predictions are on the whole borne out by experiment. Plate III shows the effect, at  $2.12^\circ\text{K.}$ , of steadily increasing the input power, the thermometer being held at a fixed distance of  $15.6\text{ cm.}$  from the heater. In Plate III (a), (b) and (c) the power flows are  $0.65$ ,  $1.7$  and  $3.6\text{ watt cm}^{-2}$  respectively, and it is clearly visible that for the larger power flows it is the leading edge that becomes elongated and the trailing edge that is steepened. (In Plate III alone a positive temperature excursion is shown by a positive deflection.) Plate IV shows the signal for a fixed power amplitude ( $3.5\text{ watt cm}^{-2}$  at  $2.12^\circ\text{K.}$ ) as the thermometer is progressively withdrawn from the heater; at long ranges the behaviour again corresponds to theory but at short ranges ( $\leq 5\text{ cm.}$ ) there appears to be an anomaly in that the leading edge is steepened as though the temperature were below  $1.96^\circ\text{K.}$

Significant quantitative measurements cannot be made for these very small signals, so that it is impossible to say whether the observed distortions agree quantitatively with the theory, but qualitatively and in order of magnitude the agreement is satisfactory.

In the neighbourhood of  $1.96^\circ\text{K.} \pm 0.1^\circ$  (i.e. where  $\rho_n = \rho_s$ ) a square pulse input results in the propagation, more or less without change of shape, of a signal with both its front and back edges elongated. This phenomenon is clearly not covered by the second order theory.

## § 5. SHOCK WAVES

The preceding section has dealt only with the progressive distortion of a wave of finite amplitude up to the stage at which the wave front reaches its limiting steepness. Temperley (1951), in addition to giving the Riemann treatment of this problem, gives also the Rankine-Hugoniot derivation of the velocity of propagation of a fully developed shock wave. This velocity  $u''$  is given by

$$u'' = u_2 + \frac{1}{2}(v_n + v_s), \quad \dots\dots(12)$$

where  $v_n$  and  $v_s$  are the normal and superfluid velocity amplitudes at the top of the shock front. Relation (12) has not been investigated in detail experimentally, but one observation at  $1.05^\circ\text{K.}$  gives a qualitative confirmation of it. The apparent velocity  $u''$  for a pulse having a power flow amplitude of  $1.3\text{ watt cm}^{-2}$  and propagated over a distance of 4 cm. was  $20.7\text{ m.sec}^{-1}$ , as opposed to the value  $18.8\text{ m.sec}^{-1}$  obtained for  $u_2$  by extrapolating to zero amplitude the velocities obtained with smaller power flows.  $v_n$  for this power flow should be about  $180\text{ cm.sec}^{-1}$ , so that the difference of  $190\text{ cm.sec}^{-1}$  corresponds rather more closely to  $v_n$  than to  $\frac{1}{2}v_n$  ( $v_s$  is negligible). On the other hand, the uncertainty of the thermal data at  $1.05^\circ\text{K.}$  does not permit accurate calculations, and the calculation of  $v_n$  from the input power flow is in any case a somewhat doubtful procedure for a fully developed shock front.

This effect is clearly of practical importance in connection with velocity measurements at the lowest temperatures. In the instance quoted the apparent velocity differed from  $u_2$  by some 8%, and at still lower temperatures the effect will be even more marked for a given power flow, since (from (11))  $v_n = W/\rho ST$ . It is essential therefore that measurements below  $1^\circ\text{K.}$  should be carried out with the smallest possible signals.

#### § 6. ATTENUATION MEASUREMENTS

Both Peshkov (1948b) and Pellam (1948, 1949) have undertaken measurements of the attenuation of second sound with distance. Peshkov's measurements were confined to one temperature, namely  $1.63^\circ\text{K.}$ , and he deduces that here the most important dissipation effects occur at the walls, due to viscosity and thermal conduction, rather than in the bulk of the liquid itself.

Pellam measured the attenuation of a  $150\text{ }\mu\text{sec.}$  pulse and found that near the lambda-point the amplitude varied exponentially with distance. His values of the quantity  $\alpha$  in the equation

$$\theta(x) = \theta(0) \exp(-\alpha x), \quad \dots\dots (13)$$

where  $\theta(x)$  is the temperature amplitude at a distance  $x$  from the heater, are given Figure in 5. Most of these data are drawn from experiments in which the thermometer was withdrawn progressively from the heater and the reduction in signal size noted, but a few of the points, especially very near the lambda-point, were taken from experiments showing multiple reflection. For these points the reflection coefficient was taken to be unity, and the reduction in amplitude of successive echoes was ascribed to attenuation *en route*.

In the present investigation these measurements have been repeated, using a  $600\text{ }\mu\text{sec.}$  pulse, with the results shown by circles in Figure 5. From the experimental errors shown by vertical lines in the Figure, it will be seen that these results differ from those of Pellam, and they do not conclusively show the existence of any attenuation at all at this particular pulse length. The important Fourier components of a  $150\text{ }\mu\text{sec.}$  pulse are in the region of  $3\text{ kc/s.}$ , while those of a  $600\text{ }\mu\text{sec.}$  pulse are in the region of  $750\text{ c/s.}$ , so that it is just possible that the greater attenuation measured by Pellam was due to the higher frequencies involved in his experiments. To test this, a small  $500\text{ }\mu\text{sec.}$  pulse was propagated at  $2.16^\circ\text{K.}$ , and its rise and decay times noted both near the heater and 2 cm. further away. If the rise and decay times increased by  $\tau_1$  because of the extra 2 cm. path length, the conclusion would be that frequencies from about  $1/2\pi\tau_1$  upwards were being attenuated appreciably within the 2 cm. The actual figures for  $W=0.64\text{ watt cm}^{-2}$  and  $\theta=0.67 \times 10^{-3}\text{ deg.}$  are as follows:



Range (cm.)	Rise time $\tau_R$ (sec.)	Decay time $\tau_D$ (sec.)
0.7	130	200
2.7	260	170
	$\Delta\tau_R = +130$	$\Delta\tau_D = -30$ /

On account of the effect described in §4, it may be calculated from the values of  $W$  and  $\theta$  that the rise time ought to increase with distance, and the decay time ought to diminish, by an amount  $\tau_2 = 85 \mu\text{sec.}$  for 2 cm. It is impossible to avoid this effect without using imperceptibly small signals. If it is assumed that  $\Delta\tau_R$  is composed of  $\tau_1 + \tau_2$ , and  $\Delta\tau_D$  is composed of  $\tau_1 - \tau_2$ , we have  $\tau_1 + \tau_2 = +130 \mu\text{sec.}$ ,  $\tau_1 - \tau_2 = -30 \mu\text{sec.}$ , whence  $\tau_1 = 50 \mu\text{sec.}$  and  $\tau_2 = 80 \mu\text{sec.}$  The value of  $\tau_2$  is in good agreement with the calculated one and it seems possible therefore that  $\tau_1$  does indeed represent an integration of the pulse, in which case it follows that frequencies upwards of 3 kc/s. ( $= 1/2\pi\tau_1$ ) are appreciably attenuated within 2 cm. at  $2.16^\circ \text{K.}$

Although this treatment is only tentative pending further experimental evidence, it suggests that the short pulse length used by Pellam should have caused some genuine attenuation due to the removal of high frequencies, but it is possible that at least part of the attenuation observed by him (Figure 5) was due to finite amplitude effects. These are much more serious in a short pulse than in a long one, because the back edge may become a 'shock front' (see §5) and new dissipative effects will then come into play which may make the attenuation much more severe. From the values of  $W$  and  $\theta$  quoted above, it may be seen that very small signals indeed ( $\sim 10^{-4}$  deg.) would have to be used in order to avoid finite amplitude effects at all safely.

This same kind of treatment can probably account for one other phenomenon, namely the difficulty of observing signals at temperatures between  $2.16^\circ \text{K.}$  and  $2.185^\circ \text{K.}$ , even though in this region the calculated value of the characteristic impedance  $\gamma$ , i.e.  $(\rho c u_2)^{-1}$  is increasing apparently without limit. The value of  $v_s$  for a given temperature amplitude  $\theta$  is becoming very large and the value of  $u_2$  is approaching zero, so that shock wave effects will become more and more important as the  $\lambda$ -point is approached. Signals of any observable size will therefore be subject to very large dissipative processes and will quickly be attenuated.

#### ACKNOWLEDGMENTS

The author wishes to thank Dr. K. R. Atkins and Mr. H. N. V. Temperley for many interesting discussions, and Mr. Temperley in particular for showing him his calculations before publication.

#### REFERENCES

- DINGLE, R. B., 1948, *Proc. Phys. Soc.*, **61**, 9.  
VAN DIJK, H., and SHOENBERG, D., 1949, *Nature, Lond.*, **164**, 151.  
FAIRBANK, H. A., and LANE, C. T., 1947, *Rev. Sci. Instrum.*, **18**, 525.  
GORTER, C. J., and MELLINK, J. H., 1949, *Physica*, **25**, 285.  
KAPITZA, P. L., 1941, *J. Phys. U.S.S.R.*, **4**, 181.  
LANE, C. T., FAIRBANK, H. A., and FAIRBANK, W. M., 1947, *Phys. Rev.*, **71**, 600.  
MAURER, R. D., and HERLIN, M. A., 1949, *Phys. Rev.*, **76**, 948.  
OSBORNE, D. V., 1948, *Nature, Lond.*, **162**, 213.  
PELLAM, J. R., 1948, *Phys. Rev.*, **74**, 841; 1949, *Ib'd.*, **75**, 1183.  
PELLAM, J. R., and SCOTT, R. B., 1949, *Phys. Rev.*, **76**, 869.  
PESHKOV, V. P., 1944, *J. Phys. U.S.S.R.*, **8**, 131; 1946, *Report of International Conference on Fundamental Particles*, Vol. I (London: Physical Society), p. 19; 1948 a, *J. Exp. Theor. Phys. U.S.S.R.*, **18**, 857; 1948 b, *Ibid.*, **18**, 867; 1948 c, *Ibid.*, **18**, 951.  
TEMPERLEY, H. N. V., 1951, *Proc. Phys. Soc. A*, **64**, 105.

## The Magnetic Susceptibility of Copper Sulphate

By R. J. BENZIE\* AND A. H. COOKE

Clarendon Laboratory, Oxford

*MS. received 25th August 1950*

**ABSTRACT.** Measurements of the magnetic susceptibility of copper sulphate pentahydrate have been made at temperatures between 20° K. and 1° K. on a single crystal specimen. It is found that the susceptibilities measured in different directions with respect to the crystallographic axes follow a Curie-Weiss law, with different Curie constants but a fixed Weiss constant of  $-0.6^\circ$ . The discrepancy between this result and that of Krishnan and Mookherji is attributed to temperature-independent paramagnetism.

### § 1. INTRODUCTION

THE first measurements of the susceptibility of copper sulphate pentahydrate as a function of temperature were made by de Haas and Gorter (1930), who found that the paramagnetic susceptibility per mole of a powdered specimen could be expressed as  $\chi = 0.457/(T + 0.7^\circ)$  between room temperature and liquid hydrogen temperatures. From a series of very delicate measurements of the anisotropy of the susceptibility of a single crystal of copper sulphate between room temperature and liquid air temperature, Krishnan and Mookherji (1936, 1938) deduced that copper sulphate is approximately magnetically uniaxial with a minimum susceptibility  $\chi_a$  along the magnetic axis and a maximum susceptibility  $\chi_e$  perpendicular to the axis. Combining their own results with those of de Haas and Gorter, they deduced that

$$\chi_a = 0.399/(T - 2.0^\circ) \text{ and } \chi_e = 0.486/(T + 1.8^\circ). \quad \dots\dots(1)$$

While the variation of the Curie constant with direction can be related to the crystal structure of the salt, the concomitant variation of Weiss constant from  $+2.0^\circ$  to  $-1.8^\circ$  is a surprising result, which would be difficult to account for theoretically. In this paper we describe a more direct measurement of the magnetic susceptibilities and Weiss constants in different directions of a single crystal, at temperatures between 20° K. and 1° K. The measurements show no significant variation of Weiss constant with direction. The discrepancy between this result and that deduced by Krishnan and Mookherji is attributed to temperature-independent effects.

### § 2. CRYSTALLINE AND MAGNETIC PROPERTIES OF COPPER SULPHATE

Crystallographic examination by Beevers and Lipson (1934) has shown that the unit cell of copper sulphate pentahydrate contains two ions, each of which is surrounded by six negatively charged oxygen atoms forming a nearly regular octahedron. Four of these belong to water molecules and are arranged in a square coplanar with the  $\text{Cu}^{++}$  ion; the other two oxygens, belonging to the  $\text{SO}_4$  group, complete the octahedron and are at a slightly greater distance. The electric field acting on the  $\text{Cu}^{++}$  ion is then of roughly cubic symmetry, but with

\* Now at the University College of the South West of England, Exeter.



a component of tetragonal symmetry whose axis is the line joining the last-mentioned oxygen atoms. According to the crystallographic measurements the angle between the tetragonal axes of the two  $\text{Cu}^{++}$  ions of the unit cell is approximately  $80^\circ$ .

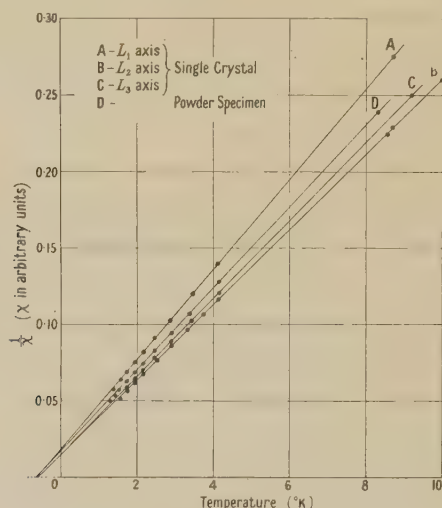
For each class of ion, the departure of the crystalline field from cubic symmetry gives rise, through spin-orbit coupling, to different susceptibilities parallel ( $\chi_{\parallel}$ ) and perpendicular ( $\chi_{\perp}$ ) to the tetragonal axes. Taking the angle between the tetragonal axes to be  $90^\circ$  and combining the effects of the two sets of ions, the magnetic susceptibility of the crystal has an axis of symmetry normal to the plane of the two tetragonal axes. In this direction the crystal has the axial susceptibility  $\chi_a = \chi_{\perp}$ , while in any direction in the plane of the tetragonal axes the susceptibility has the equatorial value  $\chi_e = \frac{1}{2}(\chi_{\parallel} + \chi_{\perp})$ . This picture, due to Krishnan and Mookherji (1938), is in agreement with the paramagnetic resonance experiments of Bagguley and Griffiths (1950), which show that the equatorial susceptibility is constant to within 1%, suggesting that the angle between the tetragonal axes is very nearly  $90^\circ$ , rather than  $80^\circ$ . The values of the axial and equatorial Curie constants derived from their measurements are respectively  $C_a = 0.407$  and  $C_e = 0.480$ . We take these figures as the most accurate available values. Figures derived from this type of experiment do not include temperature-independent magnetic effects.

### § 3. EXPERIMENTAL METHOD

Our experiments were made on a single crystal ground roughly to a sphere, and also on a powder specimen. Measurements on the sphere were made along three directions, denoted  $L_1$ ,  $L_2$ ,  $L_3$ . The direction  $L_1$  ( $154^\circ$ ,  $64^\circ$ ,  $51^\circ$  with reference to the crystallographic axes) was the direction of axial susceptibility;  $L_2$  ( $70^\circ$ ,  $41^\circ$ ,  $69^\circ$ ) was along one of the tetragonal axes;  $L_3$  was a bisector of the angle between the tetragonal axes. Susceptibility measurements were made by an A.C. mutual inductance method at temperatures from  $20^\circ\text{K.}$  to  $1^\circ\text{K.}$  The apparatus and method used have already been described elsewhere (Benzie and Cooke 1950). The measurements from  $20^\circ\text{K.}$  to  $8^\circ\text{K.}$  were made by condensing hydrogen over the specimen and pumping to various temperatures, and measurements from  $4^\circ\text{K.}$  to  $1^\circ\text{K.}$  were made in a similar way using helium. The temperatures were measured by the vapour pressures of the hydrogen and of the helium. Temperature and susceptibility measurements were much more reliable in the liquid helium region, and most weight has been given to these. The measurements at liquid and solid hydrogen temperatures were used as little more than checks on the liquid helium observations.

In each experiment the sphere was mounted with one of the chosen directions parallel to the axis of a mutual inductance coil surrounding the specimen. Changes in the susceptibility  $\chi$  in this direction give rise to proportional changes in the mutual inductance  $M$ , and if  $m$  is the difference of the value of  $M$  at a particular temperature and  $M_0$ , the infinite temperature or zero susceptibility value of  $M$ , we have  $m = k\chi$ , where  $k$  is a constant. (Strictly,  $m$  is a measure only of the temperature-dependent part of the susceptibility, but this distinction can be neglected in our measurements. In the liquid helium range the diamagnetic susceptibility, for example, is less than 0.1% of the total susceptibility.) If the susceptibility  $\chi = C/(T - \Delta)$ , the value of the Weiss constant  $\Delta$  can be obtained by plotting a graph of  $1/m$  against  $T$  and extrapolating to  $1/m = 0$ . The values

of  $M_0$  and  $\Delta$  were in fact found by successive approximation, by extrapolating graphs of  $M$  against  $1/T$  to  $1/T=0$ , and of  $1/m$  against  $T$  to  $1/m=0$ . The final graphs of  $1/m$  (or  $1/\chi$ ) against  $T$  are shown in the Figure. It will be seen that the graphs for the three directions  $L_1$ ,  $L_2$  and  $L_3$  all tend to a value of Weiss constant  $\Delta$  very near to  $-0.6^\circ$ . The diagram also shows the result for a powdered sample for which the Weiss constant appears to be slightly greater. The value of  $\Delta$  obtained with the powder ( $-0.65^\circ$ ) is very nearly the same as that found by de Haas and Gorter (1930) and is probably more reliable, as their lowest temperature of measurement was  $14^\circ\text{K}$ . A value of  $-0.65^\circ$  also fits Reekie's (1939) observations as well as the value of  $-0.7^\circ$ . However, the difference between our powder and crystal results is within experimental error, and the results can best be stated as  $\Delta = -0.60 \pm 0.05$  for all directions of the crystal. The law  $\chi = C/(T + 0.6)$  holds down to approximately  $1.8^\circ\text{K}$ , and between this temperature and  $14^\circ\text{K}$  the extreme scatter, from the mean, of  $\chi(T + 0.6)$  is less than 1% in each of the four series of measurements.



The susceptibility of copper sulphate.

In order to rotate the crystal, the apparatus had to be dismantled and reassembled between the measurements along the different axes, and as a result the slopes of the graphs are not accurately inversely proportional to the corresponding Curie constants. Our accuracy from this point of view is not better than  $\pm 1\%$ . (This, of course, does not affect the accuracy of the determination of the Weiss constants.) Further, the value for the powdered specimen had to be adjusted for the mass and shape of the sample being different from that of the single crystal. Taking these factors into account the relative slopes of the graphs are in satisfactory agreement with the Curie constants derived from the measurements of Baggeley and Griffiths (1950), which are 0.407 for the axial Curie constant, 0.480 for the equatorial, and 0.457 for a powder. These are in the ratio 1:1.18:1.12, which compares with our corresponding ratio 1:1.19:1.12. It must be pointed out that this good agreement is to some extent fortuitous, as our value for the Curie constant in the equatorial plane is the mean of two values (axes  $L_2$  and  $L_3$ ) which differ by 3%.



Combining our measurements with those of Bagguley and Griffiths we obtain

$$\chi_e = \frac{0.480}{T+0.6}, \quad \chi_a = \frac{0.407}{T+0.6}. \quad \dots\dots(3)$$

The isotropic Weiss constant is readily attributable to exchange interaction (Wright 1949).

#### § 4. DISCUSSION

The considerable discrepancy between the above results and those derived by Krishnan and Mookherji is attributable to temperature-independent paramagnetism. Our measurements give only the temperature-dependent part of the susceptibility, while theirs include temperature-independent effects which though small are important at the relatively high temperatures of their experiments. In the Table the second row of figures gives the values of paramagnetic anisotropy at different temperatures, taken from the paper of Krishnan and Mookherji, while the third row gives the values calculated from equations (3). The fourth row gives the difference of the two sets of figures.

Table

Temperature (° K.)	299	280	260	240	220	200	180	160	140	90.1
$\chi_e - \chi_a$ (K. & M.)	275	291	308	327	352	385	424	473	536	781
$\chi_e - \chi_a$ (B. & C.)	210	225	242	262	286	314	349	392	448	694
Difference	65	66	66	65	66	71	75	81	88	87

It will be seen that at the higher temperatures the difference is remarkably constant at  $66 \times 10^{-6}$  per mole. This is the region of temperature in which the scatter of the results of Krishnan and Mookherji is least; at lower temperatures there is an appreciable scatter between their experimental results, and the values in the table are smoothed values. The values of anisotropy obtained by adding a constant  $66 \times 10^{-6}$  to our figures of row 3 lie, in fact, within the scatter of their observations at all temperatures. We conclude therefore that copper sulphate possesses a temperature-independent susceptibility whose anisotropy has a value of 60 to  $70 \times 10^{-6}$ .

This is in excellent agreement with the theoretical calculations of Polder (1942) who calculated the magnetic susceptibility in terms of the splitting of the energy levels of the cupric ions. He found that for a copper ion in an electric field of tetragonal symmetry the susceptibility along the tetragonal axis,  $\chi_{||}$ , is

$$\chi_{||} = \frac{0.376}{T} \left( 1 - \frac{4\lambda}{W_1} \right)^2 + \frac{4.1 \times 10^{-16}}{W_1}, \quad \dots\dots(4)$$

while the susceptibility  $\chi_{\perp}$  perpendicular to the tetragonal axis is

$$\chi_{\perp} = \frac{0.376}{T} \left( 1 - \frac{\lambda}{W_2} \right)^2 + \frac{1.04 \times 10^{-16}}{W_2}. \quad \dots\dots(5)$$

Here  $\lambda$  is the spin-orbit coupling constant, which for the cupric ion is known from spectroscopic data to be  $-852 \text{ cm}^{-1}$ , and  $W_1$  and  $W_2$  are the energy differences of higher orbital levels of the  $\text{Cu}^{++}$  ion from the ground state, produced by the crystalline electric field. The two susceptibilities each contain a term following Curie's law and a small temperature-independent term. (Polder's theory does not take account of exchange effects, and so no Weiss constant is obtained.) Both the terms depend on the value of the splitting  $W_1$  or  $W_2$ , which to some

extent must be taken as adjustable constants in the theory, but once the values of  $W_1$  and  $W_2$  are chosen so as to give the right values for the Curie constants in the main terms, the small temperature-independent terms are fixed. Polder chose  $W_1 = 15,400 \text{ cm}^{-1}$ , and  $W_2 = 26,600 \text{ cm}^{-1}$ . Then

$$\chi_{\parallel} = \frac{0.56}{T} + 136 \times 10^{-6} \quad \text{and} \quad \chi_{\perp} = \frac{0.40}{T} + 20 \times 10^{-6}. \quad \dots\dots(6)$$

For the crystal of copper sulphate, with two ions per unit cell having their tetragonal axes at  $90^\circ$ , this gives

$$\chi_a = \frac{0.40}{T} + 20 \times 10^{-6} \quad \text{and} \quad \chi_e = \frac{0.48}{T} + 78 \times 10^{-6}. \quad \dots\dots(7)$$

The anisotropy of the temperature-independent paramagnetism is thus  $58 \times 10^{-6}$  on this theory. The agreement of theory and experiment is certainly within the margin of experimental error, and affords new evidence of the existence of the Van Vleck temperature-independent paramagnetism.

For a powdered specimen, Polder's theory gives a mean temperature-independent susceptibility of  $60 \times 10^{-6}$  per mole. We have examined the effect of this term on the experimental results of de Haas and Gorter (1930) and Reekie (1939) but it is too small to permit any conclusions being drawn. It is less than the diamagnetic correction which has to be applied, and is of the same order as the differences between the two sets of experimental results. The effect of interpreting the results of de Haas and Gorter in terms of a temperature-independent paramagnetism of  $60 \times 10^{-6}$  per mole and a Weiss constant of  $-0.6^\circ$ , instead of a Weiss constant of  $-0.7^\circ$  without temperature-independent paramagnetism, is to reduce the Curie constant by less than 1%.

#### ACKNOWLEDGMENT

We are deeply indebted to Dr. D. M. S. Bagguley, who provided us with the single crystal of copper sulphate marked with the directions  $L_1$ ,  $L_2$  and  $L_3$ , and with whom we have had many helpful discussions.

#### REFERENCES

- BAGGULEY, D.M.S., and GRIFFITHS, J. H. E., 1950, *Proc. Roy. Soc. A*, **201**, 366.  
 BEEVERS, C. A., and LIPSON, H., 1934, *Proc. Roy. Soc. A*, **146**, 570.  
 BENZIE, R. J., and COOKE, A. H., 1950, *Proc. Phys. Soc. A*, **63**, 201.  
 DE HAAS, W. J., and GORTER, C. J., 1930, *Leiden Comm.* 210d.  
 KRISHNAN, K. S., and MOOKHERJI, A., 1936, *Phys. Rev.*, **50**, 860; 1938, *Ibid.*, **54**, 533, 841.  
 POLDER, D., 1942, *Physica*, **9**, 709.  
 REEKIE, J., 1939, *Proc. Roy. Soc. A*, **173**, 367.  
 WRIGHT, A., 1949, *Phys. Rev.*, **76**, 1826.



## Theory of the Superconducting State: II

### Magnetic Properties at the Absolute Zero of Temperature

By H. FRÖHLICH

Department of Theoretical Physics, The University, Liverpool

*MS. received 4th October 1950*

**ABSTRACT.** It has previously been shown by the author that the interaction between free electrons and the lattice vibrational field (if strong enough) leads at the absolute zero to the formation of a new state. The London equations are now derived in the sense conjectured by F. London.

#### § 1.

THE electron theory of metals in the simplest form is based on the assumption that electrons can move freely except for an occasional scattering by the lattice vibrations connected with absorption or emission of a vibrational quantum. It has recently been shown by the author (Fröhlich 1950 a, referred to as I, 1950 b) that this leads to an interaction (the *S*-interaction) between electrons in a similar way as in field theories emission and absorption of quanta is closely correlated to the interaction between sources of the field. It has been found that the interaction between two electrons can be very simply represented in *k*-space ( $\hbar\mathbf{k}$  is the momentum of a free electron): it is repulsive when the difference of the absolute *k*-values of the two electrons is small and attractive otherwise; it becomes negligible when this difference is larger than  $2\sigma$  where  $\sigma = 2ms/\hbar$  ( $s$  = velocity of sound). If  $\sigma \ll k$  the energy range of the *S*-interaction is of the order  $\epsilon\sigma/k$  for electrons of energy  $\epsilon = \hbar^2 k^2/2m$ . If strong enough this interaction leads in the ground state to a distribution (denoted by  $f_1$ ) in *k*-space which differs from a Fermi  $f_0$ -distribution where electrons fill a sphere of radius  $k_0$ . In this  $f_1$ -distribution a shell whose thickness is of the order  $\sigma$  has been removed by a distance of the same order from the surface of the Fermi sphere. In ordinary space this implies that the probability of finding electrons with parallel spin at a distance smaller than  $1/\sigma \simeq 10^{-5}$  cm. is slightly larger than for completely free electrons. Subject to later confirmation this  $f_1$ -distribution has been identified with the superconducting state. It has been shown that a condition concerning the strength of the interaction has to be fulfilled in order to make the new distribution stable. This condition is not satisfied by monovalent metals but holds for most superconductors; also the correct magnitude of the energy difference  $|S|$  from the normal state was obtained. This energy difference  $|S|$  should be inversely proportional to the isotopic mass, as has been confirmed by recent experiments (Maxwell 1950, Reynolds *et al.* 1950). The methods of perturbation theory were used for the calculations; Bardeen (1950, private communication) has now shown that the results can also be obtained with the use of a different method. In the present paper it is shown that the magnetic properties follow in a simple way.

## § 2.

The electromagnetic behaviour of superconductors shows two main striking features: the existence of persistent currents in multiply connected bodies, and the Meissner-Ochsenfeld (1933) effect in simply connected bodies. Both are described in a satisfactory manner by the phenomenological theory of F. and H. London (1935). According to this theory the electric current density  $\mathbf{j}$  can be written as the sum of a normal ( $\mathbf{j}_n$ ) and a superconducting ( $\mathbf{j}_s$ ) component,

$$\mathbf{j} = \mathbf{j}_s + \mathbf{j}_n. \quad \dots\dots(1)$$

The latter component satisfies the London equation

$$d^2 \text{curl} \mathbf{j}_s = -c \mathbf{B}; \quad \mathbf{B} = \text{curl} \mathbf{A}. \quad \dots\dots(2)$$

Here  $\mathbf{B}$  is the magnetic induction and  $\mathbf{A}$  is the vector potential. If the latter is gauged in such a way that its normal component  $A_{\perp}$  vanishes at the surface of the specimen, then  $\mathbf{j}_s = -c\mathbf{A}/d^2$  follows from (2). The length  $d \simeq 10^{-5}$  cm. is denoted as penetration depth because a magnetic field can penetrate into a superconductor only to this depth. A number  $n_s$  per unit volume of superconducting electrons is introduced by the relation

$$d = (mc^2/n_s e^2)^{1/2}. \quad \dots\dots(3)$$

Recently in a most interesting analysis, F. London found that it will be sufficient to prove equation (2) for a simply connected isolated superconductor "in order to obtain the properties of a ring, and presumably also those of an open superconducting wire fed at its ends".

As a conveniently shaped body we choose a long cylinder of radius  $r_0$  with the magnetic field parallel to its axis ( $z$ -direction). Then  $\mathbf{B}$  has a  $z$ -component only, and hence to satisfy  $A_{\perp} = 0$ ,  $\mathbf{A}$  has a  $\phi$ -component  $A(r)$  only ( $\phi$  = azimuth) which depends on the distance  $r$  from the axis but not on  $\phi$  or  $z$ . The electronic states are described by the momentum  $\hbar k_z$  in the  $z$ -direction, the angular momentum  $\hbar\mu$  and a further quantum number  $\nu$ . The electronic wave functions are  $\psi = \sqrt{N} e^{ik_z z} e^{i\mu\phi} J_{|\mu|}(\nu r/r_0)$ , where  $N$  is a normalization factor and  $J_{|\mu|}$  is a Bessel function;  $\mu$  is a positive or negative integer. The density of electrons is

$$n = \sum_{\mu} |\psi|^2, \quad \dots\dots(4)$$

where the sum extends over all occupied states. The  $\phi$ -component of the momentum is the expectation value of the operator  $(\hbar/i r) \partial/\partial\phi = p_{\phi}$ . Following F. London we shall introduce an average momentum field

$$\overline{p_{\phi}} = \frac{1}{n} \sum_{\mu} \psi^* p_{\phi} \psi = \frac{1}{nr} \sum_{\mu} \mu \psi^* \psi. \quad \dots\dots(5)$$

This expression vanishes when positive and negative  $\mu$ -values have equal probability.

We shall now assume that it is permitted to treat the magnetic field as a perturbation given by the operator

$$-\frac{\hbar}{i} \frac{e}{mc} \frac{A(r)}{r} \frac{\partial}{\partial\phi} + \frac{e^2 A^2(r)}{2mc^2}. \quad \dots\dots(6)$$

For a homogeneous magnetic field this requires that the radius of curvature  $\rho$  of most electrons is large compared with  $r_0$  and that  $A(r)/r \rightarrow 0$  as  $r \rightarrow 0$ . In a field



of 600 gauss  $\rho \sim 10^{-2}$  cm. for most electrons, and for weaker fields  $\rho$  is correspondingly larger. The density of the perturbed energy can then be written as the sum of three terms,

$$U = U_D + U_p + U_k, \quad \dots\dots(7)$$

$$\text{where } U_D = \frac{e^2 n}{2mc^2} A^2(r), \quad \dots\dots(8) \quad U_p = -\frac{en}{mc} \bar{p}_\varphi A(r) \quad \dots\dots(9)$$

and  $U_k$  is the change in zero order kinetic energy. In the lowest non-vanishing approximation,  $\bar{p}_\varphi$  is (cf. §4) obtained in terms of a redistribution of occupied levels. This is enforced by the magnetic field so as to make  $U$  a minimum. It is mainly connected with a transfer of electrons from negative to positive  $\mu$ -values. Let  $\Delta z$  be the number of transferred electrons per unit volume. We then expect  $\bar{p}_\varphi$  to be proportional to  $\Delta z$ , and  $U_k \propto (\Delta z)^2$ ; also approximately

$$U_k \simeq \zeta (\Delta z)^2 / n, \quad \dots\dots(10)$$

where  $\zeta$  is the maximum zero order energy of an electron. The redistribution has been studied in detail by Welker (1938), but these details will not be required in the present paper. Since  $U_D$  is nearly independent of  $\Delta z$  we have

$$U = U_D - c_1 \Delta z + \frac{1}{2} c_2 (\Delta z)^2 \quad \dots\dots(11)$$

$$\text{where } c_1 = \frac{en}{mc} A(r) \frac{\bar{p}_\varphi}{\Delta z}. \quad \dots\dots(12)$$

In equilibrium,  $\Delta z = \Delta z_0$ ,  $U = U_0$ , where

$$\Delta z_0 = c_1 / c_2 \quad \dots\dots(13) \quad \text{and} \quad U_0 = U_D - \frac{1}{2} c_1^2 / c_2, \quad \dots\dots(14)$$

are obtained by minimizing  $U$  with respect to  $\Delta z$ . Now for free electrons it is found that  $U_0$  vanishes except for an extremely small term which gives rise to the normal diamagnetic change in energy and which can be neglected here. Then using (14) and (8)  $U_0 = 0$  yields

$$\frac{c_1^2}{2c_2} = U_D, \quad \text{i.e. } c_1 = \left( c_2 \frac{n}{m} \right)^{1/2} \frac{e}{c} A(r). \quad \dots\dots(15)$$

Hence with (15), (12) and (8), we find from (12)

$$\bar{p}_\varphi = \frac{e}{c} A(r) \frac{\Delta z}{\Delta z_0} = \left( \frac{m}{n} c_2 \right)^{1/2} \Delta z. \quad \dots\dots(16)$$

It should be noticed that  $c_2$  is nearly independent of  $r$ .

Since the current density is given by

$$j = \frac{en}{m} \bar{p}_\varphi - \frac{e^2 n}{mc} A(r), \quad \dots\dots(17)$$

$j=0$  follows if  $\Delta z = \Delta z_0$ , as must be expected for free electrons in the present approximation.

It has been stressed by F. London (1948 and earlier papers) that equations (2) and (3) with  $n = n_s$  are obtained from (17) if it can be shown that  $\bar{p}_\varphi = 0$ , i.e.  $\Delta z = 0$ . More generally, however, if only  $\Delta z < \Delta z_0$ , with the use of (16) we have

$$j = -\frac{e^2 n}{mc} \left( 1 - \frac{\Delta z}{\Delta z_0} \right) A(r). \quad \dots\dots(18)$$

Thus if  $\Delta z / \Delta z_0$  is independent of  $r$  we may define the number  $n_s$  of superconducting electrons by

$$n_s = n(1 - \Delta z / \Delta z_0). \quad \dots\dots(19)$$

For free electrons  $\Delta z = \Delta z_0$ , and hence  $n_s = 0$ .

## § 3.

We consider now the influence of  $S$ -interaction on the value of  $\Delta z$ , using perturbation theory. According to I, at the absolute zero of temperature the distribution function  $f_1$  of a superconductor is obtained from a Fermi distribution  $f_0$  by shifting a given small number  $z$  of electrons in a narrow energy range by an energy of equal amount. The energy difference between the two states was denoted by  $|S|$  per unit volume. In this  $f_1$ -distribution  $\bar{p}_\varphi = 0$  as for free electrons. Again the magnetic field tends to make this distribution non-symmetrical in momentum space by a displacement of, say,  $\Delta z$  electrons such that  $\bar{p}_\varphi \neq 0$ , because this leads to a depression of energy according to (9). The  $f_1$ -distribution on the other hand was obtained by displacing  $z$  electrons from the  $f_0$ -distribution, and  $z$  was determined by minimizing the total energy. A further displacement of  $\Delta z$  electrons must, therefore, weaken the  $S$ -interaction energy\* and hence lead to a further positive term in expression (11) for the energy density. Its order of magnitude should be expected to be  $|S|(\Delta z/z)^2$ . This is confirmed by calculations on the energy of some special non-symmetrical states carried out in I, equation (4.2) together† with equation (3.30).

That this expression gives the correct order of magnitude for any sufficiently smooth displacement follows immediately from expressions (3.21), (3.22) also Figure 1 (b)) of I. According to these equations the energy required to shift a single electron by a small energy from the surface of the distribution is larger but of the same order as its increase in zero order (kinetic) energy. The total energy required to shift  $\Delta z$  electrons must therefore be of the same order as  $U_k$ , equation (10). This agrees with the above expression because  $|S| \simeq \zeta z^2/n$  apart from numerical factors.

In order to take account of the change of  $S$ -interaction we must therefore add the above term to expression (11) for the energy density. Thus, since the contributions of the two inner surfaces to  $U_k$  and  $U_p$  cancel,

$$U = U_D - c_1 \Delta z + \frac{1}{2}(c_2 + \alpha_2)(\Delta z)^2 \quad \dots\dots(20)$$

where

$$\alpha_2 \simeq |S|/z^2 \quad \dots\dots(21)$$

and  $c_1$  and  $c_2$  satisfy relation (15). Minimizing  $U$  with respect to  $\Delta z$  one obtains as equilibrium value  $\Delta z_s$  of  $\Delta z$ ,

$$\Delta z_s = c_1/(c_2 + \alpha_2) < \Delta z_0. \quad \dots\dots(22)$$

Hence, using (20), (22), (15) and (8) the equilibrium value  $U_s$  of the energy density is given by

$$U_s = U_D - \frac{1}{2} \frac{c_1^2}{(c_2 + \alpha_2)} = \frac{1}{2} \left( \frac{c_1^2}{c_2} - \frac{c_1^2}{c_2 + \alpha_2} \right) = U_D \frac{\alpha_2}{c_2 + \alpha_2} = \frac{e^2 n}{2mc^2} A^2(r) \frac{\alpha_2}{c_2 + \alpha_2}. \quad \dots\dots(23)$$

Also from (12), (15) and (22) we find for the average momentum field

$$(\bar{p}_\varphi)_s = \frac{c_2}{c_2 + \alpha_2} \frac{eA(r)}{c}. \quad \dots\dots(24)$$

\* This makes use of the fact that  $S$ -interaction and magnetic interaction can be treated as independent perturbations in the case of our model. In this order of approximation the expressions derived in the previous section still hold.

† Only the change in  $S$ -interaction should be considered here; the increase in zero order kinetic energy is already contained in  $U_k$ .



Hence, using (17) the current density becomes

$$j = -\frac{e^2 An}{mc} \left( 1 - \frac{c_2}{c_2 + \alpha_2} \right) = -\frac{e^2 An_s}{mc}, \quad \dots\dots(25)$$

where

$$n_s = n\alpha_2/(c_2 + \alpha_2). \quad \dots\dots(26)$$

Both  $\alpha_2$  and  $c_2$  are independent of  $r$ . We have thus derived the London equations (2) and (3) which follow immediately from (25) by applying the operator curl. From equations (26), (21), (10) and  $U_k = c_2(\Delta z)^2/2$  we obtain

$$\frac{n_s}{n} \simeq \frac{S}{S + \zeta z^2/n}. \quad \dots\dots(27)$$

As mentioned before  $|S|$  and  $\zeta z^2/n$  are of equal order of magnitude.  $n_s/n$  is therefore of the order  $\frac{1}{2}$ , but detailed calculations of  $U_k$  and  $\alpha_2$  would be required to establish the exact value.

It will also be noticed that with (25), (26) and (3) the energy density (23) becomes

$$U_s = \frac{1}{2} d^2 j^2 / c^2 \quad \dots\dots(28)$$

in agreement with the London theory.

There is no need to prove the existence of a critical magnetic field for transition into the normal state, as this follows from the London equations with the thermodynamical method developed by Gorter and Casimir (1934).

Finally it should be remarked that additional terms to  $S$  may perhaps be expected to occur in the energy difference between normal and superconducting states when the radius  $r_0$  of the cylinder is small of the order  $1/\sigma$  or less, for in this case the discrete nature of the electron spectrum may be expected to make itself noticeable. It happens that  $1/\sigma$  is of the same magnitude as the penetration depth  $d$  which may make it difficult to separate the effect of finite penetration from those of additional energies. Also from the preceding derivation it will be seen that small additional terms in (20) do not essentially alter the form of the London equations; they might, however, lead to a weak dependence of  $n_s$  on either  $r$  or field strength.

#### § 4. REMARKS ON THE METHOD

The above calculations where the magnetic field as well as the electron lattice vibration interaction are treated as a perturbation holds only if  $r_0$  is sufficiently small, and if  $A(r)/r$  remains finite as  $r \rightarrow 0$ . The method of minimizing  $U$  requires that  $A(r)$  is a self consistent field due to outside sources as well as due to sources in the metal. For, if  $H_0$  is the density of the Hamiltonian of the outside sources plus that of the unperturbed metal, it is required that the integral

$$\int \left\{ H_0 + U + \frac{1}{8\pi} (\text{curl } A)^2 \right\}$$

over space is a minimum. Minimizing with respect to  $A$  leads to the Maxwell equation  $\text{curl curl } A = 4\pi j$ . Minimizing with respect to  $\Delta z(r)$  leads to  $\partial U / \partial \Delta z = 0$ , which was used to find  $\Delta z$ .

Above, both current density  $j(r)$  and momentum field  $\bar{p}(r)$  were found proportional to  $A(r)$ . As mentioned, these quantities are obtained in this order by redistribution of electrons in momentum space; perturbation of the wave functions would contribute only in higher order. In fact since  $p_{q \ 0p}$  has only diagonal

elements, and since  $\bar{p}_\varphi = 0$ , the first order perturbation of the wave function due to the first term in (6) (proportional to  $A(r)$ ) leads to vanishing contributions to  $\bar{p}_\varphi$  or  $j$ . There is no perturbation at all if  $r_0$  is so small that the magnetic field can be considered as homogeneous. For superconductors the extra energy term  $|S|(\Delta z/z)^2$  is proportional to  $C^2 A^2(r)$ , where  $C$  is the constant measuring the interaction between electrons and the vibrational field (cf. I (2.8)). Here, too, redistribution only yields terms proportional to  $C^2 A$ . It should be re-emphasized that only for superconductors is this term  $|S|(\Delta z/z)^2$  positive. It is negative for normal metals, but smaller than  $U_k$  (otherwise these metals would be superconductors). It might lead to interesting magnetic properties of normal metals at very low temperatures which will be investigated.

For other models, e.g. for a box with boundary condition  $\psi = 0$ , i.e.  $\psi = \sin k_x x \sin k_y y \sin k_z z$ , both  $j$  and  $\bar{p}$  vanish for the unperturbed wave functions. The magnetic energy is then obtained from perturbation only without redistribution (cf. Papapetrou, *Z. Phys.*, 1937, **107**, 387). In this case  $p_{\varphi \text{ op}}$  has only non-diagonal elements. Hence in contrast to the above there are perturbation terms in the wave function proportional to  $A(r)$  leading to the required order in  $j$  and  $\bar{p}$  as well as to a  $A^2(r)C^2$  term in the energy density.

Finally it should be mentioned that for the present method in the case of a cylinder it would not be permissible to gauge  $A$  by, say, adding a constant. For then  $A(r)/r$  would diverge as  $r \rightarrow 0$  and perturbation theory would be excluded. In the case of the box, however,  $A$  may be regauged in this way because a constant  $A$  yields no energy contribution even when perturbation theory is applied; second order perturbation of the linear term then just cancels the first order perturbation of the quadratic term in  $A$ .

#### APPENDIX—NOTES ON PAPER REFERRED TO AS I

Expression (3.16) for  $S_3$  is correct and does not require a further factor  $\frac{1}{2}$  as mistakenly stated in note 2 added in proof. However, a factor 2 is missing on the right-hand side of (2.6) defining  $\sigma$  as was pointed out to the author by Mr. M. J. Buckingham. Hence, factors  $\frac{1}{2}$  are required in equations (2.12)–(2.15), (2.23), (2.24), (3.15). In (3.17) and (6.9) replace  $[P(\xi) - \xi/F(4\nu)^{1/3}]$  by  $2[P(\xi) - 2\xi/F(4\nu)^{1/3}]$ . In inequalities (3.19), (6.7), (6.8) the right-hand side is 2 instead of 1. The influence of these corrections on the results is insignificant. Dr. Schafroth kindly informs me of a misprint in equation (3.22); the argument of the last log term should be multiplied by  $(y - \sigma)/(y + \sigma)$ .

#### REFERENCES

- BARDEEN, J., 1950, *Phys. Rev.*, **80**, 567.  
 FRÖHLICH, H., 1950 a, *Phys. Rev.*, **79**, 845; 1950 b, *Proc. Phys. Soc. A*, **63**, 778.  
 GORTER, C. J., and CASIMIR, H., 1934, *Physica*, **1**, 366.  
 LONDON, F., 1948, *Phys. Rev.*, **74**, 562.  
 LONDON, F., and LONDON, H., 1935, *Physica*, **2**, 341.  
 MAXWELL, E., 1950, *Phys. Rev.*, **78**, 477.  
 MEISSNER, W., and OCHSENFELD, R., 1933, *Naturwissenschaften*, **21**, 787.  
 REYNOLDS, C. A., SERIN, B., WRIGHT, W. H., and NESBITT, L. B., 1950, *Phys. Rev.*, **78**, 487.  
 WELKER, H., 1938, *Bayerischen Akad. Wiss.*, p. 115.



# The Second Order Photoelectric Effect at a Metal Surface

BY R. E. B. MAKINSON \* AND M. J. BUCKINGHAM †

School of Physics, University of Sydney

*Communicated by H. S. W. Massey; MS. received 5th September 1950*

**ABSTRACT.** An expression is derived for the photoelectric current excited at the surface of a metal by radiation of frequency below the threshold frequency of the first order photoelectric effect. A physical interpretation of the formal results is given and the possibility of detecting this current experimentally is briefly discussed.

## § 1. INTRODUCTION

IN discussions of the theory of the photoelectric effect at the surface of a metal the first order approximation alone is normally considered, corresponding to absorption of single quanta by the electrons. For light of usual intensities and of frequencies greater than the threshold frequency, the higher order corrections (corresponding to absorption of two or more quanta) are certainly exceedingly small. When the frequency of the radiation is less than the threshold, however, the first order current is zero (at zero absolute temperature) and if the frequency is greater than half the threshold frequency the second order terms give a current proportional to the square of the radiation intensity.

It is the purpose of this paper to derive a formal expression for this second order current and to estimate its order of magnitude.

These results may be of interest because of the very high intensities now available in pulses from flash tubes, also because the radiation field is here treated classically, so that some check on the conclusions so reached seems desirable either experimentally or from the quantum theory of radiation. The methods of that theory do not seem to have been applied yet to processes of this kind.

The method employed is an extension of earlier work (Makinson 1949) in which a formal expression of some generality was derived for the first order photoelectric current.

## § 2. THE SECOND ORDER CURRENT

### (i) *The Model*

It will be supposed that the conduction electrons are free in the interior of the metal and that near the surface their potential energy may be represented by the potential function  $V(x)$ ,  $x$  being a coordinate normal to the surface. Bardeen has shown that taking account of the exchange energy of the electrons in the metal necessitates the use of different effective potential barriers for each value of electron momentum. Since in the present discussion this generalization merely requires the use of a more complicated notation without altering the essential results, it will be assumed that  $V(x)$  is the same for all electrons.

The wave function  $u$  for a conduction electron in the metal satisfies

$$(\hbar^2/8\pi^2m)\nabla^2u + (i\hbar/2\pi)\partial u/\partial t - V(x)u = 0. \quad \dots\dots(1)$$

For an electron in the state with wave-vector  $\mathbf{k}(k_1, k_2, k_3)$ ,

$$u = u_k = \alpha_k \phi_k(x) \exp(i k_2 y + i k_3 z - 2\pi i E_k t/\hbar), \quad \dots\dots(2)$$

\* At present at Physics Department, University College, London

† At present at Department of Theoretical Physics, University of Liverpool

where  $E_k = \hbar k^2 / \mu - \hbar \nu_a$ ,  $\mu = 8\pi^2 m / h$  and  $\hbar \nu_a = -V(-\infty)$  the height of the surface potential barrier. Then  $\phi_k$  is the solution of

$$\phi_k'' - \{p^2 + (\mu/h)V(x)\}\phi_k = 0 \quad \dots\dots(3)$$

for which

$$\left. \begin{aligned} \phi_k &= \exp(ik_1x) + a_k \exp(-ik_1x), & x \leq 0, \\ &= b_k \exp(-px), & x \geq 0, \end{aligned} \right\} \quad \dots\dots(3a)$$

where  $|a_k| = 1$  and  $p^2 = \mu \nu_a - k_1^2$ . Without loss of generality  $k_1$  is restricted to positive values, and the normalizing factor  $\alpha_k$  is supposed chosen so that in the interior of the metal  $2\sum_k |u_k|^2 = n_0$ , the number of conduction electrons per unit volume.

### (ii) The Perturbed Wave Equation

The steady-state equation (1) is perturbed in the presence of incident light which we describe classically as plane waves with vector and scalar potentials  $\mathbf{A}$  and  $\Phi$  of frequency  $\nu$ , so that

$$\begin{aligned} (h/\mu)\nabla^2 u - (h/2\pi i)\partial u/\partial t - V(x)u \\ = -(i\hbar e/2\pi mc)\{\mathbf{A}\cdot\nabla u + \frac{1}{2}u\nabla\cdot\mathbf{A} + (i\pi e/\hbar c)\mathbf{A}^2 u\} - e\Phi u. \end{aligned} \quad \dots\dots(4)$$

We may take  $\Phi = 0$ , but must retain the term in  $\mathbf{A}^2$ . If  $\vartheta$  is the angle of incidence,

$$\mathbf{A} = \mathcal{A}\mathbf{a}(x) \exp\{-2\pi i\nu(t + y \sin \vartheta/c) + \text{conjugate},$$

where  $\mathcal{A}$  is selected so that  $\mathbf{a}(x)$  is dimensionless and has unit magnitude just outside the surface, and where the  $y$  axis is in the plane of incidence and the plane of the surface.

Let  $u = u_k + v_k + w_k$ , where  $u_k$  is the unperturbed solution (2) and  $v_k$  is the solution of the first order perturbation equation

$$(h/\mu)\nabla^2 v_k - (h/2\pi i)\partial v_k/\partial t - V(x)v_k = -(i\hbar e/2\pi mc)(\mathbf{A}\cdot\nabla u_k + \frac{1}{2}u_k\nabla\cdot\mathbf{A}). \quad \dots\dots(5)$$

The terms in  $\exp\{-2\pi i(E_k - \hbar\nu)t/h\}$  correspond to stimulated emission and do not concern us here, so that, putting

$$v_k = \alpha_k(-4\pi i e/\hbar c)\mathcal{A}\theta_q(x) \exp\{ik_2y + ik_3z - 2\pi i\nu y \sin \vartheta/c - 2\pi i(E_k + \hbar\nu)t/h\} \dots(6)$$

and taking  $\nu$  less than the threshold frequency  $\nu_0$ ,  $\theta_q(x)$  satisfies the equation

$$\theta_q'' - \{r^2 + (\mu/h)V(x)\}\theta_q = a_x\phi_k' + i\phi_k(k_2a_y + k_3a_z) + \frac{1}{2}\phi_k a_x', \quad \dots\dots(7)$$

after neglecting some small terms in  $\nu/c$ , with the boundary conditions

$$\left. \begin{aligned} \theta_q &= C_q e^{-iqx}, & q^2 &= k_1^2 + \mu\nu, & x &\leq 0, \\ \theta_q &= B_r e^{-rx}, & r^2 &= -k_1^2 + \mu(\nu_a - \nu), & x &\geq 0. \end{aligned} \right\} \quad \dots\dots(7a)$$

Since, for  $\nu < \nu_0$ ,  $r$  is real, there is no net outward electron current corresponding to  $\theta_q$ , so the first order photoelectric current under these conditions is zero.

The second order perturbation equation satisfied by  $w_k$  is then

$$\begin{aligned} (h/\mu)\nabla^2 w_k - (h/2\pi i)\partial w_k/\partial t - V(x)w_k \\ = -(i\hbar e/2\pi mc)\{\mathbf{A}\cdot\nabla v_k + \frac{1}{2}v_k\nabla\cdot\mathbf{A} + (i\pi e/\hbar c)\mathbf{A}^2 u_k\}. \end{aligned}$$

Rejecting terms corresponding to stimulated emission and putting

$$w_k = \alpha_k(-4\pi i e/\hbar c)^2 \mathcal{A}^2 \omega_l(x) \exp\{ik_2y + ik_3z - 2\pi i(E_k + 2\hbar\nu)t/h - 4\pi i\nu y \sin \vartheta/c\} \quad \dots\dots(8)$$



we find, on using (6) for  $v_k$ , that  $\omega_l(x)$  is a solution of

$$\omega_l'' + \{s^2 - (\mu/\hbar)V(x)\}\omega_l = a_x\theta_q' + i\theta_q(k_2a_y + k_3a_z) + \frac{1}{2}\theta_qa_x' - \phi_k\mathbf{a}^2/4, \quad \dots\dots(9)$$

where two small terms in  $v/c$  have been neglected\*, and

$$s^2 = k_1^2 + \mu(2\nu - \nu_a), \quad l^2 = k_1^2 + 2\mu\nu.$$

We require the solution of (9) which represents an outward stream of photoelectrons, satisfying the boundary conditions

$$\left. \begin{aligned} \omega_l &= F_l e^{-ilx}, & x \leq 0, \\ &= G_s e^{isx}, & x \geq 0, \end{aligned} \right\} \quad \dots\dots(10)$$

since the right side of (9) vanishes at large distances both inside and outside the surface.

Let  $\chi_l(x)$  be the solution† of

$$\chi_l'' + \{s^2 - (\mu/\hbar)V(x)\}\chi_l = 0,$$

which satisfies the conditions

$$\left. \begin{aligned} \chi_l &= e^{-ilx}, & x \leq 0, \\ &= P_s e^{isx} + Q_s e^{-isx}, & x \geq 0. \end{aligned} \right\} \quad \dots\dots(11)$$

To determine the magnitude of  $G_s$  and thus the photoelectric current of electrons which have absorbed energy  $2\hbar\nu$  from the radiation, we multiply both sides of (9) by  $\chi_l$  and integrate from  $-\infty$  to  $+\infty$ . Then from (10) and (11)  $2isG_sQ_s = L(\mathbf{k}, \nu)$ , where

$$L(\mathbf{k}, \nu) = \int_{-\infty}^{\infty} \{a_x\theta_q' + i\theta_q(k_2a_y + k_3a_z) + \frac{1}{2}\theta_qa_x' - \phi_k\mathbf{a}^2/4\}\chi_l dx. \quad \dots\dots(12)$$

Now the transmission coefficient of the surface barrier  $V(x)$  to the wave  $e^{-isx}$  is  $D(s) = l/(s|Q_s|^2)$  so that

$$|G_s|^2 = D(s)|L(\mathbf{k}, \nu)|^2/(4ls). \quad \dots\dots(13)$$

The photoelectric current density from the surface corresponding to  $w_k$  is given, using (8), (10) and (13), by

$$\begin{aligned} dJ_2 &= (2eh/4\pi mi)(w_k \partial w_k^*/\partial x - w_k^* \partial w_k/\partial x) \\ &= -e|\alpha_k|^2 D(s)(4\pi e^2/\hbar mc^2 l)^2 \mathcal{A}^4(4\pi ml/\hbar) |L(\mathbf{k}, \nu)|^2. \quad \dots\dots(14) \end{aligned}$$

The expression (14) represents the contribution to the current density arising from the electrons from the state  $\phi_k$  and the total second order current is then this expression summed over all the occupied states of the free electron gas in the metal.

### § 3. DISCUSSION

#### (i) Physical Interpretations

In the integrand in (12) the first three terms involve the wave function  $\theta_q$  describing an intermediate singly excited state, whereas the last term does not. We may regard the latter (arising from the term in  $\mathbf{A}^2$  in the perturbation equation (4)) as corresponding to double excitation directly.

\* The corresponding terms neglected in (7) do not affect the second order approximation, since their contribution to the current vanishes when the first order current vanishes.

† This procedure is the same as that used by Makinson (1949), cf. Mott and Massey (1949, p. 107). It is not applicable here unless the first order current is zero.

In the interaction of an electromagnetic field with a charged particle, the corresponding  $\mathbf{A}^2$  term leads in classical mechanics to a second harmonic term in the motion of the particle. The condition that one may neglect the term in  $\mathbf{A}^2$  in calculation of the classical motion of the particle (as one neglects it in quantum-particle *cum* classical-field calculations of the first order photoelectric current) is that the second harmonic term in the motion shall be much less than that with fundamental frequency. This condition may be written  $eA/c \ll mc$ , i.e. that the maximum velocity acquired in one period is very much less than  $c$ . Thus relativistic equations would be necessary in classical mechanics for sufficiently large  $A$ . However, in the present treatment the same limit would appear in the failure of the perturbation method. Since we are only concerned here with second order current under conditions where much greater first order currents are absent simply because the frequency lies below their threshold, the non-relativistic perturbation theory we have used should be adequate.

Inspection of (7) and (12) indicates that neglect of the term in  $\mathbf{a}^2$  will not greatly alter the value of  $|L|^2$ . The remaining part of  $L$  can be expressed approximately in terms of first-order excitation functions (Makinson 1949) corresponding to two transitions each involving absorption of a single quantum. Writing  $M(k, \nu)$  for the excitation integral

$$\int_{-\infty}^{\infty} \{a_x \phi_k' + i \phi_k (k_2 a_y + k_3 a_z) + \frac{1}{2} \phi_k a_x'\} \chi_q dx,$$

where  $\chi_q$  satisfies  $\chi_q'' - \{r^2 + (\mu/\hbar)V(x)\}\chi_q = 0$ ,

$$\begin{aligned} \chi_q &= e^{iqx} + h_x e^{-iqx}, & x \leq 0, \\ &= g_x e^{-rx} & x \geq 0, \end{aligned}$$

it can easily be shown, by the method used for determining  $G_s$  in (10), that in (7a)  $2iqC_q = M(k, \nu)$ . Denote by  $\phi_q$  the solution of (3) when  $r^2$  replaces  $p^2$  so that  $q$  replaces  $k_1$  in (3a); this is what the wave function would be for a conduction electron in the metal of energy equal to that of a singly excited electron. Let  $M(q, \nu)$  now denote the integral corresponding to  $M(k, \nu)$  when  $\phi_q$  replaces  $\phi_k$  and  $\chi_l$  replaces  $\chi_q$ .

Comparing the forms of  $\theta_q$  and  $C_q \phi_q$  in  $x \leq 0$  and noting that they do not in general vary violently in magnitude near the surface, we may assert that in computing  $L(\mathbf{k}, \nu)$  we shall arrive at a result of similar magnitude if we replace  $\theta_q$  in (12) by  $C_q \phi_q$ .

Thus  $|L(\mathbf{k}, \nu)| \sim |C_q| \cdot |M(q, \nu)|$  and therefore

$$|L(\mathbf{k}, \nu)| \sim |M(k, \nu)| \cdot |M(q, \nu)| / (2q). \quad \dots\dots(15)$$

Introducing an excitation function  $E(k, \nu) = (\pi e^2 / \hbar m c^2 q) \mathcal{A}^2 |M(k, \nu)|^2$ , we may write as an approximation for the expression (14) for the current density of doubly excited electrons:

$$dJ_2 \sim -e \cdot 4 |\alpha_k|^2 \cdot D(s) \cdot E(k, \nu) E(q, \nu) \cdot 4\pi m / (\hbar q). \quad \dots\dots(16)$$

This may be compared with the corresponding expression for the first order current (Makinson 1949),

$$dJ_1 = -e \cdot 4 |\alpha_k|^2 \cdot D(r) \cdot E(k, \nu). \quad \dots\dots(17)$$

Equation (16) thus describes an excitation from the unperturbed state  $\phi_k$  to the state  $\phi_q$  (with absorption of a quantum  $\hbar\nu$ ) followed by a further excitation



to the state  $\omega_l$  and transmission through the barrier. The rate at which the second excitation occurs should be proportional to the density of singly excited electrons near the surface, which is inversely proportional to their speed ( $h\mathbf{q}/(2\pi m)$  inside the barrier), and such a factor is found in (16).

### (ii) Orders of Magnitude

The order of magnitude of the second order current may be roughly estimated as follows. Let  $dJ_2(\nu)$  be the contribution to it arising from electrons with some particular wave vector  $\mathbf{k}$  in the metal, where  $\nu < \nu_0 < 2\nu$ . Let  $dJ_1(2\nu)$  be the first order current which would arise from the same electrons from light of frequency  $2\nu$  but of the same intensity  $R$  erg cm<sup>-2</sup> sec<sup>-1</sup>. From (14), (15) and (17)

$$\frac{dJ_2(\nu)}{dJ_1(2\nu)} \sim \left( \frac{2\pi e}{hcq} \right)^2 \frac{(c/2\pi\nu^2)^2 R^2}{(c/8\pi\nu^2)R} F^2,$$

where  $F$  stands for the dimensionless quantity  $|M(\mathbf{k}, \nu)| \cdot |M(\mathbf{q}, \nu)| / |M(\mathbf{k}, 2\nu)|$  which is of order unity. Thus

$$dJ_2(\nu)/dJ_1(2\nu) \sim 8\pi e^2 R / (ch^2 q^2 \nu^2) \sim 10^{-20} R$$

when values appropriate to sodium have been used. Taking the whole current densities  $J_2(\nu)$  and  $J_1(2\nu)$  as being in the same ratio, and the first order yield of sodium as  $10^{-3}$  amperes per watt, the 'second order yield' of sodium is given roughly as  $10^{-16}$  amperes per cm<sup>2</sup> per (watt cm<sup>-2</sup>)<sup>2</sup>.

The possibility of measuring such a yield depends on the availability of (i) a sufficient intensity of light, (ii) a light filter sufficiently selective to reduce the first order yield from frequencies above  $\nu_0$  to a magnitude below that of the anticipated second order yield. Flash tubes of the gas discharge type are stated to give a peak output of about  $10^6$  watts in the visible spectrum and we may suppose (in the absence of detailed measurements) that half of this lies on either side of  $\nu_0$  and that 2% of the low frequency output can be focused on the cathode (1 cm<sup>2</sup> in area) of a photomultiplier tube via the filter. The latter is then required to reduce the intensity of light of frequency above  $\nu_0$  to less than  $10^{-9}$  times that of light below  $\nu_0$ . If this very severe filtering requirement (which would be more severe for lower intensities) can be met, then second order currents from the cathode of approximately  $10^{-8}$  amperes are anticipated. This corresponds to the emission of about  $10^5$  electrons per flash of two microseconds duration.

The second-order current should thus be easily detectable in a photomultiplier tube with suitable threshold frequency. If the cathode is free of small patches of much lower work function, the whole difficulty lies in adequate filtration of the light source without too much reduction in intensity of the wanted band.

### ACKNOWLEDGMENTS

The authors wish to express their thanks to Mr. V. C. Officer of the School of Physics, University of Melbourne, whose interest in the experimental aspects of the problem led to this investigation. One of us (M. J. B.) was the holder of a Commonwealth Research Studentship while engaged on this work.

### REFERENCES

- MAKINSON, R. E. B., 1949, *Phys. Rev.*, **75**, 1908.  
MOTT, F., and MASSEY, H. S. W., 1949, *The Theory of Atomic Collisions* (Oxford: Clarendon Press).

## On the Theory of Plastic Deformation

By DORIS KUHLMANN \*

H. H. Wills Physical Laboratory, University of Bristol

*MS. received 7th October 1949, and in amended form 13th March 1950.*

**ABSTRACT.** A model for plastic deformation in soft metals, i.e. metals which are not age-hardened or severely cold-worked, is given. It is based on the assumption that in real crystals there is always a number of regions present which, by an unknown process, act as sources of dislocations. Furthermore, it is assumed that in soft metals dislocations are very mobile except in a limited number of regions which act as obstacles. The model is applied to explain a number of facts connected with plastic deformation.

### § 1. THE ASSUMPTIONS

IN the course of an experimental investigation of the plastic deformation of copper at stresses below the yield point (Kuhlmann and Masing 1948), the following model of the mechanism of creep, involving two assumptions, was adopted and subsequently developed in greater detail.

The first assumption is that in every crystal of a plastic material there is always a number of regions which act as sources of dislocations of one type and one sign only, probably dislocations in which the edge component is dominant and the screw component plays a small rôle only.†

Each source may be characterized by the limiting stress necessary to put it into action, which will be quite low for the most active sources. The process by which the dislocations are released is obscure. Possibly one has to think of some kind of notch effect, but it is doubtful whether this alone is a sufficient explanation.

Frank (1948) recently proposed a reflection mechanism for dislocations, involving edge and screw dislocations of both signs, which would explain the creation of dislocations, the formation of slip bands and the sudden extension on applying a stress to a metal. The model considered here, whilst not in conflict with this theory, will be applicable at stresses too low to cause reflection, and also probably to metals in which Frank's process has come to an end, i.e. after some degree of cold work.

The second assumption is that on each active glide plane there are several times as many obstacles hindering the movement of the dislocations as there are sources, and that the stress required to move the dislocations through these obstacles is higher than that required for their creation.

If the metal is not age-hardened or severely cold-worked, the potential energy of one dislocation on an average glide plane  $P_d$  may then have the form sketched schematically in Figure 1(a). Mott and Nabarro, on the other hand, worked out the theory of plastic deformation in severely disturbed crystal lattices such as are probably present in precipitation hardened alloys. The potential energy  $P_d$  is then as drawn in Figure 1(b). In fact there will be a continuous gradation between the two extremes. In the present paper, however, only the case of Figure 1(a) is treated.

\* Now Mrs. Wilsdorf, N.P.L., P.O. Box 395, Pretoria, South Africa.

† For the elastic theory of dislocations see, for example, Cottrell (1949).

While it has not yet been possible to give a satisfactory theoretical explanation for the first assumption, the second one seems to be well justified, as we know that in real crystals there are, or can be, inclusions, precipitates, internal stresses, dislocations on other glide planes crossing the one considered, grain boundaries, mosaic and polygonization boundaries and layers (for example oxide) on internal or external surfaces, all of which are obstacles against the movement of dislocations. Most of these obstacles act symmetrically, that is, the magnitude of the stress necessary to make the dislocations pass them is independent of the side from which they are approaching. This property of symmetrical action is of great importance in connection with after-effects and fatigue.

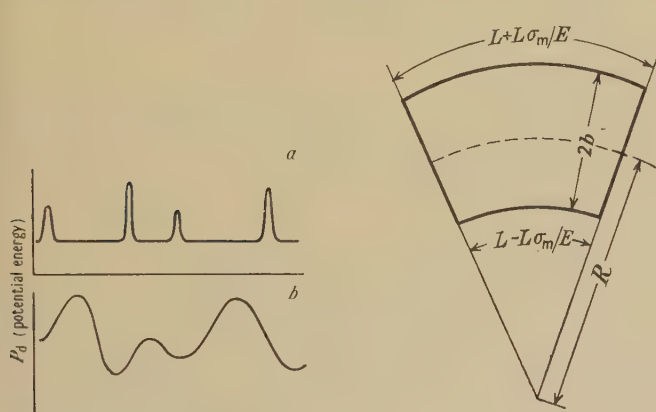


Figure 1. Potential energy of a dislocation as a function of its position: (a) in a soft metal; (b) in a cold-worked or age-hardened metal.

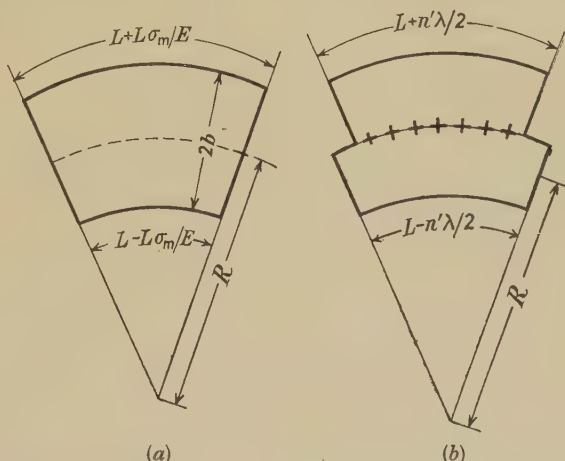


Figure 2. (a) Elastically bent slab; (b) slab in which the same radius of curvature is established by the presence of a row of dislocations.

## § 2. THREE CONSEQUENCES OF THE ASSUMPTIONS AND ELASTIC THEORY

(i) According to the modern theory of dislocations (cf. Cottrell 1949) two like dislocations distant  $d$  apart on the same glide plane each produce a shear stress  $\tau = A/d$  at the centre of the other. Here  $A = G\lambda/2\pi(1-\mu)$ , where  $G$  is the shear modulus,  $\lambda$  is the atomic spacing in the glide plane measured in the glide direction, and  $\mu$  is Poisson's ratio. These stresses produce a force  $\tau\lambda$  on each dislocation, tending to drive them apart. If one of them is fixed, an applied shear  $\tau = A/d$  is thus necessary to keep them at a distance  $d$  from one another. Therefore we expect that by the action of the shear stress  $\tau$ ,  $n$  dislocations can be piled up between two obstacles separated from each other by a distance  $l$ , where  $n$  is given approximately by  $n \sim l\tau/A$ .

The exact evaluation of  $n$  is difficult and has not yet been solved completely. With the assumptions that the first dislocation is held by an obstacle which does not exert any forces on the following dislocations, that there is a repulsive shear stress  $A/d$  between two dislocations tending to repel them, and that the external shear stress  $\tau$  acts on each dislocation, Heilbronn (private communication) found  $n > D\tau/2A$ , where  $D$  is the distance between the first and the last dislocation.  $n \sim D\tau/2A$  is a good approximation for large  $n$ . Nabarro (1950) found the upper limit  $n < 1 + D\tau/A$ .



Thus so far there is uncertainty about the exact value of the number of dislocations  $N$  which can be piled up on a glide plane of length  $L$ ; but at least for large  $N$  there is a linear connection between  $L$  and  $N$ , and in the following we shall use Heilbronn's approximate formula and set  $N = L\tau/2A$ .

(ii) The dislocations in each slip band are considered to have originated from one source and, therefore, are of one type and one sign only, for instance, positive edge dislocations. The bending stress set up by these dislocations will be partly relieved if the neighbouring slip bands contain like dislocations, but not if—in our example—they contain negative edge dislocations. Therefore there is a high probability that a slip band which develops between two adjacent slip bands with like dislocations will contain the same sort of dislocations as its neighbours. Thus we expect whole packets of slip bands with one sort of dislocation only, as was observed by Nye (1949).

(iii) Cottrell (1949) has shown that when  $n$  dislocations are piled up behind an obstacle under an applied shear stress  $\tau$ , their pressure “produces a high local stress in the vicinity of the obstacle of  $n$  times the external stress”. In our model this stress will, in equilibrium, be  $l\tau^2/2A$ .

### § 3. THE MOVEMENT OF THE DISLOCATIONS

The dislocations, which according to the assumptions of the first section are formed on a single atomic plane or on a few very closely spaced planes, will move one after the other along their glide planes until the first one from each course is held up by an obstacle. The subsequent dislocations will now distribute themselves behind the first ones in a way determined by the resolved shear stress and their mutual repulsive interaction. If the shear stress or the number of piled-up dislocations is sufficiently large, the first dislocation will pass the obstacle and leave the part of the glide plane under consideration, either moving on to the next obstacle or, if there are no more obstacles, leaving the glide plane altogether through the surface of the metal. After the first dislocation has surmounted the obstacle, the following ones will move up in the ‘queue’, and as a consequence another dislocation will leave the source; the next dislocation will then pass the obstacle, and so on until either the second free region of the glide plane is filled up and the process stops, or the first dislocation passes the second obstacle and moves on to the third one.

Obviously the number of obstacles in comparison with the number of sources in action, the mean distance between the obstacles, and their opacity will depend on the state of the material and can change during plastic deformation. These differences will give rise to the observed differences in the mechanical properties.

### § 4. THE $\Delta G$ -EFFECT

Before discussing the model in greater detail, we must deal with a special aspect of it. Masing (1944, 1948) has pointed out that every model of plastic deformation which involves the presence of an appreciable number of dislocations in the material will lead to an apparent modulus of rigidity which is lower than that for an ideal crystal. In our case, under a given stress there will be a certain number of dislocations in each slip band, divided into groups by the obstacles. On relieving or reversing the stress there will be a rearrangement of the dislocations within each group, but there will be no appreciable interchange between the groups if the obstacles are symmetrical in the sense of § 1, unless the real resolved shear stress is nearly equal and opposite to that which was required to move them into

the glide plane. The rearrangement of the dislocations, however, will cause a reversible deformation in addition to the elastic strain.

If the stress is reduced from  $\tau$  to zero the dislocations will rearrange and on the average move by  $ql$ , where  $q$  is a pure number which must be less than  $\frac{1}{2}$ . The additional shear strain caused by this rearrangement will be  $\Delta\gamma = (N/W)(ql/L)$ , where  $W$  is the average distance between neighbouring slip bands normal to the glide plane and the other symbols have the same meaning as in § 2. Let the observed modulus of rigidity be denoted by  $G'$ , the elastic shear strain by  $\gamma$ ; we find

$$G' = \frac{\tau}{\gamma + \Delta\gamma} = \frac{G}{1 + \Delta\gamma/\gamma}.$$

Thus

$$\frac{\Delta\gamma}{\gamma} = \frac{G - G'}{G'} = \frac{G N q l \lambda}{\tau W L},$$

and with the relation  $N = L\tau/2A$  of § 2,  $\Delta\gamma/\gamma = lq\pi(1 - \mu)/W \lesssim 1.2l/W$ .

Changes of several per cent in the modulus of rigidity or Young's modulus after cold work, or abnormally low values of these quantities by factors as large as or greater than two, have been observed repeatedly (see for example Kawai 1930, Laurent and Eudier 1949, Crussard 1945, Maddin, Mathewson and Hibbard 1948, Raffelsieper 1950), and there is no obvious disagreement between the above formula and experiment. On the other hand, detailed experimental investigation of the  $\Delta G$ -effect could give very valuable information about the magnitude of  $l$  and its dependence on degree of cold work, grain size and so on.

As a rough estimate of the maximum number of dislocations which can be piled up in each interval we may take the ratio of theoretical yield stress to the true breaking stress at low temperatures, provided failure does not occur by cleavage. Until more information is available it therefore seems reasonable to think of values for  $n$  from 1 to 10 or 20, but hardly higher.

## § 5. FACTS WHICH MUST BE EXPLAINED BY A THEORY OF PLASTIC DEFORMATION

A theory of plastic deformation should explain, or at least not contradict, the main facts connected with slip. They are: (i) the behaviour of slip bands; (ii) the stress-strain curve and its dependence on grain size and temperature; (iii) the creep curve under constant stress; (iv) the great influence which thin surface layers can have on the creep properties of single crystals; (v) the lattice bendings, which often develop in the course of plastic deformation and which manifest themselves in asterism, deformation bands and kinks; (vi) Bauschinger effect, after-effects and recovery.

It is thought that the two assumptions of § 1, together with their three consequences, which led to the model of the movement of the dislocations described in § 3, are in qualitative or quantitative agreement with these facts. In the following sections we shall try to justify this.

## § 6. SLIP BANDS

The existence of slip bands follows at once from the first assumption, but their fine structure, which was discovered by Heidenreich and Shockley (1947, 1948), apparently cannot be explained on the basis of this model alone.

The fact that slip bands often start and end within the crystal suggests that the sources need not necessarily lie at the surface of the specimen or the grain boundaries, but may lie within the crystals.

It is difficult to think of a way in which internal sources of dislocations of one type and sign only can act without producing fine cracks, but such cracks would probably be filled up to a certain extent by slip in the neighbouring parts of the metal. This difficulty would be removed if we assumed that the sources release pairs of dislocations or dislocation loops. The assumption, however, that only such sources exist, or that they are in the great majority, at present seems to lead to several other difficulties, and we shall therefore not consider it. We shall continue to consider sources of dislocations of one type and one sign only, and believe that this is no great restriction because the other type of sources can be regarded as pairs of sources of opposite sign next to each other.

The number of active sources, and hence of slip bands, at a given *stress* in this model will, if it depends on the temperature at all, increase slowly with increasing temperature, because if there is an energy of activation involved in the starting of a slip band at all it is assumed to be small. The energy of activation necessary to move the dislocations through the obstacles, on the other hand, is assumed to be larger than the former, and therefore the number of dislocations which leave an average source at a given *stress* within a given time will increase more rapidly with increasing temperature than the number of active sources. The strain due to the dislocations of one slip band increases proportionally to their number and the length of the slip band. Thus while with increasing temperature the number of slip bands for a given *stress* will slowly increase, for a given *strain* it will decrease. This is in agreement with the result of Yamaguchi and Togino (1929) for aluminium single crystals.

It is thought, however, that the spacing of the slip bands and the fact that they tend to be arranged regularly (Kuhlmann 1950) is not a consequence of the number and distribution of the sources alone, but that some sort of stress mechanism and/or an energy principle, as proposed by Orowan (1941) and Bragg (1942, 1948), is acting. Thus, especially at stresses well beyond the yield stress, the number of sources whose threshold stress is smaller than, or equal to, the applied stress is presumably much higher than the number of slip bands.

The following energy consideration may be useful in this connection: the elastic energy of a sheet of metal which is bent elastically to a given radius of curvature is higher than that of a similar sheet in which the same curvature is produced by a row of parallel edge dislocations lying in the neutral plane when its thickness exceeds a certain value. This may be seen as follows: Let the thickness of the slab be  $2b$ , its length in the glide direction  $L$ , and its width one atomic distance (Figure 2). The elastic energy of the slab is (Figure 2(a))  $U_{el} = L\lambda\sigma_m^2 b/3E$  if  $\pm\sigma_m$  is the stress at its upper and lower surface. The number of dislocations which will produce the same radius of curvature (Figure 2(b)) is  $n' = 2L\sigma_m/E\lambda$  and their energy  $U_d = n'P$ , where  $P$ , the energy of one dislocation per atomic plane, is a few electron volts (Koehler 1941). For a given stress  $\sigma_m$  the energy of the slab with the dislocations will be smaller than that of the elastically bent slab if  $U_d < U_{el}$ , so that

$$L\lambda\sigma_m^2 b/3E > 2L\sigma_m P/E\lambda \quad \text{or} \quad b > 6P/\lambda^2\sigma_m.$$

For  $\sigma_m = 3 \text{ kg/mm}^2$  and  $P = 3 \text{ ev}$ .  $b$  is then greater than about  $10^{-4} \text{ cm.}$ , while for aluminium single crystals at a resolved shear stress of  $3 \text{ kg/mm}^2$  Yamaguchi (1928) found that the thickness of the lamellae between the slip bands was about  $2 \times 10^{-4} \text{ cm.}$  Moreover, Yamaguchi found a linear increase of the density of slip bands with increasing shear stress, while the present calculation entails a



proportionality between  $1/b$  and  $\sigma_m$ ; and finally the conception that bending stresses play an important rôle in plastic deformation seems to be sound because, as has already been mentioned in § 2, and will be discussed in § 9, the dislocations themselves set up bending stresses.

Thus it is very tempting to pursue this idea, which may possibly lead to a theoretical explanation of the sources of dislocations, but it needs some modification and, therefore, so far, is to be regarded as a suggestion only.

## § 7. THE STRESS-STRAIN CURVE

### (i) Yield Stress

The magnitude of the yield stress for unstrained metals in this model is governed by the number of obstacles and their opacity. In agreement with generally adopted ideas on the structure of real crystals, we assume that either or both increase sharply with decreasing grain size and crystal perfection.

Let us follow the ideas of Orowan (1934a) and take the yield stress,  $\tau_y$ , as that stress under which the dislocations start to pass the first obstacles at such a rate that the velocity of deformation equals the testing velocity. The formula derived by Becker (1925) may be applied here :

$$W = K \exp\{-V(\tau_R - \tau)^2/2GkT\}$$

It gives the probability that within the volume  $V$  the applied stress  $\tau$  is increased to  $\tau_R$  by thermal activation.  $K$  is a constant,  $k$  and  $T$  have the usual meanings, and  $G$  is, as before, the modulus of rigidity. Thus if it is necessary for the stress  $\tau_R$  to act within the volume  $V$  for a dislocation to pass through an average obstacle, where in most cases  $\tau_R$  will be much smaller than the theoretical yield stress, the probability that this will happen under the applied stress  $\tau$  is given by Becker's formula. Therefore the yield stress will be reached when  $W$  assumes a certain value, say  $W_0$ , and we get

$$\ln\left(\frac{W_0}{K}\right) = -p = -\frac{V(\tau_R - \tau_y)^2}{2GkT}.$$

In § 2 it has been pointed out that the stress in the vicinity of an obstacle behind which  $n$  dislocations are piled up is  $n\tau$ , and if  $l$  is taken not only as a measure for the average distance between two successive obstacles but also for that between the sources and the first obstacles, we have  $n\tau = l\tau^2/2A$ . This leads to the equation

$$p = \frac{V}{2GkT} \left( \dot{\tau}_R - \frac{l}{2A} \tau_y^2 \right)^2, \text{ so that } \tau_y^2 = \frac{2A}{l} \{ \tau_R - (2GkTp/V)^{1/2} \},$$

or, if we set  $(2A\tau_R/l)^{1/2} = \tau_0$ ,  $V\tau_R^2/2G = U_0$ , and  $U_0/kp = T_s$ , we have  $\tau_y = \tau_0 \{ 1 - (T/T_s)^{1/2} \}^{1/2}$ . This formula is in qualitative agreement with experiment, because with decreasing grain size and crystal perfection  $l$  will decrease and  $\tau_R$  increase and, therefore, both  $\tau_0$  and  $T_s$  will increase with decreasing grain size.  $T_s$  is the temperature at which, in our equation, the yield stress becomes zero, but it is not the melting point, although it will be near to it. This is obvious from the fact that  $T_s$  depends on  $p$  and therefore on the testing velocity. With decreasing testing velocity  $p$  decreases slowly and hence  $T_s$  increases.

As we have taken all constants to be independent of temperature, which certainly is incorrect for  $G$ , and possibly for  $V$  and  $\tau_R$ , the above formula will only be a first approximation. Another complication arises at high temperatures because, as Orowan (1935) has pointed out, Becker's formula is not valid for very low stresses.

There a second term, of the form  $K \exp \{ -V(\tau_R + \tau)^2 / 2GkT \}$ , which takes account of the stress fluctuations in the unfavourable direction, and which cannot be neglected. On this basis Kochendörfer (1941) explained the striking result of Schmid and his co-workers (1926, 1929, 1930) that near the melting point the yield stress of single crystals of cadmium, bismuth, zinc and magnesium remained constant, or even increased, with increasing temperature. In view of the strong influence which surface layers may have on the plastic properties of single crystals, however, we think that this effect was probably due to oxide layers, especially as at that time the effect which surface layers may have was not known, and, therefore, apparently no precautions against oxidation were taken.

In Figure 3 the above-mentioned results of Schmid and his co-workers have

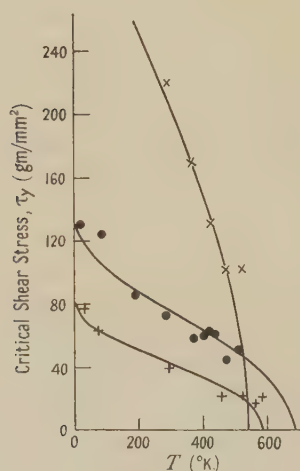


Figure 3. Experimental points for bismuth (x), zinc (•) and cadmium (+) are from Schmid and co-workers (1926, 1929, 1930). The curves represent  $\tau_y = \tau_0 \{ 1 - (T/T_s)^{1/2} \}^{1/2}$ , where  $T_s$  in all cases is taken as the melting point.

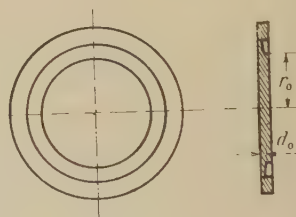


Figure 4. Plan and cross section of specimen as used in the creep experiment by Andrade (1949). If the thickness of the annulus is  $d$  at a distance  $r$  from the axis, then  $d/d_0 = r_0^2/r^2$ .

been used to test our equation for  $\tau_y(T)$ . The curves are calculated with  $T_s$  equal to the melting temperature, although a better fit can be obtained if  $T_s$  is chosen freely.

For very soft materials and low speeds of deformation the critical shear stress is often taken as the stress which produces the first detectable deformation. Here another consideration may be useful. Until now we have calculated as though the first dislocations would move right up to the obstacles even under very low stresses, but in fact some types of obstacles—as for instance an oxide layer—will give rise to an image force which in the most extreme case could have the same effect as if the dislocations which approach them were repelled by their mirror image with respect to the oxide layer. In §2 we mentioned that two like dislocations on the same glide plane repel each other with a force  $\lambda\tau = \lambda A/d$ ; hence no dislocations at all can leave the sources at stresses below  $\tau = A/2l$ . With the experimental value  $\tau_y \approx 5 \text{ gm/mm}^2$  for the softest single crystals we find from this formula  $l \geq G\lambda/4\pi(1-\mu)\tau_y \approx 3 \times 10^{-3} \text{ cm}$ . This is a reasonable value, but because of our ignorance of the nature of the sources and the image force of the obstacles the above consideration may only be regarded as a qualitative suggestion.

(ii) *Work Hardening*

For single crystals of cadmium at low strain rates Andrade and Roscoe (1937) observed a linear law of work hardening and found that the number of slip bands was independent of strain. Therefore they suggested that the law of work hardening for each individual slip band is linear, and pointed out that this, together with the result of Yamaguchi (1928) that in aluminium single crystals the number of slip bands increases linearly with the shear stress, would also explain the parabolic law of work hardening in aluminium.

The mutual interaction of the dislocations in the slip bands leads to such a linear law of work hardening because, as was stated in §2, the equilibrium number of dislocations in each individual slip band is  $N = L\tau/2A$ . The strain produced by them is  $\gamma = \frac{1}{2}N\lambda/W = L\lambda\tau/4AW$ , i.e. increases linearly with stress, as soon as the length of the slip bands  $L$  has reached its final value. The hardening coefficient is then  $h = \partial\tau/\partial\gamma = 4AW/\lambda L$ , where  $W$ , as before, is the average distance between two successive slip bands normal to the glide plane and is assumed to be constant. However, this cannot in general be the only cause of work hardening, though it may be so in favourable circumstances. The fact that the stress in single crystals can increase to five times the yield stress or more, and the marked temperature dependence of the work hardening coefficient at low temperatures, especially in hexagonal single crystals, show this. Therefore we must look for other reasons for work hardening and, apart from the trivial redistribution of stress during deformation (stress hardening = Spannungsverfestigung), in our model these can only be an increase in number and height of the obstacles which we shall call 'real' work hardening. Among the kinds of obstacles mentioned in §1 only slip bands of other glide systems, internal stresses and mosaic, polygonization and grain boundaries can increase in number or opacity, or both, during plastic deformation, and we cannot believe that this increase is in general very strongly dependent on the temperature. But there is another obstacle we have not yet mentioned which was first introduced by G. I. Taylor (1934): the mutual interaction of dislocations in neighbouring slip bands of the same glide system, especially when they are unlike and, therefore, move in different directions. It is thought that this interaction may play an important rôle at low temperatures, but the second consequence in §2 should be borne in mind. In the present paper we shall not attempt to investigate the matter in detail however, and shall only discuss it briefly later.

#### §8. THE NORMAL CREEP CURVE AND THE INFLUENCE OF SURFACE LAYERS ON THE CREEP RATE

The normal creep curve under constant stress consists of three parts—the sudden extension, the transient creep and the steady creep (Andrade 1910, 1914).

A sudden extension due to the movement of the dislocations from the sources to the first obstacles on each active glide plane is to be expected, but this explanation can only be valid for sudden extensions below a shear of at most one-tenth of one per cent. However, the sudden extension at higher stresses may rise to much greater values because some rapid creep in the most efficient slip bands, which is completed almost immediately after the application of the load, will be indistinguishable from the sudden extension as defined above.

The transient creep is due to the gradual decrease of the creep rate as the slip bands are being filled up with dislocations and as 'real' work hardening goes on. Where mosaic boundaries are the dominant obstacles the real work hardening will



arise as follows: Before the deformation these boundaries will have positions such that the blocks fit between their neighbours as well as possible; the passage of dislocations through a boundary will shift the part above and below the glide plane relative to the lattice into a necessarily less favourable position, and consequently the energy of activation for the passage of dislocations will rise, at least for the first few.

In a single crystal the glide plane extends through the whole specimen and the dislocations will finally leave the specimen through the surface. For polycrystalline material the situation is rather more complicated, as the glide planes end at the crystal boundaries. The dislocations, when leaving the grains, create steps in their surfaces, to which the neighbouring grains set up an increasing resistance, and either the creep comes to an end for this reason or, if the applied stress is sufficient, equilibrium may be reached by the initiation of a suitable complex slip in the neighbouring grains. As before, the dislocations can ultimately leave the specimen only through the surface. Thus steady creep means that a dynamic equilibrium is reached in which as many dislocations leave the specimen through its surface as are formed. Naturally the rate of steady creep will be determined by the number and opacity of the dominant obstacles.

If the external stress is too small to force the dislocations through the highest obstacles, or if for geometric or other reasons the dislocations cannot leave the specimen, no steady creep will occur. The latter case is illustrated in a recent experiment by Andrade and his co-workers (1949)\*:

"A polycrystalline metal wire loaded by a device that keeps the longitudinal stress constant shows, in a suitable temperature range, a sudden extension, followed by a creep that can be divided into a transient component and a permanent or quasi-viscous component. Experiments have been carried out on creep under a different system of stressing. The metal is in the form of a circular disc in which is cut a deep coaxial groove, so that a thin annulus of metal separates an inner and an outer part of the thick disc. In the stressing apparatus the outer part of the disc is firmly held, while a constant torque is applied to the inner part of the disc, which is gripped between metal plates. The cut face of the annulus is subjected to a uniform shear. [See Figure 4 of the present paper.]

"Under these conditions, when the surfaces through which the stress is applied are not free, the law of flow with the two metals so far tested, lead and cadmium, are modified. There is a transient component obeying the Andrade  $t^{1/3}$  law, but the permanent or quasi-viscous flow does not take place."

The explanation of this result on the basis of our model is straightforward. Under the conditions described the dislocations will on the average travel everywhere parallel to the surfaces and, therefore, cannot leave the specimen, and hence no steady creep can occur.

Andrade and Randall (1948) discovered that the creep rate of a cadmium crystal suddenly changes if the crystal is immersed in certain electrolytes. Andrade (1949), Phillips (1949) and Hall (private communication) independently proved that the effect is due to a surface layer, probably of oxide, which dissolves or thickens in the electrolyte. If the surface layer is removed by electrolytic polishing the creep rate can no longer be increased by immersing in an electrolyte. The layers concerned in considerably lowering the creep rate are much too thin for it to be possible to explain the effect by their mechanical strength. According to the model of creep

\* I am indebted to Professor E. N. da C. Andrade for this description of his experiment.

presented here, the explanation is that in these very soft single crystals the surface layer is the dominant obstacle, so that when it is removed the creep rate increases because now the less efficient obstacles become dominant. In agreement with this explanation the effect is absent in polycrystalline material. There the grain boundaries are the obstacles which govern the creep rate.

### § 9. ASTERISM, DEFORMATION BANDS AND KINKS

As was stated in § 2, it is to be expected that—contrary to the assumption of G. I. Taylor (1934)—packets of slip bands with like dislocations will form in the course of plastic deformation. Now any block of material which contains a number of parallel slip bands with, say,  $N$  positive edge dislocations each, is bent (see Figure 5). If  $W$  is the distance between neighbouring slip bands and  $L$  their

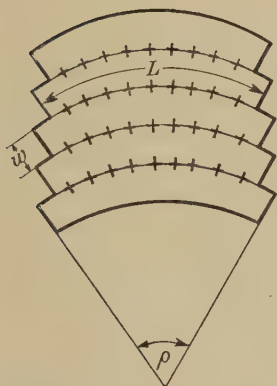


Figure 5. Schematic illustration of the bending set up by the presence of parallel rows of dislocations.

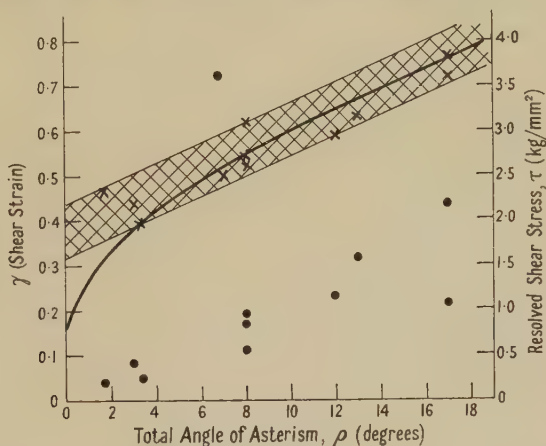


Figure 6. Values of shear stress ( $\times$ ) and shear strain ( $\bullet$ ) corresponding to the same experiments are plotted for varying values of the angle of asterism. Experimental data from Yamaguchi (1929) for aluminium single crystals.

length, the angle of rotation is  $\rho = N\lambda/W$ , where, as before,  $\lambda$  is the atomic distance in the glide plane and in the glide direction and, if equilibrium is reached,  $N = l\tau/2A$ .

This bend will manifest itself as asterism in the Laue pattern, and its axis of rotation is the same as that found experimentally by Taylor (1928), Yamaguchi (1929) and Burgers and Louwerse (1931), namely, parallel to the glide plane and perpendicular to the glide direction. From the foregoing it follows that asterism will occur even when great care is taken to avoid inhomogeneous deformation, because it is merely a consequence of the presence of regions with a large surplus of dislocations of one type and sign, which is a characteristic feature of our model. It seems more difficult to find reasons why in some materials, for instance  $\alpha$ - and  $\beta$ -brass (Elam 1936, Maddin, Mathewson and Hibbard 1948, 1949, Treuting and Brick 1942), the asterism is practically absent.

As the density of dislocations within the material depends on the stress, but not directly on the strain, we expect a close connection between asterism and stress but not between asterism and strain. This seems to agree with experiment. Figure 6 shows the values of  $\rho$  for aluminium single crystals taken from the paper by Yamaguchi (1928), plotted against stress and against strain. While the crosses

all lie within a narrow region the dots are scattered. Taking for  $1/W$  the experimental result of Yamaguchi (1928) for the same material, namely

$$1/W = C(\tau - \tau_y), \text{ where } \tau_y \simeq 0.8 \text{ kg/mm}^2 \text{ and } C \simeq 200 (\text{mm.kg/mm}^2)^{-1}$$

we find

$$\rho = L\pi(1 - \mu)G^{-1}C(\tau^2 - \tau\tau_y) \simeq 0.1L(\tau^2 - \tau\tau_y)$$

for  $L$  in millimetres and  $\tau$  in  $\text{kg/mm}^2$ . The curve plotted in Figure 6 is  $\rho = 0.027(\tau^2 - 0.8\tau)$ , so that  $L \simeq \frac{1}{4} \text{ mm}$ .

$L$  is only an approximate measure for the average width of the bent regions, for we have neglected the interaction between neighbouring glide bands as well as glide packets, and assumed that the equilibrium number of dislocations is always reached.

Deformation bands, in particular regions in which the lattice curvature changes sign, will occur at the boundaries where a region containing dislocations of one sign meets a region containing dislocations of the opposite sign. We have to expect a greater number of deformation bands at low temperatures than at high temperatures, for in §6 we showed that at a given stress the number of active sources does not vary very much with temperature, but that the average length of the slip band increases markedly, and according to §2 each slip band sets up in its neighbourhood a region in which only slip bands with the same type of dislocation are likely to be formed. Therefore at high temperatures the relatively few sources which act first, and are thus almost independent of each other, will be the origin of long slip bands, and hence will influence comparatively large regions, while at low temperatures their region of influence will be much smaller because there will be a great number of sources acting before the slip bands reach an appreciable length and their zones come into contact with each other. From then on the number of deformation bands will to a first approximation be independent of stress and strain until secondary slip starts. As the energy of a number of like dislocations on different glide planes, according to elasticity theory, is lowest when they are arranged in a wall perpendicular to the glide plane, there will be a tendency for the deformation bands also to form planes perpendicular to the glide direction and to the glide plane.

The deformation bands will act as strong obstacles against the movement of dislocations because the unlike dislocations lock each other. They thus will be a source of real work hardening of the type mentioned in §7.

If single crystals of zinc or cadmium with the hexagonal axis perpendicular to the specimen axis are axially compressed, a type of deformation called 'kinking' occurs (Orowan 1942). It consists of sharp lattice bendings or 'kinks'. Hess and Barrett (1949) in an experimental investigation found that kink bends are a special type of deformation band. They explained kinks as produced by a great number of pairs of edge dislocations which under the applied stress originate in a section of the specimen and separate, thus producing a great surplus of like dislocations within restricted regions.

The close relation between the ideas of Hess and Barrett and those put forward here is obvious. The only difference between kinks and the lattice bendings which produce deformation bands and asterism is that the latter arise unintentionally even in 'homogeneous' deformation, while those which cause kinking are of a larger scale and are formed under the influence of macroscopic bending stresses.



## § 10. RECOVERY, BAUSCHINGER EFFECT AND AFTER-EFFECT

(i) *Recovery*

According to § 8, steady creep goes on without further work hardening, i.e. the process has become stationary. If now a single crystal which has crept at a steady rate for a while is suddenly unloaded, no more dislocations are created, but under the influence of their mutual repulsive forces a movement of the dislocations will go on, though with a smaller speed. If the obstacles are of the symmetrical type as many dislocations will move back to their sources and be annihilated there as will be annihilated at the surfaces of the specimen, i.e. leave the specimen through the surface. While this elimination of dislocations goes on, the number and opacity of the obstacles will remain unchanged and the net plastic flow will be zero. But the properties of the material which depend on the number of dislocations present (for instance hardness, yield stress, conductivity, modulus of rigidity, thermoelectric power and so on) will change: the material will recover.

In an earlier paper (Kuhlmann, Masing and Raffelsieper 1949) such a recovery has been considered, and with some simplifications the following law of recovery has been derived:  $x = B - A^* \ln(t + t_0)$ . Here  $x$  is the number of dislocations present in the material and  $t$  is the time of recovery,  $A^*$  is proportional to the absolute temperature at which the recovery has taken place,  $B = A^* \ln(A/K_1) + K_2$ , where  $K_1$  and  $K_2$  are constants, and  $t_0 = A^*/v_0$  where  $v_0$  is the velocity of recovery,  $dx/dt$ , at  $t=0$ . Although the agreement between this law and the experiments seems to be good (Kuhlmann, Masing and Raffelsieper 1949, Cottrell and Aytakin 1950) the author is aware that the calculation is too much simplified and needs improvement, and hopes to do this in a later paper.

(ii) *After-effect and Bauschinger Effect*

If, in the course of a deformation, macroscopic parts of the material (i.e. grains or regions which are comparable with the dimensions of the specimen) behave elastically, while others undergo plastic deformation, large-scale internal stresses will be set up (Wartenberg 1918) such that after unloading some part of the deformation will slowly disappear. This reversed creep is called after-effect, and its time and temperature law has been derived in a recent paper (Kuhlmann 1947). It is the same as for recovery.

Similarly, but without the help of large-scale internal stresses, an after-effect will occur when a specimen which has been strained but has not yet reached the stationary state of steady creep is unloaded. In this case the dislocations will be preferentially eliminated at their sources, at least in the initial stages of the process, and thus a small plastic deformation will be connected with the recovery. As before, its direction will be opposite to that of the original deformation. We therefore expect an after-effect (or reversed creep) in all cases where steady creep has not been reached. The after-effect independent of large-scale internal stresses can be calculated in very much the same way as that which occurs when they are present.

The Bauschinger effect is closely connected with the after-effect because the tendency of the material to creep back spontaneously and partially to annihilate the preceding deformation will naturally lead to a lowered critical yield stress of the material when the direction of the stress is reversed. Masing (1923, 1926, Masing and Mauksch 1925) has treated the case where large-scale internal

stresses are involved. The corresponding case without large-scale stresses, investigated for instance by Sachs and Shoji (1927) for  $\alpha$ -brass single crystals, can be understood in the light of the above considerations on after-effect.

Apparently no after-effect has yet been observed in single crystals, although, according to this model of plastic deformation, it is to be expected in certain cases. The reason may be that it takes place too slowly.

#### § 11. EXPLANATION OF A SPECIAL EFFECT CONNECTED WITH SUDDEN ALTERATIONS OF THE STRESS IN CREEP EXPERIMENTS

The best way to test the present model of plastic deformation seems to be to employ it for the explanation of creep experiments, preferably in the region of steady creep. Here, as discussed in § 8, we do not expect changes of the number and opacity of the obstacles or the number of the active sources. In the steady creep range we, therefore, on the one hand avoid the great complications connected with asterism, deformation bands, true work hardening and changes in the number of slip bands, and on the other hand cannot employ these in a theoretical explanation of the observations, so that an agreement in this region will be of greater significance.

Fortunately there are a few experimental investigations which are suitable for testing the model, namely the creep experiments employing small changes of load during steady creep carried out by Carreker, Leschen and Lubahn (1949), by Phillips (1949) and by Cottrell and Aytakin (1950). The last investigation is the most complete of these, and we shall discuss it.

When the stress on single crystals of zinc was lowered by different small amounts  $\Delta\tau$  after the steady creep rate had been reached, it was found that for a certain period of time the creep rate was reduced to a very small value and then increased to a steady value again. The time  $\delta$  which elapsed before the creep rate reached its new steady value was in approximate agreement with that expected from the rate of recovery  $r$  calculated from the relation  $r = vh$  (Orowan 1934 b), where  $v$  is the rate of steady creep and  $h$  is the hardening coefficient, i.e.  $\delta \simeq \Delta\tau/vh$ .

Both the creep rate  $v$  and the rate of recovery  $r$  (determined by strain hardening and annealing experiments) were proportional to  $\exp\{-(U_0 - \alpha\tau)/RT\}$ , in which  $\alpha$  is a constant,  $\tau$  is, as usual, the resolved shear stress, and  $U_0$  an energy of activation. The magnitudes of  $U_0$  and  $\alpha$  were found to be the same in creep and in recovery, and the coefficients of proportionality were essentially the same when allowance was made for the presence of the hardening coefficient.

The idea adopted by Cottrell and Aytakin was that while creep had been going on at the higher stress, the yield stress remained constant because of a balance between strain hardening and recovery, and that when the applied stress was suddenly lowered the creep rate would be small until the yield stress had fallen by the same amount, due to recovery.

Obviously the experiments of Cottrell and Aytakin are in agreement with our model, in so far as, according to § 10, the same energy of activation  $U_0$  is involved in creep and in recovery, namely that necessary for a dislocation to pass an average obstacle, and, moreover, in the cases where recovery takes place under stress, as in the experiments of Cottrell and Aytakin, the energy supplied by the acting stress,  $\alpha\tau$ , is the same for recovery as for creep.

To understand these experiments quantitatively let us make a simplified model of the process and consider a slip band of length  $L$  with a sequence of

$\nu$  obstacles, to a first approximation of equal opacity and regularly arranged at intervals,  $l = L/\nu$ . The equilibrium number of dislocations in such a slip band is (§ 2)  $N = Ln/l = L\tau/2A\ddagger$ .

The dislocations will leave the slip band at a rate proportional to  $\exp\{-(U_0 - \alpha\tau)/RT\}$  and will be replaced by new dislocations from the sources in the manner discussed in § 3.

Let the stress now be reduced by  $\Delta\tau = \tau/n$  to  $\tau'$  so that  $(n-1)L/l$  dislocations are the equilibrium number with the new stress. There will now be a surplus of  $\nu$  dislocations in the slip band. The first one will leave the glide plane through the surface of the specimen more rapidly than would be normal for the new stress, but this just brings the density of the dislocations to its equilibrium value in the last segment, and no dislocation from the preceding one can move up. As the strain produced by moving dislocations is proportional to the total distance traversed by them, and as the first dislocation only causes a slight readjustment of the dislocations between the last two obstacles, it will lead only to a negligible strain. The next dislocation will leave the surface after a life-time corresponding to the steady creep rate at the new stress and will cause all dislocations in the last section to move up and enable one dislocation to pass over from the penultimate to the last segment, but for the same reason as above it will not be replaced from the preceding section. The slip produced by the second dislocation to leave the surface after the stress was lowered will thus to a first approximation be  $\lambda/\nu$ , where, as before,  $\lambda$  is the interatomic distance in the glide plane in the glide direction. This process will go on, the rate at which the surplus dislocations leave the surface being  $K \exp\{-(U_0 - \alpha\tau')/RT\}$  while the slip produced is  $(k-1)\lambda/\nu$  for the  $k$ th dislocation. When the  $\nu$ th dislocation has left the glide plane, the new equilibrium number of dislocations in the slip band is reached and thereafter each dislocation which leaves the slip band will, as before, be replaced by one from the source and produce the slip  $\lambda$ . Thus this simplified model leads to a creep velocity which rises linearly with time until the new steady rate is reached, and the strain increment  $\Delta$  during that time will be half as large as it would be if the final velocity  $v$  had acted all the time.

Though it cannot be expected that the creep rate will necessarily increase in a truly linear manner from zero to its final velocity, as this simple model predicts, the second prediction, that the strain increment during the transition time will be  $\Delta \simeq \frac{1}{2}v\delta$ , should be fulfilled. The reason is that we start with a certain number of surplus dislocations, of which practically all leave the specimen at the rate appropriate to the new stress, but on the average they travel only over half the length of the slip bands. The reverse effect to that discussed, namely that a sudden increase of the stress gives rise to a transient rapid creep, can probably be explained on the same basis. There, in addition to the normal creep, the dislocation density is brought up to its new equilibrium value. The present calculation is equally applicable to polycrystalline material and to single crystals, but to single crystals with an oxide layer only as long as other obstacles besides the layer are present.

Expressing the result in symbols, we find that the time  $\delta$  which elapses before the last surplus dislocation has left the average slip band is  $\delta = (\nu/K) \exp\{(U_0 - \alpha\tau')/RT\}$ ,

† As  $n = l\tau/2A$  dislocations are piled up behind each obstacle there will be a stress magnification factor  $n$ , but the difference between  $U = U_0 - \alpha\tau$ , the experimental result from Cottrell and Aytakin, and  $U = U^* - \beta\tau^2$ , which follows from the present model, would hardly have been noticeable because: the stress range in which measurements of  $U$  for single crystals are practicable is rather narrow, so that, taking into account the normal scatter of experimental values, the curve  $U(\tau) = U^* - \beta\tau^2$  cannot be distinguished from its tangent  $U = U_0 - \alpha\tau$ . The same applies to any other reasonable function  $U(\tau) = U^* - f(\tau)$ .



or in general, since  $N = L\tau/2A$ ,  $\delta = (L\Delta\tau/2AK) \exp \{(U_0 - \alpha\tau')/RT\}$ . The new steady rate is  $v = (\lambda/W)K \exp \{(U_0 - \alpha\tau')/RT\}$ . For the present case there is no change in the number and opacity of the obstacles during plastic deformation. We also assume that  $W$  is constant during deformation; according to Andrade and Roscoe (1937) this is true for single crystals of cadmium at very slow strain rates. The same is true, according to Hoyt (1927), for single crystals of zinc provided a certain minimum deformation has been exceeded. For such a case

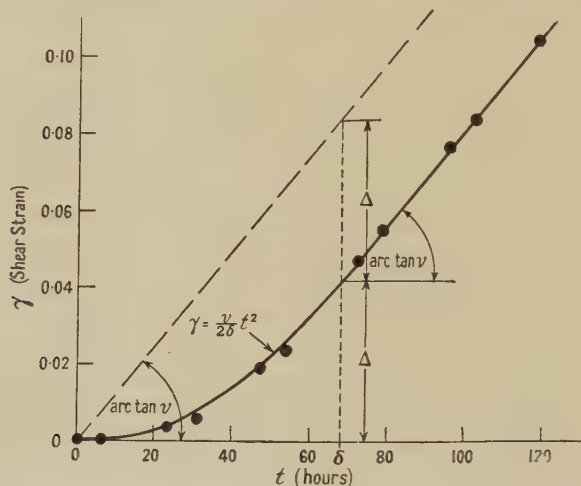


Figure 7. Experimental points by Cottrell and Aytakin (1950) for the creep of a single crystal of zinc. After the crystal had crept for some time with a constant rate at  $82^\circ\text{C}$ . and  $\tau = 27.7\text{ gm/mm}^2$  the stress was reduced to  $26.3\text{ gm/mm}^2$  at  $t = 0$ . (The curve is that predicted in § 11.)

we found in § 7 the relation  $h = 4AW/\lambda L$ . From this we get  $\delta = 2\Delta\tau/hv$ . This formula is in good agreement with the result of Cottrell and Aytakin,  $\delta \simeq \Delta\tau/hv$ . Considering the time law, we find that the shear during the transition time is given by  $\gamma = (v/2\delta)t^2$ . In Figure 7 the readings for one of Cottrell and Aytakin's creep experiments are plotted together with that curve. It will be seen that the agreement is very satisfactory.

#### ACKNOWLEDGMENTS

The author wishes to express her thanks to Professor N. F. Mott for extending to her the facilities of the H. H. Wills Physical Laboratory and for his kind interest and encouragement. Thanks are also due to Messrs. F. R. N. Nabarro and F. C. Frank, and especially to Mr. G. Wyllie of that laboratory, for helpful discussions, and to Professor E. N. da C. Andrade and Professor A. H. Cottrell for kindly allowing the use of some unpublished results.

#### REFERENCES

- ANDRADE, E. N. DA C., 1910, *Proc. Roy. Soc. A*, **84**, 1; 1914, *Ibid*, **90**, 329; 1949, Lecture on Surface Effects in Plastic Deformation; Conference on Plastic Deformation and Recrystallization, Cambridge, September 1949; see also *The Strength of Solids* (London: Physical Society), 1948, p. 20.  
 ANDRADE, E. N. DA C., and RANDALL, R. F. Y., 1948, *Nature, Lond.*, **162**, 890.  
 ANDRADE, E. N. DA C., and ROSCOE, R., 1937, *Proc. Phys. Soc.*, **49**, 152.  
 BECKER, R., 1925, *Phys. Z. Sowjet*, **26**, 919.

- BRAGG, L., 1942, *Nature, Lond.*, **149**, 511; 1948, *Proc. Camb. Phil. Soc.*, **45**, 125; 1948, *The Strength of Solids* (London : Physical Society), p. 26.
- BURGERS, W. G., and LOUWERSE, P. C., 1931, *Z. Phys.*, **67**, 605.
- CARREKER, R. P., LESCHEN, J. G., and LUBAHN, J. D., 1949, *Trans. Amer. Inst. Min. Metall. Engrs.*, **180**, 139.
- COTTRELL, A. H., 1949, *Progress in Metal Physics*, **1**, 77 (London : Butterworth).
- COTTRELL, A. H., and AYTEKIN, V., 1950, *J. Inst. Met.*, in the press.
- CRUSSARD, C., 1945, *Rev. Metall*, **42**, 286, 321.
- ELAM, C. F., 1936, *Proc. Roy. Soc. A*, **153**, 273.
- FRANK, F. C., 1948, *The Strength of Solids* (London : Physical Society), p. 46.
- HEIDENREICH, R. D., and SHOCKLEY, W., 1947, *J. Appl. Phys.*, **18**, 1029; 1948, *The Strength of Solids* (London : Physical Society), p. 57.
- HESS, J. B., and BARRETT, C. S., 1949, *Metals Trans. (A.I.M.M.E.)*, **185**, 599.
- HOYT, S. L., 1927, *Trans. Amer. Inst. Min. Metall. Engrs.*, **74**, 116.
- KAWAI, T., 1930, *Sci. Rep. Tôhoku Univ.*, **19**, 209.
- KOCHENDÖRFER, A., 1941, *Plastische Eigenschaften von Kristallen und metallischen Werkstoffen* (Berlin: Springer), p. 81.
- KOEHLER, J. S., 1941, *Phys. Rev.*, **60**, 397.
- KUHLMANN, D., 1947, *Z. Phys.*, **124**, 468; 1950, *Z. Metallkunde*, **41**, 129.
- KUHLMANN, D., and MASING, G., 1948, *Z. Metallkunde*, **39**, 361.
- KUHLMANN, D., MASING, G., and RAFFELSIEPER, J., 1949, *Z. Metallkunde*, **40**, 241.
- LAURENT, P., and EUDIER, M., 1949, *C. R. Acad. Sci., Paris*, **228**, 225.
- MADDIN, R., MATHEWSON, C. H., and HIBBARD, W. R., 1948, *Trans. Amer. Inst. Min. Metall. Engrs.*, **175**, 86; 1949, *Metals Trans. (A.I.M.M.E.)*, **185**, 527.
- MASING, G., 1923, *Wiss. Veröff. Siemens Konzern*, **3**, 231; 1926, *Ibid.*, **5**, 135; 1944, *Nachr. Wiss. Göttingen*, p. 81; 1948, *Z. Phys.*, **124**, 586.
- MASING, G., and MAUKSCH, W., 1925, *Wiss. Veröff. Siemens Konzern*, **4**, 74.
- MOTT, N. F., 1946, *J. Inst. Met.*, **72**, 367.
- MOTT, N. F., and NABARRO, F. R. N., 1940, *Proc. Phys. Soc.*, **52**, 86; 1948, *The Strength of Solids*, (London : Physical Society), p. 1.
- NABARRO, F. R. N., 1946, *Proc. Phys. Soc.*, **58**, 669; 1949, *Z. Metallkunde*, **40**, 81; 1950, to be published.
- NYE, J. F., 1949, *Rev. Metall.*, **46**, 371.
- OROWAN, E., 1934a, *Z. Phys.*, **89**, 605; 1934b, *Ibid.*, **89**, 614; 1935, *Ibid.*, **98**, 382; 1941, *Nature, Lond.*, **147**, 452; 1942, *Ibid.*, **149**, 643.
- PHILLIPS, D. J., 1949, *Thesis*, Bristol.
- RAFFELSIEPER, J., 1950, *Z. Metallkunde*, in the press.
- SACHS, H., and SHOJI, H., 1927, *Z. Phys.*, **45**, 776.
- SCHMID, E., and BOAS, W., 1929, *Z. Phys.*, **57**, 575; 1930, *Ibid.*, **61**, 767; also GEORGIEFF, M., and SCHMID, E., 1926, *Ibid.*, **36**, 759; FAHRENHORST, W., and SCHMID, E., 1930, *Ibid.*, **64**, 845.
- TAYLOR, G. I., 1928, *Trans. Faraday Soc.*, **24**, 121; 1934, *Proc. Roy. Soc. A*, **145**, 362, 388.
- TREUTING, R. G., and BRICK, R. M., 1942, *Trans. Amer. Inst. Min. Metall. Engrs.*, **147**, 128.
- VON WARTENBERG, H., 1918, *Verh. dtsch. phys. Ges.*, **20**, 113.
- YAMAGUCHI, K., 1928, *Sci. Pap. Inst. Phys. Chem. Res. Tokio*, **8**, 289; 1929, *Ibid.*, **11**, 151.
- YAMAGUCHI, K., and TOGINO, S., 1929, *Sci. Pap. Inst. Phys. Chem. Res. Tokio*, **9**, 277.

## Factors Controlling Dislocation Widths

By A. J. FOREMAN, M. A. JASWON AND J. K. WOOD

Department of Mathematics, Imperial College, London

*Communicated by H. Jones ; MS. received 21st July 1950*

**ABSTRACT.** The work of Peierls and Nabarro is extended to a family of edge dislocations of greater widths. The weaker the shearing forces between adjacent atoms in the slip plane, the wider is the dislocation. The external shear stress required to move the dislocations is extremely sensitive to the width, becoming vanishingly small at widths of the order of three atomic spacings. The theory is applied to bubble raft dislocations, and satisfactory agreement is found with experiment.

### § 1. INTRODUCTION

THE early theories of the edge dislocation (Taylor 1934) were based on the classical elastic dislocations of Volterra, in which singularities of stress and strain occur at the centre. A more direct approach was made by Peierls (1940) and Nabarro (1947), who took into account the atomic structure along the slip plane whilst still making use of classical elasticity theory elsewhere, and in this way determined the atomic displacements throughout the dislocation. Their calculations, however, were based on an assumed form for the interaction forces between adjacent atoms in the slip plane. It is the purpose of the present paper to extend this work by showing how the width of a dislocation and the external shear stress required to move it depend on the nature of the assumed interatomic forces. It is concluded that dislocations in single pure annealed crystals have a greater width than that obtained by Peierls and Nabarro, and that the external shear stress required to move them is less than the observed yield stress. Finally an interesting illustration of the theory is provided by the bubble raft dislocations constructed by Bragg and his collaborators.

### § 2. THE PEIERLS-NABARRO DISLOCATION

A diagram of the cross section, one atom thick, of a single positive edge dislocation is shown in Figure 1, the problem being two-dimensional. Following Peierls, it is convenient to regard the dislocation as constructed by slicing the material along the slip direction  $x'Ox$ , thus forming two semi-infinite planes. The upper plane is cut along  $Oy$  and an extra row of atoms inserted. The two planes are then 'stitched' together along  $x'Ox$ , the upper one being compressed, the lower extended, so that there is perfect alignment of corresponding atoms at infinity, as illustrated in Figure 1. Each half-plane is now separately in equilibrium under the action of the forces applied to the boundaries  $A'A$ ,  $B'B$  respectively, it being assumed, for purposes of calculation, that the planes can be treated as isotropic elastic continua.

The forces acting along  $A'A$  which maintain the upper half-plane in its deformed state, are taken to be a system of shear stresses directed towards the origin, these being equal and opposite to the shear stresses in  $B'B$ . The displacement  $U(x)$  along the slip direction, caused by these stresses, of an atom at the point  $x$  in  $A'A$  will be equal and opposite to the displacement  $\bar{U}(x)$  of the corresponding



atom in B'B, provided that  $U(x)$  varies slowly from atom to atom. It follows therefore that the relative displacement  $r(x)$  of the two atoms is given by

$$\left. \begin{aligned} r(x) &= U(x) - \bar{U}(x) + \frac{1}{2}d = 2U(x) + \frac{1}{2}d & (x > 0) \\ r(x) &= U(x) - \bar{U}(x) - \frac{1}{2}d = 2U(x) - \frac{1}{2}d & (x < 0), \end{aligned} \right\} \dots\dots(1)$$

the initial relative displacement in the undeformed state being  $\pm \frac{1}{2}d$ . Since there is perfect alignment at infinity,  $r(\pm \infty) = 0$ , so that

$$U(\infty) = -U(-\infty) = -d/4. \dots\dots(2)$$

It has been shown by Nabarro and by Leibfried and Lücke (1949), on the basis of classical elasticity theory, that the shear stress  $p(x)$  and the displacement  $U(x)$  at  $x$  are related by the equation

$$\frac{\pi(1-\nu)}{G} p(x) = \int_{-\infty}^{\infty} \frac{dU(x')}{dx'} \frac{dx'}{x' - x}, \dots\dots(3)$$

where  $G$  is the shear modulus and  $\nu$  is Poisson's ratio.

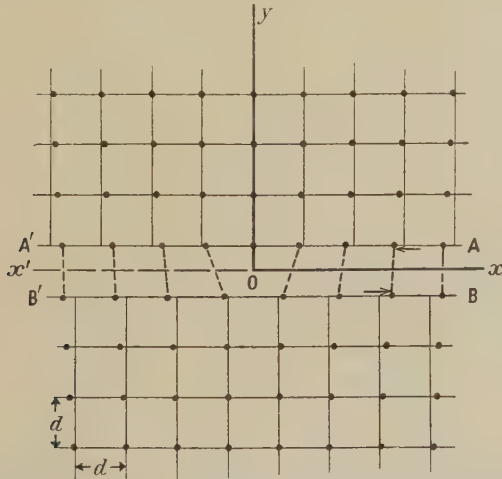


Figure 1. Cross section of a positive edge dislocation. The arrows indicate directions of shear stress and displacement for a pair of corresponding atoms.

The shear stress distribution along A'A is provided by the interaction forces between the atoms in A'A, B'B, so that  $p(x)$  is a function of  $r(x)$ . This function  $p(r)$  has not yet been calculated, but it must be periodic with period  $d$ , and alternately positive and negative in each half-period. Furthermore, it has the limiting form  $p = Gr/d$  for small relative displacements, in accordance with Hooke's law. A simple function of this type, viz.

$$p = \frac{G}{2\pi} \sin \frac{2\pi r}{d}, \dots\dots(4)$$

was put forward by Peierls (1940) as the most convenient assumption as to the law of force.

It is clear that each assumed function  $p(r)$  implies a corresponding displacement function  $U(x)$  and a corresponding distribution of shear stress  $p(x)$ . Thus, substituting for  $r$  in (4) from (1) gives

$$p = -\frac{G}{2\pi} \sin \frac{4\pi U}{d} \dots\dots(5)$$

which, when put into (3), leads to the integral equation for  $U$ :

$$-\frac{(1-\nu)}{2} \sin \frac{4\pi U}{d} = \int_{-\infty}^{\infty} \frac{dU(x')}{dx'} \frac{dx'}{x' - x}. \quad \dots\dots(6)$$

As may be verified by substitution, a solution of (6) which satisfies the boundary conditions (2), and which represents a single dislocation, is given by

$$U(\xi) = -\frac{d}{2\pi} \tan^{-1} \xi, \quad \xi = \frac{2(1-\nu)}{d} x. \quad \dots\dots(7)$$

From (5) and (7) the distribution of shear stress which maintains these displacements is

$$p(\xi) = \frac{G}{\pi} \frac{\xi}{1 + \xi^2}. \quad \dots\dots(8)$$

These displacements and stresses are both odd functions as required, and their general shape is entirely satisfactory, but it is unfortunate that they vary rather rapidly from atom to atom at the centre. As a result of this, the equation (1) for relative displacements is slightly in error at the first pair of atoms. Furthermore, the strain along the slip direction, i.e.  $dU/dx$ , reaches a maximum of the order of  $1/5$ , which is above the limit usually accepted in classical elasticity. It is, however, considered unlikely that the errors in the theory are serious on this account, particularly as the elastic problem is essentially one of simple tension and compression.

The dislocation described above is such that the atoms in the slip plane become fairly well aligned at a short distance from the centre, so that the major part of the slip caused by the dislocation takes place over a region of only a few atoms. This is classed as a narrow dislocation, the strains near the centre being large. It is found convenient to define the width of a dislocation as the range of  $x$  for which  $U(x)$  is numerically less than  $d/8$ , i.e. half its limiting value. The dislocation represented by equation (7) is then of width

$$w = d/(1 - \nu),$$

i.e. about 1.5 atomic spacings if  $\nu \sim 0.3$ , which is very narrow. It is probable that in actual crystals the dislocations are wider than this. The extreme narrowness here is due to the assumed law of force (4) between atoms, which is very unlikely to hold in real crystals. In consequence, a flatter type of periodic function of stress against relative displacement has been suggested. This would almost certainly lead to a wider dislocation, for the tendency of adjacent atoms to align themselves correctly on either side of the dislocation will not be so marked if they are attracted by weaker forces. It has been found possible to investigate this question quantitatively, and hence to determine how the width of a dislocation varies with the assumed law of force. In order to obviate the difficulty of having to solve integral equations of the type mentioned, the method of approach adopted here is to choose some suitable type of function  $U(x)$ , find the corresponding stress distribution from (3) and, by eliminating  $x$  between them, find  $p$  as a function of  $U$  and hence of  $r$ .

### §3. MODIFICATION OF THE PEIERLS-NABARRO DISLOCATION

It is required to find displacement functions  $U(x)$  such that they (i) represent wider dislocations than that obtained by Peierls and Nabarro, and (ii) give curves of stress against relative displacement having the same initial slope as the previously assumed sinusoidal curve (4), thus ensuring that Hooke's law holds for small values of  $r/d$ .

One type of displacement curve which implies a greater dislocation width is given by

$$U = -\frac{d}{2\pi} \tan^{-1} \frac{\zeta}{a}, \quad \dots\dots(9)$$

where  $\zeta = 2(1-\nu)x/d$  and  $a$  is a parameter greater than unity. When  $a=1$ , this becomes the solution (7). The width  $w$  of the dislocation (9) is easily seen to be  $ad/(1-\nu)$ , and so increases linearly with  $a$ . On substituting from (9) into the relation (3), the corresponding stress distribution is found to be

$$p = \frac{G}{\pi} \frac{\zeta}{a^2 + \zeta^2}, \quad \dots\dots(10)$$

from which the function  $p(r)$  is given by

$$p = \frac{G}{2\pi a} \sin 2\pi r/d. \quad \dots\dots(11)$$

This is a sinusoidal curve as before, but has an incorrect initial slope, except when  $a=1$ . This example shows at once that the main difficulty of the problem is to find some type of function  $U(x)$  which will ensure that the initial slope of the corresponding function  $p(r)$  is given by Hooke's law, i.e.  $p = Gr/d$  for  $r/d$  small.

A displacement function which satisfies the conditions mentioned, and which is of a suitable form, is

$$U = -\frac{d}{2\pi} \left\{ \tan^{-1} \frac{\zeta}{a} + (a-1) \frac{\zeta}{a^2 + \zeta^2} \right\}, \quad \dots\dots(12)$$

where  $\zeta = 2(1-\nu)x/d$ , and the parameter  $a$  determines the width. When  $a=1$ ,  $U$  reduces to the function (7), whilst for larger values of  $a$  the dislocation is wider. Displacement curves are shown in Figure 2 for the cases  $a=1, 2, 4, 10$ . In these wider dislocations  $U(x)$  varies more slowly from atom to atom, so that the maximum elastic strains are smaller, and the theory accordingly more consistent.

Setting the displacements (12) into (3) gives the corresponding stress distribution, the integration being facilitated by observing that (12) may be written as

$$U = -\frac{d}{2\pi} \left\{ 1 - (a-1) \frac{\partial}{\partial a} \right\} \tan^{-1} \frac{\zeta}{a},$$

and that the operator can be brought outside the integral sign. The resulting stress distribution is then

$$\begin{aligned} p &= \left\{ 1 - (a-1) \frac{\partial}{\partial a} \right\} \frac{G}{\pi} \frac{\zeta}{a^2 + \zeta^2} \\ &= \frac{G}{\pi} \left\{ \frac{\zeta}{a^2 + \zeta^2} + 2a(a-1) \frac{\zeta}{(a^2 + \zeta^2)^2} \right\}. \quad \dots\dots(13) \end{aligned}$$

As the dislocation widens, that is as  $a$  increases, it is found that the maximum stress decreases, its position moves outwards, and the sharp rise in stress which occurs when  $a=1$  gives way to a smoother type of curve (Figure 2).

It will be noted from (13) that as  $|\zeta| \rightarrow \infty$ , the relation between  $p$  and  $\zeta$  becomes, for all values of the parameter  $a$ ,

$$p = \frac{G}{\pi \zeta}, \quad \dots\dots(14)$$



which is the shear stress along the slip plane in Koehler's classical dislocation (1941). It will also be noted that the limiting form for  $U$  as  $|\zeta| \rightarrow \infty$  is, from (12),

$$\left. \begin{aligned} U &= -\frac{d}{4} + \frac{d}{2\pi\zeta} & (\zeta > 0), \\ U &= \frac{d}{4} + \frac{d}{2\pi\zeta} & (\zeta < 0). \end{aligned} \right\} \dots\dots (15)$$

Hence from (1), for  $|\zeta|$  large and, therefore, for the relative displacement  $r$  small, we have

$$r/d = 1/\pi\zeta. \dots\dots (16)$$

It follows from (16) and (14) that as  $r \rightarrow 0$ , the relation between  $p$  and  $r$  is  $p = Gr/d$ , which is Hooke's law, as required.

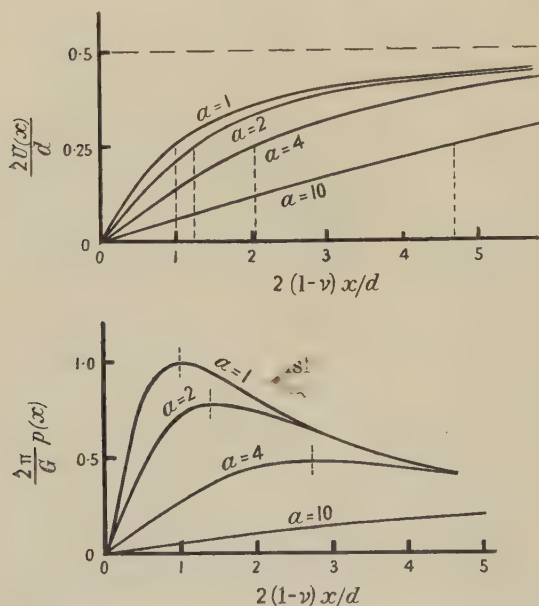


Figure 2. The upper diagram illustrates the family of displacement curves assumed. The lower one illustrates the corresponding shear stress distributions.

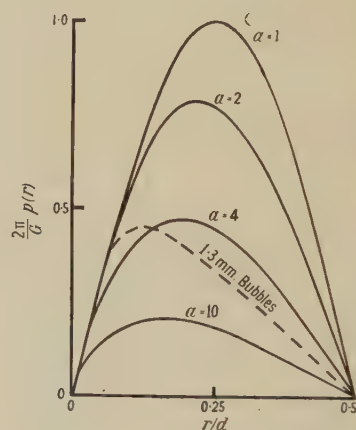


Figure 3. Curves of stress against relative displacement.

From (12) and (13), using (1), the function  $p(r)$  corresponding to the assumed displacements is written most conveniently in the parametric form

$$\left. \begin{aligned} \frac{2\pi}{G} p &= \frac{1}{2a^2} \{2(2a-1) \sin \theta - (a-1) \sin 2\theta\}, \\ \frac{2\pi r}{d} &= \theta - \frac{a-1}{a} \sin \theta, \end{aligned} \right\} \dots\dots (17)$$

where  $\theta$  is given by  $\zeta = a \cot \theta/2$ . The cases  $a=1, 2, 4, 10$  are illustrated in Figure 3. As can be seen, the initial slopes of the  $p(r)$  curves are constant for all values of  $a$ , but the amplitudes decrease as  $a$  increases, i.e. as the width increases.

It is interesting to note that the relation between the width  $w$  and the amplitude  $p_{\max}$  is given very closely by the equation

$$w = \frac{Gd}{2\pi(1-\nu)} \frac{1}{p_{\max}}, \dots\dots (18)$$

as is illustrated by Table 1. This relation has been found to hold approximately for several families of dislocations of the same type as that described here. This

Table 1

$a$	1	2	3	4	5	10	$\infty$
$(1-\nu)w/d$	1.000	1.255	1.653	2.076	2.507	4.697	0.442a
$(2\pi/G)p_{\max}$	1.000	0.787	0.594	0.471	0.389	0.207	2.202/a
$2\pi(1-\nu)wp_{\max}/Gd$	1.000	0.988	0.982	0.978	0.975	0.973	0.973

suggests that the form of a dislocation depends primarily on the amplitude of the corresponding  $p(r)$  function rather than on its precise shape.

#### § 4. EXTERNAL STRESS REQUIRED TO MOVE A DISLOCATION

We now consider the minimum external shear stress  $T$  which will move the dislocation through the lattice. In the case of the dislocation discussed by Nabarro this was found to be

$$T_n = \frac{2G}{1-\nu} \exp \{-2\pi/(1-\nu)\}, \quad \dots\dots(19)$$

which is very much smaller than the theoretical shear strength  $G/2\pi$  of the lattice. The value of  $T$  for the dislocation represented by the displacements (12) may be found following the methods of Nabarro (1947); the procedure is outlined below.

The interaction energy of the atoms in A'A and B'B when the centre of the dislocation is displaced by  $\alpha d$  has been given by Nabarro as

$$V_n = \frac{Gd^2}{8\pi^2} \sum_{n=-\infty}^{\infty} \left[ 1 + \cos \left\{ 2 \tan^{-1} 2(1-\nu) \left( \alpha + \frac{n}{2} \right) \right\} \right],$$

apart from a constant term; the series may be transformed into a more rapidly converging one by the relation (Titchmarsh 1937)

$$\sum_{n=-\infty}^{\infty} f(n) = \sum_{s=-\infty}^{\infty} \int_{-\infty}^{\infty} f(t) \cos 2\pi ts \, dt. \quad \dots\dots(20)$$

The corresponding energy for the dislocation (12) may be shown to be

$$V = \left\{ 1 - (a-1) \frac{\partial}{\partial a} + \frac{1}{6} (a-1)^2 \frac{\partial^2}{\partial a^2} \right\} \frac{Gd^2}{8\pi^2 a} \sum_{n=-\infty}^{\infty} \left[ 1 + \cos \left\{ 2 \tan^{-1} 2(1-\nu) \left( \frac{\alpha + \frac{1}{2}n}{a} \right) \right\} \right],$$

the subsequent analysis being simplified by the use of this operational form and by the use of the relation (20). Equating the constraining force  $F$  on the dislocation to  $-d^{-1} \partial V / \partial \alpha$  gives

$$F = \left\{ 1 - (a-1) \frac{\partial}{\partial a} + \frac{1}{6} (a-1)^2 \frac{\partial^2}{\partial a^2} \right\} \frac{2G}{1-\nu} \sum_{s=1}^{\infty} s \exp \{-2\pi sa/(1-\nu)\} \sin 4\pi s \alpha,$$

in which the series is dominated by the first term. From this it follows, using the Mott-Nabarro relation  $F = \tau d$ , that the shear stress is given by

$$T = T_n e^{-K} (1 + K + K^2/6) \quad \dots\dots(21)$$

where  $K = 2\pi(a-1)/(1-\nu)$ .

The shear stress  $T$  is extremely sensitive to the parameter  $a$  and hence to the width  $w$  of the dislocation, as can be seen from Table 2. It has been pointed out by Cottrell (1949) that the value of  $T$  for  $a=1$  is from ten to fifty times larger than the observed yield stress for annealed pure single crystals.

Table 2

	$a$	1	2	4	10
$\nu=1/3$	$w$	$1.5d$	$1.9d$	$3.1d$	$7.1d$
	$T$	$2 \times 10^{-4}G$	$5 \times 10^{-7}G$	$2 \times 10^{-14}G$	$4 \times 10^{-36}G$
$\nu=1/4$	$w$	$1.3d$	$1.7d$	$2.8d$	$6.3d$
	$T$	$6 \times 10^{-4}G$	$3 \times 10^{-6}G$	$1 \times 10^{-12}G$	$1 \times 10^{-33}G$

If the yield stress is determined by the force required to move a single dislocation which is straight and parallel to a simple crystallographic axis, then the above results suggest that the widths of dislocations in crystals are greater than  $1.5d$ . A dislocation of width  $2d$  would provide a lower limiting value for  $w$ , as it would require a stress of the order of magnitude of the observed yield stress to move it.

#### § 5. BUBBLE RAFT DISLOCATIONS

A useful check on the theory is provided by the edge dislocations which have been obtained experimentally in bubble rafts by Bragg and Nye (1947), even though the lattice of bubbles differs from the simple cubical structure, and it is a case of plane stress rather than of plane strain.\* By shearing of adjacent rows past each other Bragg and Lomer (1949) have obtained what is effectively the function  $p(r)$  for bubbles of 1.3 mm. diameter (Figure 3). This function is of the same form as those described here except that the region in which Hooke's law holds is more clearly defined. The amplitude of Bragg and Lomer's curve is rather less than half that of the sine curve with the same initial slope, and is very nearly equal to that for the case  $a=4$  described here. As the width of a dislocation depends primarily on the amplitude of the function  $p(r)$ , see equation (18), the displacements corresponding to  $a=4$  will provide a reasonable approximation to those in the bubble raft dislocation. If a small correction is made for the slightly different spacing of the bubbles, and Poisson's ratio taken as 0.5 for 1.3 mm. bubbles as indicated by Bragg and Lomer (1949), it is found that the calculated displacements of the bubbles in the slip plane of the dislocation are in reasonable agreement with the measured values, as indicated in Table 3.†

Table 3

$x/d$	1	2	3	4	5	6	7	8	9	10
$2u(x)/d$ meas.	0.18	0.32	0.39	0.43	0.45	0.47	0.48	0.48	0.48	0.48
calc.	0.20	0.32	0.39	0.43	0.46	0.47	0.47	0.47	0.48	0.48

It is interesting to note that the widths of these bubble raft dislocations are very dependent on the size of the bubbles used in the experiments, and hence it is possible to obtain wide or narrow dislocations by varying the size of the bubbles.

\* The theory for plane stress may be derived from that of plane strain by replacing  $1-\nu$  by  $1/(1+\nu)$ .

† Dr. W. M. Lomer has kindly supplied a photograph of a dislocation in 1.32 mm. bubbles.



For example, the dislocations in 0.7 mm. bubbles correspond to about  $a=10$  in the theory, whilst for 1.9 mm. bubbles they are very narrow, being of the type  $a=2$ . It is hoped to check the theory more fully when the experimental ( $p, r$ ) curves for bubbles of varying sizes become available.

## ACKNOWLEDGMENT

The authors wish to acknowledge the benefit of valuable advice from Professor H. Jones throughout the course of the work.

## REFERENCES

- BRAGG, W. L., and LOMER, W. M., 1949, *Proc. Roy. Soc. A*, **196**, 171.  
 BRAGG, W. L., and NYE, J. F., 1947, *Proc. Roy. Soc. A*, **190**, 474.  
 COTTRELL, A. H., 1949, *Progress in Metal Physics*, I (London: Butterworth), p. 91.  
 KOEHLER, J. S., 1941, *Phys. Rev.*, **60**, 397.  
 LEIBFRIED, G., and LÜCKE, K., 1949, *Z. Phys.*, **126**, 450.  
 LOMER, W. M., 1949, *Proc. Roy. Soc. A*, **196**, 182.  
 NABARRO, F. R. N., 1947, *Proc. Phys. Soc.*, **59**, 256.  
 PEIERLS, R. E., 1940, *Proc. Phys. Soc.*, **52**, 34.  
 TAYLOR, G. I., 1934, *Proc. Roy. Soc. A*, **145**, 362.  
 TITCHMARSH, E. C., 1937, *Fourier Integrals* (Oxford: Clarendon Press), p. 60.

## Further Studies — Experimental and Theoretical — of a Wide-Angle $\beta$ -Spectrometer which uses a Prolate Spheroidal Magnetic Field

BY T. H. BRAID AND H. O. W. RICHARDSON

Department of Natural Philosophy, The University, Edinburgh

*Communicated by N. Feather; MS. received 4th August 1950*

**ABSTRACT.** A  $\beta$ -spectrometer is described which focuses a conical sheaf of rays emitted at about  $80^\circ$  to the axis of a prolate spheroidal magnetic field. In agreement with a previous theoretical prediction, the trajectories cross over at two sites in the rotating meridional plane. The field behaves in some ways like a magnetic mirror and can be arranged to form an aberration-free image of a point on the axis of symmetry. It cannot, however, give a clear image of an area because the Abbe sine condition is not fulfilled.

The wide-angle focusing action is compared with that recently found by Slätis and Siegbahn, for which a different optical analogue is suggested, based on the isolation of a meridional focal line between two refractions.

The adjustment of the spectrometer and measurements of its resolving power and solid angle of collection are described, an example being  $1.4\%$  of  $4\pi$  with a line-width of  $1/113$  at half-height. By working at less than unit magnification it is possible to focus rays emitted at less than  $80^\circ$  to the axis.

## § 1. INTRODUCTION

THE mode of focusing in the present instrument (Richardson 1949) bears some resemblance to the forming of an optical real image by a curved mirror. The resemblance appears when the paths of particles emitted from a point source on the axis of symmetry are plotted in the usual rotating meridional  $r, z$  plane. The particles are repelled by the bowl-shaped meridional potential barrier and adjacent 'rays' cross over near the turning point rather in

the manner of a specular reflection. The turning back, however, is gradual so that it cannot be sharply distinguished from refraction. In spite of this it is convenient to describe a system in which a strong repulsion coincides with a cross-over as a magnetic mirror. The concept has proved helpful in predicting the behaviour of the rays. An alternative description of a similar system in terms of refraction is discussed in § 5\*.

A remarkable feature of the focusing is that it seems possible to form an image of a particular object point which is corrected for spherical aberration, in the sense that the point at which the rays return to the axis is stationary over a narrow range of angles of emission. This angular range is defined by stops which select a 'sheaf' of rays emitted at a fairly large inclination to the axis.

The magnetic field has lines of force which are, approximately, ellipses lying on confocal prolate spheroids, so that the equipotentials are the orthogonal family of confocal hyperboloids of revolution. The field is maintained between two soft-iron poles of roughly hyperboloidal shape.

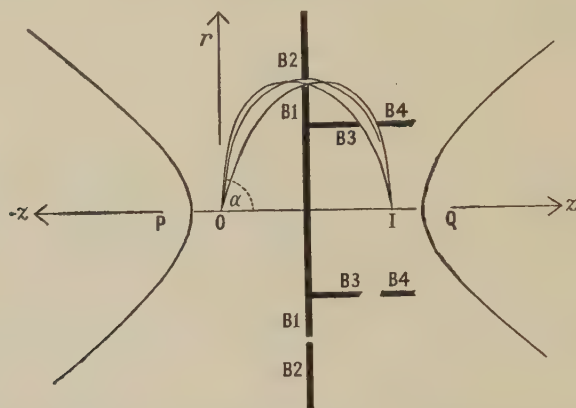


Figure 1. Wide-angle focusing in the spheroidal field. A sheaf of mono-energetic trajectories represented in the rotating meridional  $r, z$  plane, showing the selecting ring-slits B1 B2 and B3 B4.

An earlier computation of electron trajectories in this field had predicted promising focusing properties with a large solid angle of collection. The theory indicated (Richardson 1949) that the focused conical sheaf of rays has the property of crossing over at two sites in the meridional plane, as shown in Figure 1. The first cross-over, which simulates reflection, takes place at the outer envelope or caustic formed by mono-energetic rays of different inclinations. The second cross-over can be arranged to be on or near the axis, at a site suited for entry into a small Geiger-Müller tube.

The site of this second cross-over is controlled by choosing the correct radius for the ring-slit B1B2 between the central stop B1 and the ring baffle B2. The radius given by the theory was 9 cm. for the case of an object point O and an image I symmetrically placed 12 cm. apart on the axis, in a field in which the distance PQ between the foci of the confocal spheroids was 20 cm.

These dimensions were used in the design, the gap between the magnet poles being set at 16 cm. The equivalent hyperboloids 16 cm. apart at the vertices are shown in Figure 1 and the actual magnet profile in Figure 3.

\* The measurements made with the 'short' slit, with Figures 3, 4 and 5, were presented in a paper read at the Edinburgh Meeting of the Physical Society of 19th February, 1949.

The momentum-resolving action of the baffles can be seen by considering first a 'central' ray, defined as a ray falling normally on the mid-plane, half-way between the pole-pieces. The central ray of the selected mono-energetic sheaf is inclined at  $81^\circ$  to the axis at O. After traversing the ring-slit B1B2 it reaches I by a path symmetrical about the mid-plane. The central rays of sheaves of other energy would be stopped either by B1 or by B2 which also stop all rays of lower energy. The non-central asymmetrical rays of higher energy can still enter B1B2 obliquely but most of them will be stopped by the second set of baffles B3 and B4, which define the angular width of the accepted sheaf.

## § 2. COMPARISON WITH A THIN MAGNETIC LENS

Some insight into the nature of the correction of spherical aberration at large angles may be gained by considering the passage of the thin wide-angle sheaf of Figure 1 through a thin magnetic lens. The real image would then have a large aberration with two focal lines. The first, a focal ring round the axis, is the figure of revolution formed from the meridional intersection of the sheaf where it touches the caustic, while the second is a short straight line along the axis. The radius of the focal ring increases rapidly with the angle of emission  $\alpha$  and the sign of the aberration is positive because rays with larger  $\alpha$  return to the axis nearer to O.

Let the field now be transformed to the spheroidal form, with a strength chosen to focus the mono-energetic sheaf from O on the axis, as in Figure 1. The focal ring will have migrated to the mid-plane and, if the sheaf is thin, the axial focal line will have shortened to a point. The shortened second focal line is now both an axial and a second meridional intersection of the sheaf and so constitutes a three-dimensional point image of the particular object point O.

The point image I will in general only be partially corrected. In the special case in which O and I are equidistant from the mid-plane, perfect correction is possible if certain conditions of symmetry and reversibility of rays between O and I are satisfied. Consider two rays emitted at angles  $\alpha_1$  and  $\alpha_2$ , above and below the central ray of the same mono-energetic sheaf. Let these two rays be incident on the mid-plane at angles  $i_1$  and  $i_2$  at the same point. Then, if  $i_1 = -i_2$ , the symmetry of the field ensures that the part of one ray lying on one side of the mid-plane will be a mirror image in that plane of the part of the other ray lying on the other side. Hence, both rays pass through O and I. Several such symmetrical pairs of rays must form an envelope which is also symmetrical about the mid-plane and the extent of its symmetrical part will be a measure of the range  $\Delta\alpha$  over which correction holds good. A point image at I will certainly exist for a small  $\Delta\alpha$  if the envelope has a horizontal tangent where it crosses the mid-plane.

A second symmetry property is shown by the central rays which, being incident normally, are necessarily mirrored in the mid-plane. If the baffles are removed, all central rays from O converge to a perfect image at I, which is achromatic since these rays all have different energies.

In the spectrometer the radius of the ring-slit B1B2 is chosen to be a little larger than is appropriate for a point image. The resulting astigmatism introduces a second focal ring which is adjusted to fall on the ring-slit S around the counter (Figure 4). The second meridional cross-over at this ring reverses the order of the rays at the axis so that the spherical aberration is now negative.



The use of a partially corrected wide-angle sheaf makes possible an increase in the solid angle of collection. Suppose that  $\Delta\alpha_0$  is the semi-angular width of a paraxial beam which can be focused without intolerable aberration and that  $\Delta\alpha$  is the corresponding thickness of a wide-angle sheaf. The ratio of the two solid angles is  $\Delta\alpha_0^2 : 2\Delta\alpha \sin\alpha$ . If  $\Delta\alpha_0$  and  $\Delta\alpha$  are small and nearly equal it is clear that an appreciable gain is possible in passing from paraxial to wide-angle conditions of operation.

### § 3. THE QUALITY OF THE IMAGE AND THE POSSIBILITY OF MAGNIFICATION

The question arises of the applicability of this kind of magnetic reflection to forming sharp magnified images with an appreciable solid angle of collection. It is usually considered impossible to correct an electron beam for spherical aberration in a system consisting of any combination of electrostatic and magnetic lenses. This is because each component of the system always has a positive spherical aberration. However, Cosslett (1946) has remarked that an electrostatic electron mirror has negative spherical aberration so that a combination of mirror and lens is potentially capable of correction. This suggests that the correction of a particular zone in the present case may be due to some combination of lens and mirror action.

In order to make a rough estimate of the quality of the image formed of a small disc source at O, with its normal along the axis, we adopt a simple aspherical mirror as the equivalent optical instrument and leave any lens action out of account. This would be fully justified if all the bending occurred suddenly, at the first cross-over, as in specular reflection. In fact, the bending has a broad maximum near the cross-over and then falls smoothly to zero at the axis, where the bottom of the meridional potential valley is flat. However, as the mirror gives values for the inclinations of conjugate rays at O and I in rough agreement with the computed trajectories, it should also give an approximate description of the conjugate rays through neighbouring points, which build up the image.

The symmetry of the sheaf in Figure 1 with respect to the mid-plane means that the part of the aspherical mirror selected by the ring-slit B1B2 must have all its centres of curvature in that plane. The fact that this ring zone of the mirror is able to form an aberration-free image of O shows that these centres of curvature must coincide with those of the particular aplanatic surface for reflection from O to I which is tangential to the mirror round the ring. This surface is the well-known prolate spheroid with foci at O and I which passes through the slit B1B2 and satisfies Fermat's principle.

The mid-plane is not the only site of the ring-slit which gives aberration-free images of O. The slit may be moved along the axis and its radius adjusted to form again a sharp image I. The ring B1B2 now defines a zone of a spheroidal aplanatic surface which is no longer equatorial so that the magnification is not unity. By considering the image formation using different zones we can get what is an 'upper limit' to its quality, because additional defects such as the equivalent of chromatic aberration are present in the electron-optical case.

Proceeding in this way it is evident that the imaging of an area near O is very poor because the image of a point distant  $\Delta r$  from O has meridional and sagittal intersections which are separated by distances of order  $2\Delta r$ . The image can easily be drawn for rays which intersect the axis, using successive zones of the

spheroid. It is erect and of unit magnification for the equatorial zone. As the reflecting zone is moved towards the image end of the spheroid, the image of a disc becomes a cone which finally turns into an inverted diminished disc. Most of the intensity at the image, however, is due to the skew rays which do not intersect at the same points as the axial rays. The only case giving a common intersection is the final polar site of the zone, when the arrangement becomes an ordinary concave mirror giving a paraxial image.

The image diffuseness is connected with a failure to satisfy the Abbe sine condition for aplanatic imaging with absence of coma, except in the paraxial polar zone near the long axis. Since this zone is obstructed by the magnet pole-piece, there seems little practical possibility of getting good images. This is in accord with the work of Schwarzschild (1905) and others who have shown that aplanatic wide-angle imaging by a single mirror is impossible but that it can be obtained if two reflections are used, arranged for mutual correction as in the reflecting microscope (Burch 1947).

From the point of view of  $\beta$ -spectroscopy it seems that the best image of a disc will be a diffuse sphere of similar radius  $r$  so that the resolution will not be improved by making the collecting slit  $S$  much narrower than  $r$ . By working with the ring-slit B1B2 displaced from the mid-plane towards the image, a small advantage may, however, arise from the magnification being less than unity.

#### § 4. THE USE OF OTHER SHAPES OF FIELD

Wide-angle focusing is clearly possible for field shapes differing from the spheroidal form. The criterion is that the surfaces of equal vector potential must delineate the contours of a bowl-shaped meridional potential barrier with a curvature capable of reflecting a diverging beam of incident particles back to a single point on the axis. The appropriate sheaf of rays must be selected by ring-baffles with radii chosen to bring the second cross-over on to the axis.

A quite different shape of field has recently been shown by the independent experiments of Slätis and Siegbahn (1949) to give wide-angle focusing. They keep the radius of the ring-slit B1B2 fixed and vary the shape of the field by adjusting the ratios of the currents flowing in five adjacent short coaxial coils. The contours of the meridional barrier may be plotted from the published diagram of the magnetic lines of force.

Two features of the focusing distinguish this from the spheroidal case. First, the bending of the trajectories in the rotating meridional plane, instead of being greatest near the first cross-over, has two well separated maxima about 8 cm. from each of the poles (which are 61 cm. apart). Secondly, the contours in the regions of strong bending are convex towards the axis and so have curvatures opposite to those of the rays which cross them. This antithesis is characteristic of the short magnetic lens but not of the spheroidal field in which the contours are concave to the axis between the poles.

The lines of equal vector potential are very similar to those of the field plotted in Figure 2(a) due to two coils of one turn separated by a distance of twice their diameter, obtained by the graphical method of Størmer (1933). It is thus clear that wide-angle focusing can also be obtained using two thin magnetic lenses placed near the object and image, with an interposed ring-slit B1B2 to select the first cross-over in the mid-plane.

## § 5. AN EQUIVALENT REFRACTING OPTICAL INSTRUMENT

For fields such as that of Slätis and Siegbahn, in which the first ray cross-over does not take place in a region of strong bending, the analogy with reflection at an aspherical mirror is not close. It is, however, possible with a very simple refracting device to reproduce crudely the feature of a cross-over at some distance from the axis, taking place between two refractions which bring a wide-angle sheaf from O back to an aberration-free point image I. This alternative to the mirror is the thick symmetrical lens of Figure 2 (b).

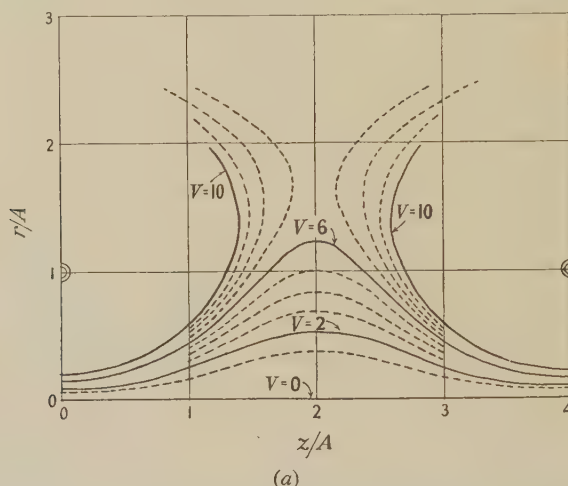


Figure 2 (a). The field of two equal circular currents of radius  $A$  placed coaxially  $4A$  apart, showing the lines of equal magnetic vector potential and equal potential energy  $V$  in the rotating meridional plane.

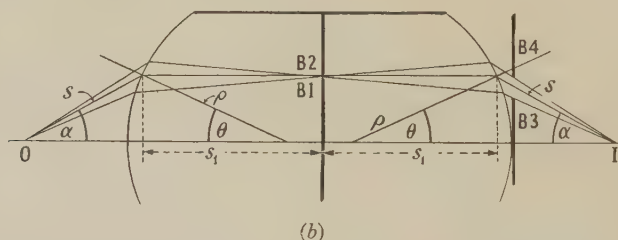


Figure 2 (b). An optical analogue of wide-angle focusing in a field of the type shown in Figure 2 (a) in which a focal ring is isolated inside a thick lens. The vertical scale is exaggerated, an actual set of values in equation (1) being  $n=2.24$ ,  $\rho=12.6$  cm.,  $s_1=18.76$  cm.,  $\theta=23.38^\circ$ ,  $\alpha=39.43^\circ$ .

Define a 'central' ray of the sheaf from O as a ray which is refracted parallel to the axis inside the lens. Then the large positive spherical aberration will cause a pencil from O which includes a central ray to intersect again in a focal line perpendicular to the meridional plane. The pencil, if rotated around the axis, sweeps out a wide-angle sheaf which now intersects in a focal ring. If we choose the thickness of the lens so that this ring lies in its mid-plane then, by symmetry, all the meridional pencils leaving points on the focal ring are brought to a second intersection on the axis at I, which is both meridional and axial and so is an aberration-free point image of O. The focal ring and the width of the sheaf must be defined by ring-baffles B1B2, B3B4, as in Figure 1. As the refractive index determines the position of the ring, the instrument will select a narrow range of wavelength.



The half-width of the lens can be found easily from the two standard equations for astigmatism at a spherical refracting surface (Flint 1936). On inserting the condition that the axial intersection is at infinity, appropriate because the central ray is parallel to the axis, the equation for  $s_1$ , the distance of the meridional intersection from the lens surface, reduces to

$$s_1 = \frac{s \cot^2 \theta}{n} = \frac{\rho \cot^2 \theta}{n [n \cos \theta - (1 - n^2 \sin^2 \theta)^{1/2}]} \dots\dots (1)$$

Here  $\rho$  is the radius of the surface,  $n$  the refractive index and  $s$  and  $\theta$  are as indicated in Figure 2 (b).

This method of selecting an intermediate focal ring and so neutralizing the aberration of a wide-angle sheaf, should be feasible with more general optical systems having many different magnetic analogues.\*

All systems in which the order of the rays is reversed by an intervening meridional cross-over resemble a mirror in being contra-current and in failing to satisfy the Abbe sine condition with a wide-angle sheaf, so that the images of off-axis points will be blurred.

It is possible that systems in which the first cross-over occurs between two regions of sharper bending are less adaptable for other than unit magnification than are more mirror-like systems in which the sharpest bending is near the cross-over.

#### § 6. CHOICE OF POLE-PIECE SHAPE

Unless large diameter coils and cores are used the outward leakage of flux round the edges of the pole-pieces distorts the inner part of the field from the spheroidal form. This effect can be much reduced if peripheral ridges are used as shown in Figure 4. The pole profile was chosen after a study of the magnetostatic equipotentials by the electrolytic tank method of solving Laplace's equation.

A full-scale wooden model was made of a portion of the magnet, with conducting surfaces to represent the known equipotentials. It was assumed that the pole-faces were equipotentials and that the 9-in. long cylindrical iron cores inside the magnetizing coils had a uniform axial potential gradient. The rest of the iron circuit was given the potential of the mid-plane half-way between the poles. These assumptions were tested roughly by plotting the actual lines of force with a compass.

In order to have good axial symmetry, the return part of the magnetic circuit consists of 12 flat soft-iron plates, each 12 in. wide, securely flanged on to dodecagonal end-plates of 48-in. diameter.

The symmetry of the dodecagon makes it possible to reproduce the equipotentials by using a model of a 30° sector of the magnet in a tank tilted at this angle.

The shape of the model pole-face was changed until it gave the equipotentials drawn in Figure 3 which show only small deviations from hyperbolae in the region traversed by the  $\beta$ -rays.

To avoid changes in the shape of the field with changing intensity of magnetization it is necessary to operate far from saturation so that the

\* Bothe (1950 a, b) has recently treated the formation of a focal ring between two thin magnetic lenses by assuming that the deviation  $d$  of a ray occurs suddenly as it crosses the mid-plane of each lens and that  $d$  may be expressed as a power series in the radial distance ( $r - r_0$ ) of the point of crossing from a corrected ring-zone of radius  $r_0$ . This leads to expressions for the effect of slit-width on the aberrations and on the resolving power.

permeability remains high at the pole-faces. With the available coils with 7-in. diameter cores the upper limit of the spectrometer was thus fixed at about 1.5 mev.

### § 7. THE GEIGER-MÜLLER TUBE

The Geiger-Müller tube is designed to accept rays incident perpendicularly all round the axis over a range of about  $290^\circ$  of azimuth. The anode wire of 0.1 mm. diameter lies along the axis and the cathode cylinder of 1 cm. inside

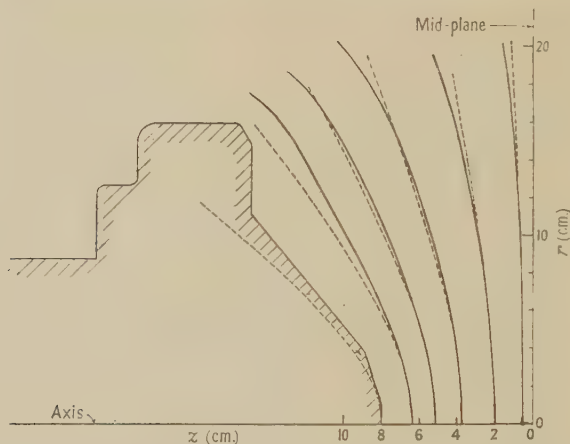


Figure 3. Magnetostatic equipotentials (—) plotted using the electrolytic tank, compared with the hyperbolae (---) of the spheroidal field.

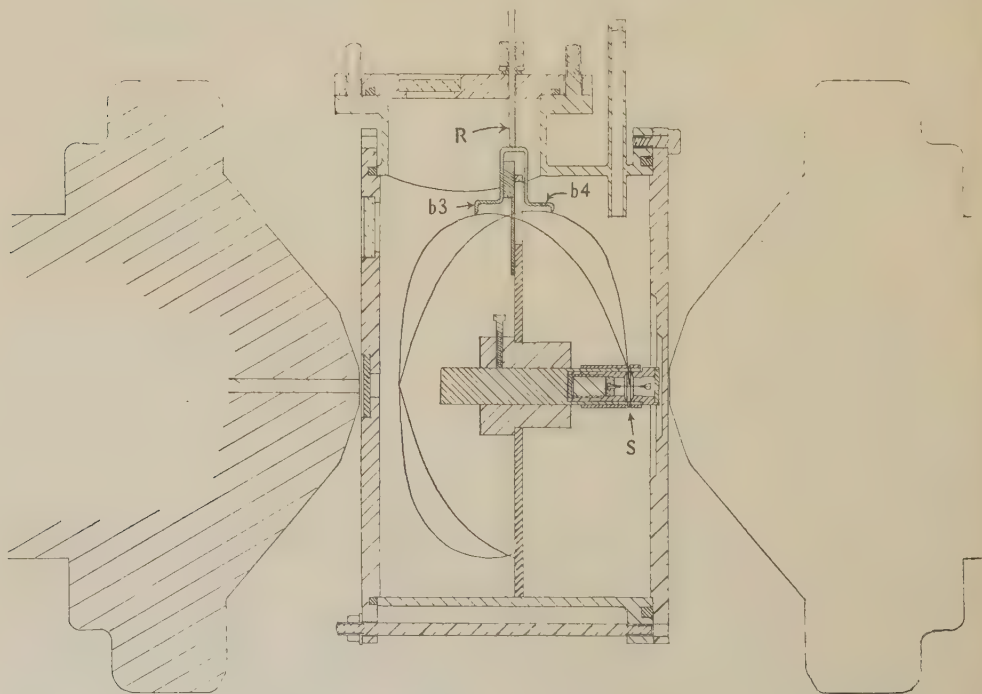


Figure 4. An axial section of the spectrometer showing the preliminary 'short' slit attached to its driving rod R giving a small radial motion.

and 1.5 cm. outside diameter receives the rays through a ring-window 2.4 mm. wide cut round its circumference and crossed by three bridge-pieces necessary for mechanical strength. The bridges obstruct about  $70^\circ$  of azimuth and one of them serves as a seating for a joint in a nylon film of  $0.5 \text{ mg/cm}^2$  which is clamped round the cathode cylinder with a rubber gasket seal about 0.3 mm. thick. When the tube is filled with argon and alcohol vapour at 12 cm. pressure, the plateau is about 200 volts long and the background counting rate is 6 per minute. The insulating bushes are of quartz and polystyrene and the tube is joined to a gas reservoir of about 150 ml.

Although the cathode is irregular in shape, the plateau for focused  $\beta$ -rays is remarkably flat (about  $0.01\%$  per volt), showing that the ions which they produce in their passage across the tube reach the middle part of the wire where the electric field is highest. In contrast the unfocused  $\beta$ -rays ejected by a  $\gamma$ -ray source give a plateau with a slope as large as  $0.25\%$  per volt.

Encircling the ring-window is the narrow collecting ring-slit S of diameter 2.2 cm., on to which the  $\beta$ -rays are focused.

### § 8. RESOLVING POWER TESTS

It was first necessary to find the correct radius for the ring-slit B1B2 to give a sharp focal ring round the counter slit S. The value predicted by the theory was 9.1 cm. but the actual field is not truly spheroidal. To allow the radius to be varied, a short portion of a ring-slit 1.25 cm. long, corresponding to  $8^\circ$  of

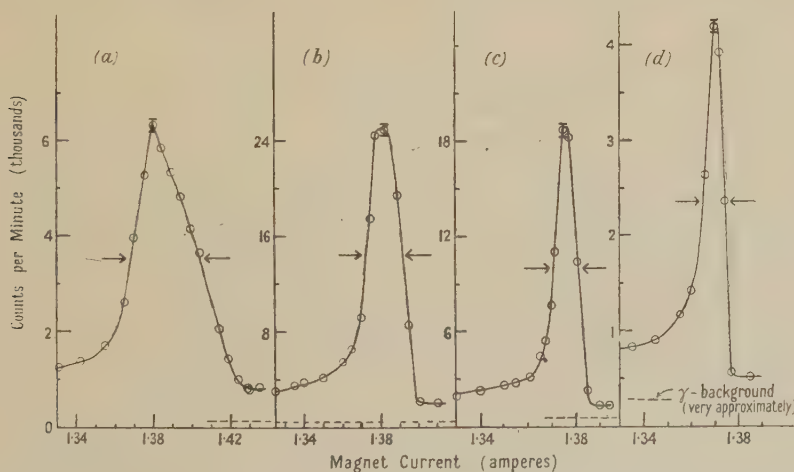


Figure 5. Measurements of the F line of thorium B with the short preliminary slit B1B2. The values of the three parameters, viz. line-width at half-height,  $\Delta(H\rho)/H\rho$ , slit-width B1B2 (mm.), and source diameter (mm.), in that order are as follows for the four lines: (a) 1/40; 2.2; 2.0; (b) 1/75; 2.2; 1.0; (c) 1/143; 0.95; 1.0; (d) 1/200; 0.95; 0.34. A solid angle of about  $2.5\%$  of  $4\pi$  was found for line (b) when normalized to correspond to collection over  $290^\circ$  of azimuth instead of the  $8^\circ$  accepted by the short slit.

azimuth, was machined to a radius of 9 cm. and provided with a radial sliding motion and a driving rod, shown in Figure 4, passing through a rubber vacuum gland. Wing-like baffles b3 and b4 were attached to the slit and moved with it. They did the work of B3 and B4 in Figure 1 by defining the width  $\Delta\alpha$  of the accepted sheaf and excluding rays of higher momentum.



An advantage of a short slit is that the image it forms is not sensitive to small deviations from axial symmetry so that it should give an upper limit of attainable resolving power.

The correct radius of B1B2 was found to be 1 or 2% larger than the predicted value. Some shapes of the F-line of thorium B at 0.148 mev. are shown in Figure 5. Fairly high resolutions are possible with a disc source which is sufficiently small.

The preliminary short slit has now been replaced by a nearly complete annular slit built up of 18 movable 20° sectors possessing a concentric radial motion of about 3 mm. to permit adjustment.  $\beta$ -ray lines found with this annulus are shown in Figure 6.

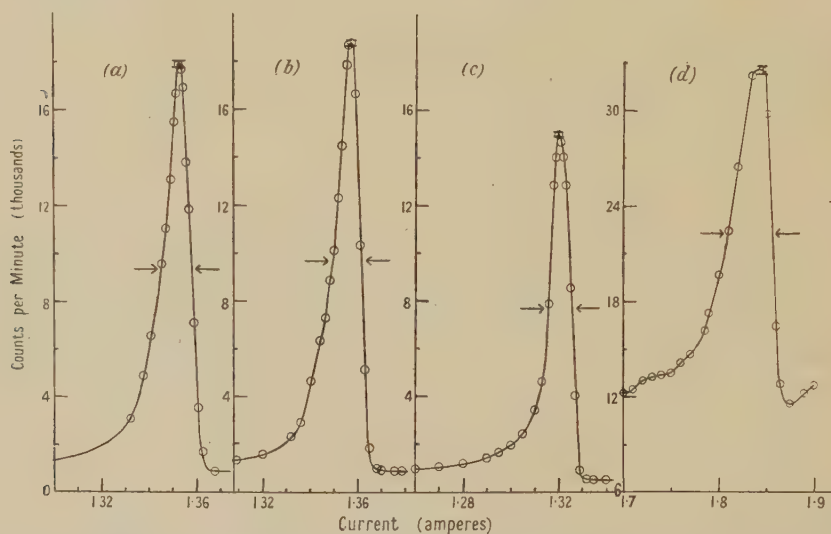


Figure 6.  $\beta$ -ray lines measured with the complete adjustable ring-slit B1B2 set at a radius of 9.3 cm. and a width 0.7 mm. Line (a) had this slit in the mid-plane with B3B4 of width 1 cm. and radius 7 cm. In (b) and (c) B1B2 was displaced from the mid-plane 5 mm. towards the image. In (c) only 100° of azimuth was used and B3B4 was narrowed to 3 mm. at a radius of 4.5 cm. In these lines the source diameter was 0.34 mm. and the  $\gamma$ -ray background was negligible. The values of  $\Delta(H\rho)/H\rho$  and the solid angle  $\times 1/4\pi$  normalized to 290° of azimuth were: (a) 1/104; 0.8%; (b) 1/113; 1.36%; (c) 1/140; 0.75%.

Line (d). The H line (1925  $H\rho$ ) of radium B, taken with a thin radon tube lying along the axis, of diameter 0.25 mm. and length 8 mm.

The large solid angle of collection makes it possible to work with only a fraction of the 360° range of azimuth  $\phi$  when broadening due to axial asymmetry is suspected. Figure 6(c) shows a resolution of 1 in 140 obtained using a range of  $\phi$  of about 100° selected by closing part of the smaller ring-slit B3B4.

#### § 9. PROCEDURE FOR CENTRING AND ADJUSTMENT

The alignment of the pole-pieces was verified by passing pointed test rods through  $\frac{1}{4}$ -in. test holes bored accurately along their axes. The centring of the Geiger tube and other parts was checked by these rods or by sighting through the  $\frac{1}{4}$ -in. holes in the pole-pieces. The axial symmetry of the field was tested by swinging a search coil around the axis.

A striking feature of the focusing is the narrowness of the beam which enters the receiving slit S. This can be shown by moving the source along the axis and

finding the variation in counting rate as in Figure 7(a). For small axial motions  $\Delta z$  of the source we can expect an equal but opposite displacement  $-\Delta z$  of the image, if the ring slit B1B2 is in the mid-plane. This behaviour is a consequence of reflection which makes the system 'contra-current'. The curves show that the counting rate from a disc source is appreciable over a region  $\Delta z$  of length about 0.5 mm. If we subtract from this the width 0.35 mm. of the collecting slit S we see that the focal ring at S must be very narrow. The curves were obtained with slit widths of 0.7 mm. at B1B2 and 6 mm. at B3B4, using a flat part of a continuous  $\beta$ -spectrum to ensure that the number of incident rays entering the ring B1B2 did not vary with source position. The beam at S broadens markedly if the centring is poor.

It is clearly necessary to adjust the axial position of the source with care. This may be done by moving it longitudinally by a screw, passing through a vacuum

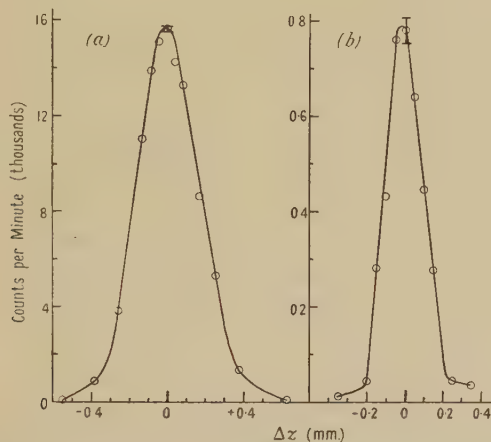


Figure 7. Longitudinal adjustment curves, showing the thinness of the sheaf near the 0.35 mm. wide collecting-slit S. (a) Axial displacement of the source alone, reckoned positive towards the counter. (b) Displacement *en bloc* of source, counter and slits.

The tail at the right of curve (b) is due to a small 'stray' radioactivity on the sides of the  $\frac{1}{8}$  mm. platinum wire, whose flat polished end received the active deposit from thoron. In (a) the deposition occurred through a masking hole of  $\frac{1}{8}$  mm. diameter, on to a larger disc.

gland, until the peak counting rate is found. A simple alternative is to move the whole vacuum tank axially between the magnet poles. A curve found in this way is shown in Figure 7(b) and is narrower than curve (a), presumably because the previously mentioned 'contra-current' motion of the image is now combined with an opposite 'concurrent' motion of the counter slit.

The width and triangular shape of these curves suggest that most of the incident beam is spread evenly over a width  $\Delta z$  nearly equal to that of the collecting slit S. This width of 0.35 mm. is nearly equal to the diameter of the disc source, and so is in rough agreement with the estimated image diffuseness.

#### § 10. RESOLVING POWER WITH AN AXIAL LINE SOURCE

The remarkable result that rays are only counted if they come from a region of the axis within about 0.6 mm. of the object point O allows fairly good resolution to be obtained from a long line source along the axis. The source is effectively shortened by the selecting action of the slits. The shape of the 0.264 mev. H-line of radium B is shown in Figure 6(d). This was obtained with a glass radon tube

of about  $3.5 \text{ mg. cm}^2$  wall thickness. This thickness of glass should give a standard straggling curve with a width at half-height of about  $H_p/90$ , according to White and Millington (1928). This accounts for only 10% of the width of the line, to which it contributes as a statistically independent source of variance.

#### § 11. FOCUSING WITH LESS THAN UNIT MAGNIFICATION

The lines shown in Figures 6(b), (c) and (d) were obtained with the ring-slit B1B2 displaced from the mid-plane about 5 mm. towards the counter. In such a case the angle of emission  $\alpha_1$  at O will be less than the angle  $\alpha_2$  at entry into the counting slit S and the focused sheaf will no longer fall normally on the mid-plane. Such an unsymmetrical arrangement makes it possible to study rays coming from the source at smaller values of  $\alpha_1$  than  $80^\circ$ .

#### § 12. TESTS OF THE SOLID ANGLE OF COLLECTION

Experimental values for the solid angle are attached to some of the curves in Figures 5 and 6. Each value assumes that the rays are collected over a range of azimuth of  $290^\circ$ , the full limit of the Geiger tube. For the 'short' slit in Figure 5 the absolute source strength was found by counting the  $\alpha$ -rays with a spark counter kindly made available by Dr. R. D. Connor. In the other cases they were counted with a proportional counter insensitive to  $\beta$ -rays.

The values given are probably lower limits because the slit S was rather narrower than was justified by the aberrations and errors in centring. In such a case widening the slits would at first increase the solid angle without much loss in resolution.

#### ACKNOWLEDGMENTS

We wish to thank Messrs. Colvilles Limited and the Torpedo Experimental Establishment, Greenock, for their help in manufacture and also Mr. C. D. Mollison and other colleagues of the technical staff. We are greatly indebted to Professor Feather for his constant encouragement and to Mr. D. A. Silverston for lending a very thin radon tube.

#### REFERENCES

- BOTHE, W., 1950 a, *Naturwissenschaften*, **37**, 41; 1950 b, *Sitz. Heidelberger Akad.*, 3 Abh., p. 191.  
 BURCH, C. R., 1947, *Proc. Phys. Soc.*, **59**, 41.  
 COSSLETT, V. E., 1946, *Introduction to Electron Optics* (Oxford: University Press).  
 FLINT, H. T., 1936, *Geometrical Optics* (London: Methuen), p. 152.  
 RICHARDSON, H. O. W., 1949, *Phil Mag.*, **40**, 233.  
 SCHWARZSCHILD, W., 1905, *Theorie der Spiegelteleskop* (Göttingen: Observatory).  
 SLÄTIS, H., and SIEGBAHN, K., 1949, *Ark. Fys.*, **1**, No. 17, p. 339.  
 STÖRMER, C., 1933, *Ann. Phys. Lpz.*, **16**, 685.  
 WHITE, P., and MILLINGTON, G., 1928, *Proc. Roy. Soc. A*, **120**, 701.



## Observations of Slow Mesons and Nuclear Disintegrations in Photographic Plates exposed under Carbon Absorbers

By J. C. BARTON, E. P. GEORGE AND A. C. JASON

Birkbeck College, University of London

*MS. received 27th June 1950*

**ABSTRACT.** The exposure was made at the Jungfraujoch, altitude 3,457 m., using Ilford type C2 nuclear research emulsions. The frequency of stars under thicknesses of carbon up to  $220 \text{ gm/cm}^2$  was measured, the experimental value of the absorption length of the radiation causing them being  $166 \pm 8 \text{ gm/cm}^2$ . The proportion of the stars due to fast  $\pi$ -mesons has been evaluated and, on subtracting this proportion, the absorption length of the radiation responsible for the remainder is found to be  $143 \pm 10 \text{ gm/cm}^2$ . The energy distribution of the stars having from 3 to 20 tracks is found to be of the form  $dE/E^{2.6}$ , with no apparent discontinuity. The frequencies of slow  $\pi$ - and  $\mu$ -mesons at various depths is reported. The  $\pi$ -mesons exhibit a transition effect which is interpreted in terms of their production in stars occurring in the carbon absorber. The ratio of negative to positive  $\pi$ -mesons is found to be 3.1 to 1.

### § 1. INTRODUCTION

IN a recent paper (George and Jason 1949a) an account was given of experiments with Nuclear Research photographic emulsions exposed under lead absorbers to the cosmic radiation at the Jungfraujoch at a height of 3,457 m. In the present paper we describe similar observations on emulsions exposed under carbon absorbers, also at the Jungfraujoch. For brevity we shall continue to refer to the strongly interacting component of the cosmic radiation causing the disintegration 'stars' as the 'N-radiation'.

A comparison of the absorption of the N-radiation in lead and in air had led us to the conclusion that the N-radiation consisted of nucleons. From the cloud chamber observations of Blackett, W. M. Powell and Hazen, it was thought that protons formed only a small part of the N-radiation, and that most of the stars were therefore produced by cosmic-ray neutrons. A similar conclusion was also published by Bernardini, Cortini and Manfredini (1949).

Perkins (1947) and Bielovitski *et al.* (1949), on the other hand, have suggested that the stronger absorption of the N-radiation in air than in lead might be due to the fact that the particles of the N-radiation were unstable. This would then give an absorption anomaly similar to that reported by Rossi, Hilberry and Hoag (1940) for the  $\mu$ -mesons.

The present investigation was undertaken in order to decide between these viewpoints by comparing the absorption of the N-radiation in air and carbon. The preliminary results, consistent with the nucleon hypothesis, were communicated to the Cosmic-Ray Conference at Bristol. A more detailed account of the observations is given here, together with a discussion of the transition effects in carbon observed for the  $\pi$ - and the  $\mu$ -mesons.

## § 2. EXPERIMENTAL

The absorber was constructed of bricks of compressed coal dust, built up in three cylindrical sections in the manner indicated in Figure 1. The plates were exposed with the plane of the emulsion vertical and were placed at various depths in the absorber at intervals of about  $50 \text{ gm/cm}^2$ , as shown. An additional packet of plates at the bottom of the absorber was screened with a further  $7.5 \text{ cm. Pb}$ . The shape of the pile was chosen so as to give, as nearly as possible, a constant path length in the absorber for N-radiation incident at angles less than  $45^\circ$  from the vertical. The errors introduced by the absorber geometry at angles greater than  $45^\circ$  are discussed below. The pile was covered with roofing felt to prevent water from melting snow dripping into the cracks between the bricks. Ilford Nuclear Research plates, type C2, 100 microns thick were used. Each packet was supplied

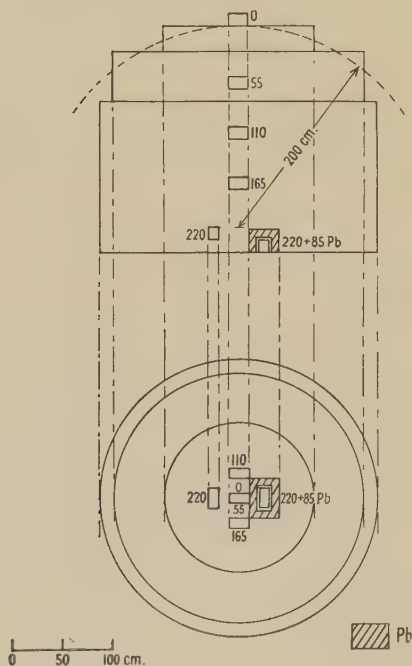


Figure 1. Arrangement of carbon absorber.

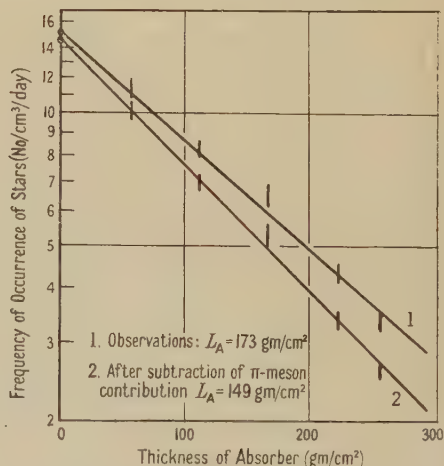


Figure 2. Frequency of 'stars' plotted against absorber thickness.

with an electrical heater, and, using a distant reading thermometer, the temperature of the plates was maintained between the limits of  $10^\circ$  and  $25^\circ \text{ C}$ . In order to minimize the effect of the background events accumulated while they were not in the absorber, the plates were taken to Switzerland on the day of manufacture, and were processed at the Jungfrauoch immediately on removal from the absorber. Corrections for the background, amounting to a few per cent, have been applied where appropriate.

The absorber was built on the edge of the main roof of the Scientific Station in order to minimize the screening effect of local rocks. The roof beneath consisted of granite and concrete and was about  $60 \text{ cm.}$  thick. Throughout the experiment the absorber was kept clear of snow, which fell frequently.

A sample of the coal was analysed and the results are shown in Table 1.

Table 1. Analysis of Coal Absorber

Constituent % by weight	H	C	N	O	S	Moisture	Ash
	3.9	80.9	1.9	0.2	2.0	1.3	9.8

Although impurities constitute 19% of the total weight, fortunately they consist mostly of substances with atomic weights close to that of carbon. The absorption length  $L_A$  in gm/cm<sup>2</sup> of the N-radiation in the coal would be 4% greater than the value for pure carbon, assuming  $L_A \propto A^{1/3}$ . Our final result, therefore, will be reduced by 4% in order to give the value of  $L_A$  for carbon.

### § 3. EXPERIMENTAL RESULTS CONCERNING THE NUCLEAR DISINTEGRATIONS

The plates were examined microscopically, using 4 mm. objectives. Nuclear disintegrations giving rise to 'stars' of three or more tracks, of which at least one was longer than 60 microns, were recorded. In this section we give the experimental results concerning (i) the frequency of occurrence of stars at various depths in the absorber, and (ii) the size-frequency distribution of the stars.

#### (i) Frequency of Occurrence of Stars as Function of Depth

The frequencies of occurrence of stars at various depths in the absorber are given in Table 2. The stars produced by  $\pi^-$ -particles at the ends of their ranges are not included in this Table. The upper set of points in Figure 2 shows the logarithm of the star frequency plotted against thickness of absorber.

Table 2

Absorber thickness $T$ (gm/cm <sup>2</sup> )	0	55	110	165	220	220 C + 85 Pb
Number of stars	1837	417	652	258	415	533
Frequency per cm <sup>3</sup> /day	15.2 $\pm 0.35$	11.4 $\pm 0.56$	8.3 $\pm 0.33$	6.53 $\pm 0.41$	4.35 $\pm 0.21$	3.37 $\pm 0.15$

In plotting the last point, we have assumed the  $A^{1/3}$  law connecting absorption length with atomic weight. On this basis 85 gm/cm<sup>2</sup> Pb is equivalent to 33 gm/cm<sup>2</sup> C. From Figure 2 we deduce the absorption length of the N-radiation in the material of the absorber to be  $L_A = 173 \pm 8$  gm/cm<sup>2</sup>. This must be reduced by 4% to give the absorption length for carbon, with the result

$$L_A = 166 \pm 8 \text{ gm/cm}^2. \quad \dots\dots(1)$$

#### (ii) The Size-Frequency Distribution of the Stars

In previous communications (George and Jason 1949 a, b) we have plotted the logarithm of the frequency of occurrence of stars with  $n$  or more tracks,  $I(\geq n)$ , against  $n$  the number of tracks. The results appeared to lie on the two straight lines

$$\left. \begin{aligned} I(\geq n) &= I_0 \exp(-0.48n), \quad 3 \leq n \leq 8 \\ \text{and} \quad I(\geq n) &= 0.28 I_0 \exp(-0.33n), \quad n > 8. \end{aligned} \right\} \quad \dots\dots(2)$$

A similar result has been published by Page (1950). Taking the stars at all depths together, the present results may also be expressed in the same form.



The reason for the result (2) was never very clear, and we decided to plot the frequency of occurrence of stars against the energy released  $E$ , rather than against the number of tracks  $n$ . In order to do this we obviously need a relation connecting  $E$  with  $n$ . From observations on stars produced in 'electron sensitive' plates, a formula has been given by Brown *et al.* (1949b) of the form

$$E(\text{MeV.}) = 37n + 4n^2 \quad \dots\dots(3)$$

However, before using a formula of the type (3) to convert from an  $n$  scale to an  $E$  scale, two modifications have to be introduced for the following reasons: (i) due to

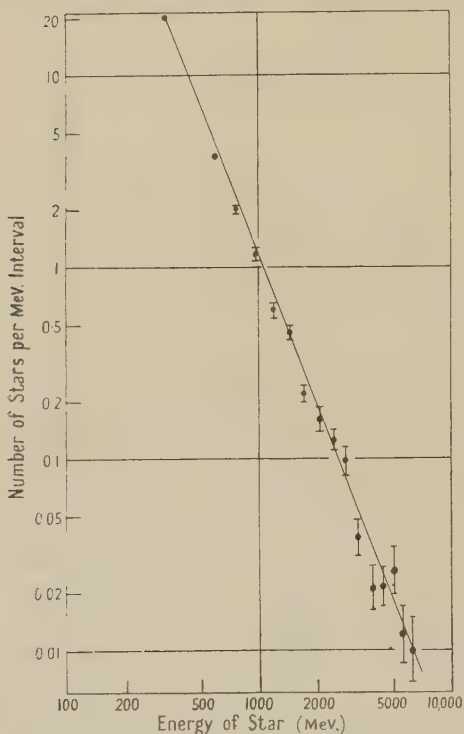


Figure 3. Differential energy distribution of stars.

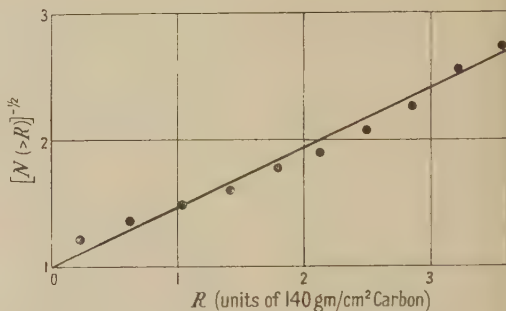


Figure 4. The dependence of  $[N(>R)]^{-1/2}$  on  $R$ .  $N(>R)$  is the integral range spectrum of  $\pi$ -mesons emitted from stars. The experimental points are those of Camerini *et al.* The full line is a plot of  $1 + R/b$ , with  $b = 2.12$ .

the limited sensitivity of the C2 plates, the value of  $n$  observed in our plates will be smaller than that in the plates of Brown *et al.*; (ii) as stated by Brown *et al.*, the energy total of the 'shower' particles has not been included by them.

Taking into account these two effects, we find that the relation between  $E$  and  $n$  in our plates may be represented approximately by

$$E(\text{MeV.}) = 26n + 12.8n^2. \quad \dots\dots(4)$$

The details of the argument leading to (4) are given in the Appendix. Figure 3 shows the differential energy distribution of the stars, plotted on a logarithmic scale. The energy has been obtained from the star size, using the relation expressed approximately by equation (4). It is seen that over a wide range of energy the differential energy distribution may be represented by the relation

$$I(E)dE \propto dE/E^\gamma, \quad \dots\dots(5)$$

where  $\gamma = 2.6 \pm 0.1$ .

## §4. DISCUSSION OF RESULTS CONCERNING NUCLEAR DISINTEGRATIONS

(i) *The Absorption of the N-Radiation*

From the absorption length of the N-radiation in air,  $L_A = 150 \pm 4$  gm/cm<sup>2</sup> (George and Jason 1949 b) and, assuming  $L_A \propto A^{1/3}$ , we deduce that the value of  $L_A$  for carbon should be  $L_A = 141$  gm/cm<sup>2</sup>. The result of the present investigation,  $166 \pm 8$  gm/cm<sup>2</sup>, appears to be significantly greater than the expected value. Thus we may conclude either that the assumption  $L_A \propto A^{1/3}$  is not valid in going from air to carbon, or that there is a small absorption anomaly due to unstable particles that produce stars in the carbon absorber but decay before doing so in the air. The extrapolation of the expected value of  $L_A$  is hardly likely to be in error over such a small range of atomic number and it therefore appears that the presence of unstable particles must be assumed.

It seems reasonable to attribute this excess of stars in carbon to the fast  $\pi$ -mesons emitted in the more energetic nuclear disintegrations (Brown *et al.* 1949 a). These are known to produce stars with an efficiency comparable with that of protons (Camerini *et al.* 1950), and hence must make some contribution to the star population observed in the carbon absorber. We now propose to evaluate this contribution approximately.

To do this we shall need the range spectrum of the emitted mesons. Sands (1950) gives this for mesons produced in the atmosphere in the form

$$N(>R) = \frac{b^\gamma}{(b+R)^\gamma} \text{ with } \gamma = 1.9. \quad \dots\dots (6)$$

Camerini *et al.* (1950) have shown that there is no appreciable difference in the energy spectra of the mesons produced in stars with different numbers of heavy branches, and that therefore the energy spectrum is, within the limits of measurement, independent of the nature of the nucleus in which the mesons are created. Also, they find good agreement with the spectrum given by Sands for the mesons produced in air. We may therefore take it that the energy spectrum of the mesons emitted in stars produced in the carbon absorber is the same as that found for stars produced in nuclear emulsion.

For the purpose in hand, i.e. the evaluation of a correction, we have assumed for simplicity  $\gamma = 2$ . Then we have attempted to fit an expression of the form (6) with  $\gamma = 2$ , to the data concerning the energy spectrum of  $\pi$ -mesons emitted from stars kindly supplied to us by Camerini *et al.* (1950), now published by them. For such a relation we should have, simply,

$$[N(>R)]^{-1/2} = 1 + \frac{R}{b}. \quad \dots\dots (7)$$

In Figure 4 we have plotted the empirical values of  $[N(>R)]^{-1/2}$  against  $R$  and it is seen that they may be reasonably well represented by an expression of the form (7). For later convenience we have chosen to take 140 gm/cm<sup>2</sup> as the unit of length in the carbon pile. Expressing  $R$  in terms of this unit,  $b$  has the value

$$b = 2.12. \quad \dots\dots (8)$$

We shall also need the angular distribution of the emitted mesons, but as yet no complete data are available and we have to proceed by assumption. One would expect the low energy mesons to be emitted almost isotropically, and those of high energy to be emitted at small angles to the incident particles, themselves strongly

collimated in the vertical direction. This would lead to a gradual change of the angular distribution with increasing energy of emitted mesons from the isotropic to the vertically collimated distribution.

In the next section we show that from the observations on the frequency of slow  $\pi$ -mesons stopping in the emulsions, approximately one-half of the emitted mesons fall into the low energy isotropic class. In order to display the main features of the argument we therefore make the assumption that mesons emitted with energy below the median value of their energy spectrum (270 mev.) are emitted isotropically, while those with energy greater than 270 mev. are collimated in the vertical direction. This is obviously a crude model, but it will serve to give us a reasonable approximation to the effects due to  $\pi$ -mesons on the star absorption curve.

Camerini *et al.* (1950) have shown that the interaction length of  $\pi$ -mesons of energy less than 1,500 mev. is close to that of protons of energy less than 600 mev. The mean free path of neutrons will presumably be the same as that of protons. Hence, in what follows, we assume that the mean free path of the  $\pi$ -mesons in the carbon absorber is the same as that of the stable N-radiation. A more refined calculation in which the difference in path length of mesons and nucleons is included is hardly justified at present.

We now calculate the contribution to the star population caused by  $\pi$ -mesons in the carbon absorber, neglecting the loss due to decay, which is negligible under the conditions of our experiment. The median range from (7) is given by  $R_0 = 0.414b = 0.88 = 123 \text{ gm/cm}^2$ . In view of the unit of length chosen ( $140 \text{ gm/cm}^2$ ), the frequency of stars at depth  $x$  produced by the stable component of the N-radiation may be taken as  $Ae^{-x}$  and for the purpose of this calculation we may put  $A=1$ . Let  $a$  be the number of mesons emitted per star. Those emitted with ionization range less than  $R_0$  are assumed to be isotropic, and the number of stars they produce at depth  $x$  will be given by

$$S_1(x) = \frac{a}{4\pi} \int_0^{R_0} \int_0^\pi [\exp - (x - R \cos \theta + R)] 2\pi \sin \theta \left[ \left( \frac{b}{b+R} \right)^2 - 0.5 \right] dR d\theta.$$

For  $x > R_0$ , this becomes

$$S_1(x) = 0.5 a e^{-x} \int_0^{R_0} \left( \frac{1 - e^{-2R}}{R} \right) \left[ \left( \frac{b}{b+R} \right)^2 - 0.5 \right] dR$$

or

$$S_1(x) = 0.27 a e^{-x} \quad (x > R_0). \quad \dots\dots(9)$$

For  $x < R_0$  the lower limit in the integration over  $\theta$  is modified and the integral for  $S_1(x)$  has been evaluated by numerical methods. We may express the result in general as

$$S_1(x) = a e^{-x} F_1(x) \quad \dots\dots(10)$$

and values of  $F_1(x)$  will be given after we have discussed the star contribution of the remainder of the emitted mesons.

For those mesons emitted with range greater than  $R_0$ , we are assuming that they are collimated in the vertical direction. Their integral range spectrum may therefore be written

$$\left. \begin{aligned} f(R) &= 0.5 && \text{for } R < R_0 \\ &= \left( \frac{b}{b+R} \right)^2 && \text{for } R > R_0. \end{aligned} \right\} \quad \dots\dots(11)$$



The star frequency at  $x$  due to all of these collimated mesons produced above  $x$  is

$$S_C(x) = ae^{-x} \int_0^x f(R) dR$$

$$\text{or } \left. \begin{aligned} S_C(x) &= 0.5axe^{-x} & x < R_0 \\ S_C(x) &= 0.5ae^{-x} \left[ R_0 + \frac{(b+R_0)(x-R_0)}{(x+b)} \right] & x > R_0. \end{aligned} \right\} \dots\dots(12)$$

Let us express this result as

$$S_C(x) = ae^{-x} F_2(x). \dots\dots(13)$$

In order to be able to derive numerical values from equations (9), (10) and (13) we shall need to know the value of  $a$  for carbon. The value for nuclear emulsion may be derived as follows: Table III of Brown *et al.* (1949 b) shows that the number of 'shower' particles per star is 0.25, while, according to Fowler (1950), at least 90% of the 'shower' particles are  $\pi$ -mesons. Hence there are at least 0.22  $\pi$ -mesons per star emitted with energies greater than 70 mev. To this we must add 0.05, representing the number of mesons emitted with energies less than 70 mev. (Fowler 1950), giving a total of 0.27  $\pi$ -mesons per star. This will err on the low side, but only by a small amount, since we have ignored those mesons emitted in stars with 0, 1 or 2 heavy branches. Thus we may take  $a = 0.27$  for nuclear emulsion at the

Table 3

$T$ (gm/cm <sup>2</sup> )	$x$	$aF_1(x)$	$aF_2(x)$	$S(x)$ $\{1 + aF_1(x) + aF_2(x)\}$
0	0	0.033	0	14.7 $\pm$ 0.35
55	0.393	0.073	0.052	10.1 $\pm$ 0.49
110	0.786	0.076	0.106	7.0 $\pm$ 0.28
165	1.18	0.080	0.156	5.28 $\pm$ 0.32
220	1.57	0.080	0.195	3.41 $\pm$ 0.16
253	1.81	0.080	0.215	2.60 $\pm$ 0.11
$\infty$		0.080	0.52	

Jungfraujoch, and we believe that the same value may be taken for carbon for the following reasons. From the number of slow  $\pi$ -mesons stopping in our emulsions we are able to deduce that there are 0.15 mesons per star in carbon emitted with a range less than 120 gm/cm<sup>2</sup> (cf. Harding and Perkins 1949 and § 6 (i) below). The centre packet of plates is screened by this amount of carbon in all directions. From the fact that the energy spectrum of the mesons produced is substantially the same in nuclear emulsion and carbon, and that 120 gm/cm<sup>2</sup> is the median value of the range spectrum (7), it follows therefore that the total number of emitted mesons is approximately twice the number deduced from those stopping, that is, the total number of emitted mesons in carbon must be close to 0.3 per star. We have chosen to keep to the measured value of  $a$  equal to 0.27.

In order to compare the results under carbon absorbers with those found for absorption in air, we must obviously eliminate the  $\pi$ -meson contribution. This is done by dividing the observed star frequencies by  $1 + a[F_1(x) + F_2(x)]$  with  $a = 0.27$ . The numerical values are given in Table 3.

The results corrected in this way are given in the last column of Table 3, and are plotted in Figure 2. The absorption length of the stars after elimination of the meson contribution is found to be  $149 \pm 10$  gm/cm<sup>2</sup> coal, corresponding to  $143 \pm 10$  gm/cm<sup>2</sup> carbon.

It therefore appears that if one subtracts the stars attributable to  $\pi$ -mesons generated in the carbon absorber, the absorption length of the radiation responsible for the remainder is very close to the value expected from the absorption of the N-radiation in air. This radiation may be taken to consist of nucleons. In dense absorbers there is an additional component of the N-radiation, the  $\pi$ -mesons. In absorbers of thickness up to several hundred gm/cm<sup>2</sup> at the Jungfraujoch, these  $\pi$ -mesons may contribute up to 30% of the observed star frequencies, and this contribution does not vary exponentially with depth. The resulting curve of the frequency of stars due to both nucleons and  $\pi$ -mesons together plotted against absorber thickness does not however depart very strongly from an exponential curve, but the absorption length deduced from this quasi-exponential will of course be greater than that for nucleons alone. In the atmosphere the  $\pi$ -mesons decay, in general, before causing further stars.

The above deals with the major contributions to the star population in dense absorbers of moderate thickness, but is by no means the whole story, since we know that the  $\mu$ -mesons also make a small contribution which under sufficiently thick absorbers may be quite important (George and Evans 1950). We estimate that the  $\mu$ -meson contribution is approximately 0.1 stars/cm<sup>3</sup>/day at the Jungfraujoch, which means that, because of their small absorption, they make the dominant contribution under carbon absorbers more than 700 gm/cm<sup>2</sup> thick. At this thickness of absorber, therefore, the departure from the exponential absorption of the N-radiation should be quite marked, the star frequency thereafter decreasing only in the slow manner characteristic of the hard component. The results of Barford *et al.* (private communication) on the star frequency under large thicknesses of ice show a departure from the exponential curve at this depth which might be explained by this  $\mu$ -meson contribution.

The possibility must be considered that stars may be caused by particles of the cosmic radiation other than the nucleons,  $\pi$ -mesons and  $\mu$ -mesons discussed above, for instance, photons, heavier mesons, etc. It would appear, however, that the contributions of these additional particles must be small, since the main features of the star absorption curve at all depths up to 6,000 gm/cm<sup>2</sup> can be understood without invoking them.

It has been found by Cortini and Manfredini (1949) and by Malaspina *et al.* (1950) that a maximum occurs in the transition curve for stars of three and four heavy branches at approximately 1 cm. Pb and approximately 2 cm. Al. No maximum is found for larger stars. This result has been interpreted by Dallaporta, Merlin and Puppi (1950) in terms of secondary neutrons generated in evaporation processes in the condensed material surrounding the plates. It is clear that the  $\pi$ -mesons discussed above must make some contribution to the frequency of the stars under these thicknesses of absorber, but on evaluating it from equations (9) and (13), the contribution is found to be much smaller than the magnitude of these transition maxima found experimentally. Thus the transition effect due to  $\pi$ -mesons discussed above is different from, and should not be confused with, the transition effect observed in small stars under small thicknesses of absorber.

#### (ii) *The Size-Frequency Distribution of the Stars*

It has been seen that when we convert the size distribution to an energy distribution, the resulting differential energy distribution of the stars may be represented by a power law of the form  $N(E)dE \propto dE/E^\gamma$  with  $\gamma = 2.6 \pm 0.1$ , for

values of  $E$  in the range 300 to 6,000 mev., corresponding to stars with from three to twenty branches in C2 emulsions. We note that a similar value for the exponent in the energy distribution of the  $\mu$ -mesons has been found by Wilson (1950). The use of equation (4) may have caused some fortuitous smoothing of the energy spectrum due to fluctuations, but this is hardly likely to account for the linearity of Figure 3 over such a wide range.

A simple interpretation of the observed energy spectrum of stars is that it is a reflection of the energy spectrum of the N-radiation, which in its turn is determined by the energy spectrum of the primary radiation. These would all be power spectra with the same exponent if the energy loss  $E$ , in a nuclear collision of an incident particle of energy  $E_0$ , were a homogeneous function of  $E/E_0$ . This latter assumption is one very frequently made in the literature (Clementel 1950, Heitler and Jánossy 1949 a, b). Granted its validity, then a primary energy spectrum of the form (5) would give rise to a similar distribution in the star energies and (apart from effects due to decay) in the energy spectra of the  $\pi$ - and  $\mu$ -mesons. This appears to be in agreement with the energy spectrum of the protons ejected from stars measured by Camerini *et al.* (1950), who have shown that the differential spectrum follows a power law of the form  $dE/E^{2.5}$  for values of the kinetic energy of the order of 1,000 mev.

The fact that the size distribution in C2 plates may be represented as the sum of two exponentials must be regarded as fortuitous. The interpretation in terms of an energy spectrum would appear to be far more logical, and in any case easier to understand. Other interpretations are not excluded, but we have none to offer.

## § 5. EXPERIMENTAL RESULTS CONCERNING SLOW MESONS

Mesons stopping in the emulsion were identified by means of their characteristic scattering and variation of grain density with range. They were classified according to their behaviour, following the scheme initiated by Lattes, Occhialini and Powell, into :

- (i)  $\rho$ -mesons: mesons stopping in the emulsion and not accompanied by tracks of secondary particles.
- (ii)  $\sigma$ -mesons: mesons stopping in the emulsion, accompanied by nuclear disintegrations at the ends of their ranges.
- (iii)  $\pi$ -mesons: mesons stopping in the emulsions, accompanied by the track of a secondary meson ( $\mu$ -meson) commencing at the end of the range of the first particle.
- (iv)  $\mu$ -mesons: the secondary particles arising from  $\pi$ -mesons above.

It is known that only 71% of negative  $\pi$ -mesons stopping in photographic nuclear emulsions give rise to recognizable 'stars'; the remainder are presumably captured by atomic nuclei with the resultant emission of neutrons only. Hence some  $\pi^-$ -mesons will be included in the category of  $\rho$ -mesons.

### (i) $\rho$ -Mesons

The  $\rho$ -mesons stopping in the emulsion and possessing a projected range greater than 60 microns were divided into two groups according to whether they entered the emulsion from above or below the horizontal. Then, using the geometric factor given by Lattes, Occhialini and Powell (1947), it follows that only 0.56 of the  $\rho$ -mesons stopping in the emulsion would be recorded. The observed numbers



were accordingly divided by 0.56 in order to give the total numbers of  $\rho$ -mesons stopping in the emulsion. The results at various depths in the absorber obtained in this way are given in Table 4.

The frequency of downward  $\rho$ -mesons at  $T=0$ ,  $4.15 \pm 0.25/\text{cm}^3/\text{day}$ , is in good agreement with the value  $4.1/\text{cm}^3/\text{day}$  reported by Camerini, Muirhead, Powell and Ritson (1948), also obtained using nuclear emulsions exposed at the Jungfraujoch.

Table 4

Thickness, $T$ , of absorber (gm/cm <sup>2</sup> C)	0	55	110	165	220	220 C + 85 Pb
Total $\rho$ -mesons downward/cm <sup>3</sup> /day	4.15 $\pm 0.25$	4.18 $\pm 0.43$	3.95 $\pm 0.28$	4.80 $\pm 0.47$	3.60 $\pm 0.25$	3.86 $\pm 0.21$
Total $\rho$ -mesons upward/cm <sup>3</sup> /day	0.54 $\pm 0.09$	0.46 $\pm 0.14$	0.33 $\pm 0.07$	0.46 $\pm 0.14$	0.34 $\pm 0.07$	0.26 $\pm 0.05$

These results may be compared with the number expected from the observations of various investigators using systems of Geiger counters. Thus if  $i_v$  is the number of mesons stopping per gramme of air per sterad per second in the vertical direction, under very thin absorbers, then since the slow meson intensity varies as  $\cos^3 \theta$  (Kraushaar 1949), and taking 4.0 as the density of C2 nuclear emulsion, we obtain the following expression for the expected number of  $\mu$ -mesons stopping per cm<sup>3</sup> per day in the emulsion:

$$i_v \times \frac{2\pi}{4.3} \times \frac{4}{1.5} \times 8.6 \times 10^4 = i_v \times 3.2 \times 10^5 \quad \dots\dots(14)$$

(the 1.5 in the denominator is the relative stopping power of air to emulsion). The earlier measurements of Rossi, Sands and Sard (1947) give

$$i_v = 1.8 \times 10^{-5} \text{ gm/sec/sterad}$$

at a height corresponding to the Jungfraujoch, while the more extensive measurements of Kraushaar give  $i_v = 1.3 \times 10^{-5} \text{ gm/sec/sterad}$ .

Using (14) these results give 5.8 and 4.2 respectively for the expected number of  $\mu$ -mesons stopping per cm<sup>3</sup> per day in the emulsion and these are seen to be in good agreement with the observed number of  $\rho$ -mesons.

The differential range spectrum of the downward stream of  $\rho$ -mesons is seen from Table 4 to be constant in the range 0 to 265 gm/cm<sup>2</sup> (for ionization loss 85 gm/cm<sup>2</sup> Pb = 45 gm/cm<sup>2</sup> C). By way of illustration, we assumed the frequency of mesons stopping to be the same at all thicknesses of the absorber, and then applied the  $\chi^2$  test to the observations to see whether they were consistent with this assumption. The best fit was obtained for an assumed constant value of 3.9  $\rho$ -mesons/cm<sup>3</sup>/day, and the corresponding value of  $\chi^2$  is 6. According to Fisher's tables, this value of  $\chi^2$  would be expected in 40% of the cases as a result of random fluctuations.

There are no measurements using nuclear emulsions with which our  $\rho$ -meson results under absorbers may be compared. Using systems of counters, the differential range spectrum has been shown to be flat up to 100 gm/cm<sup>2</sup> air equivalent at Echo Lake by Kraushaar (1949), and a similar result at several points in the atmosphere was obtained by Rossi, Sands and Sard. We may note that if the differential range spectrum at the Jungfraujoch is at all similar to that at sea level, then it should remain fairly flat up to about 1,000 gm/cm<sup>2</sup>, after which it

should fall rapidly (Rossi 1948). Our maximum absorber was considerably less than  $1,000 \text{ gm/cm}^2$ .

The upward stream of  $\rho$ -mesons has been attributed by Camerini, Muirhead, Powell and Ritson (1948) to the decay in flight of the upward stream of  $\pi$ -mesons. We may note here that the frequency of upward  $\rho$ -mesons is of an order of magnitude comparable with that of the  $\pi$ -mesons (Table 5).

We will leave the discussion of the upward  $\rho$ -meson results until we have considered the results for  $\pi$ -mesons.

### (ii) $\pi$ -Mesons

The frequencies of  $\sigma$ -mesons giving rise to stars,  $N(\sigma)$ , and those showing  $\mu$ -decay,  $N(\pi, \mu)$ , were noted, as well as their directions of motion on entering the emulsion. In order to determine the total numbers of  $\pi^+$ - and  $\pi^-$ -particles stopping in the emulsions, the observed frequencies were corrected for the loss due to the geometry of the emulsion. A simple extension of the method of Lattes, Occhialini and Powell (1947) shows that 18.6% of the positive and 11.3% of the negative mesons would not be recorded for reasons of geometry. Furthermore, Adelman and Jones (1949) have shown that only 71% of  $\pi^-$ -mesons give rise to nuclear disintegrations. Hence the actual frequencies of  $\pi^-$ - and  $\pi^+$ -particles were obtained as follows:

$$\left. \begin{aligned} N(\pi^+) &= 1.23 N(\pi, \mu), \\ N(\pi^-) &= (1.13/0.71) N(\sigma) = 1.6 N(\sigma). \end{aligned} \right\} \dots\dots (15)$$

The total frequencies of  $\pi$ -mesons stopping in the emulsion at various depths in the absorber, obtained with the aid of equation (15), are given in Table 5.

In Table 5,  $\pi$ -mesons of both signs of charge have been added in order to give the total frequencies entering the emulsion in the downward and upward directions.

Table 5

Thickness, $T$ , of absorber ( $\text{gm/cm}^2 \text{ C}$ )	0	55	110	165	220	220 C + 85 Pb
$\pi$ -mesons down/ $\text{cm}^3/\text{day}$	0.36 $\pm 0.05$	0.72 $\pm 0.14$	0.77 $\pm 0.09$	0.73 $\pm 0.13$	0.56 $\pm 0.08$	0.36 $\pm 0.05$
$\pi$ -mesons up/ $\text{cm}^3/\text{day}$	0.86 $\pm 0.08$	0.80 $\pm 0.15$	0.54 $\pm 0.08$	0.55 $\pm 0.12$	0.47 $\pm 0.07$	0.23 $\pm 0.04$

The results are plotted on a logarithmic scale in Figure 5. The downward stream of  $\pi$ -mesons appears to exhibit a transition effect, passing through a flat maximum in the vicinity of  $100 \text{ gm/cm}^2$  (cf. Harding and Perkins 1949). The results for the upward stream of  $\pi$ -mesons may be fitted to an exponential curve, Figure 5(b); the line drawn has the same slope as the line in Figure 2, giving the variation of nuclear disintegrations with depth. We show below that the frequency of upward  $\pi$ -mesons would be expected to be proportional to the frequency of nuclear disintegrations, and it is seen that, bearing in mind the limited accuracy of the results, the observed points fit the line reasonably well.

The total frequency of  $\pi$ -mesons for  $T=0$  is  $1.22 \pm 0.1$  and is consistent with the figure of  $1.42 \pm 0.16$  given by Camerini, Muirhead, Powell and Ritson (1948) for unscreened plates exposed at the Jungfrauoch.

Another feature of the results that may be obtained is the ratio of negative to positive  $\pi$ -mesons. In Table 6, we give the results obtained by disregarding the direction of motion of the  $\pi$ -mesons, and taking simply the ratio of  $N(\pi^-)$  to  $N(\pi^+)$ .

It will be seen that the ratio of  $\pi^-$  to  $\pi^+$ -mesons remains substantially constant with depth in the absorber, and the mean value, averaged over all depths, is found to be

$$\frac{N(\pi^-)}{N(\pi^+)} = 3.1 \pm 0.25. \quad \dots\dots(16)$$

The only result with which this may be compared is that of Camerini, Muirhead, Powell and Ritson (1948), who report that the values of  $N(\sigma)$  and  $N(\pi, \mu)$  are

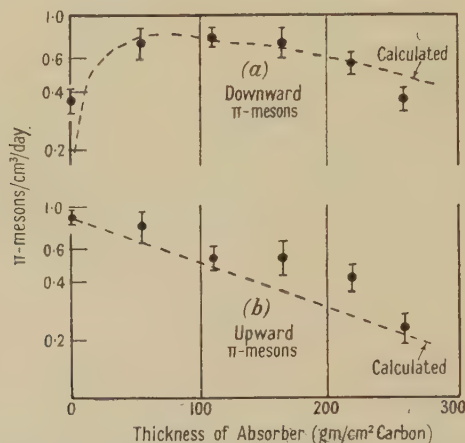


Figure 5. The frequency of occurrence of slow  $\pi$ -mesons. The calculated values are those given in Table 5.

Table 6

Thickness, $T$ , of absorber (gm/cm <sup>2</sup> C)	0	55	110	165	220	220 C +85 Pb
$N(\pi^-)$ /cm <sup>3</sup> /day	0.93	1.14	1.0	0.97	0.74	0.44
	$\pm 0.09$	$\pm 0.18$	$\pm 0.11$	$\pm 0.16$	$\pm 0.09$	$\pm 0.05$
$N(\pi^+)$ /cm <sup>3</sup> /day	0.30	0.38	0.28	0.31	0.29	0.15
	$\pm 0.05$	$\pm 0.10$	$\pm 0.06$	$\pm 0.09$	$\pm 0.09$	$\pm 0.03$
$N(\pi^-)/N(\pi^+)$	3.1	3.0	3.6	3.1	2.6	3.0
	$\pm 0.6$	$\pm 0.9$	$\pm 0.8$	$\pm 1.0$	$\pm 0.6$	$\pm 0.7$

$0.74 \pm 0.11$  and  $0.68 \pm 0.23$ /cm<sup>3</sup>/day respectively. This gives for the ratio of negative to positive mesons

$$\frac{N(\pi^-)}{N(\pi^+)} = \frac{(0.74 \pm 0.11)}{0.71(0.68 \pm 0.23)} = 1.4 \pm 0.5,$$

which does not seem consistent with the value (16). Examination of Table 2 of these authors reveals that they would appear to have used a much larger factor ( $\sim 4$ ) to correct for the loss of positive mesons than for the negative ones. In the light of present knowledge concerning  $\pi$ -mesons, we believe that the values (15) are to be preferred.



## § 6. DISCUSSION OF MESON RESULTS

In the previous section it was seen that the results for the downward stream of  $\rho$ -mesons were consistent with the observations of other workers using nuclear emulsions and systems of Geiger counters. In this section we discuss the frequency of the downward and upward stream of  $\pi$ -mesons, the upward stream of  $\rho$ -mesons and the negative/positive ratio of  $\pi$ -mesons.

(i) *The Frequency of  $\pi$ -Mesons as a Function of Depth in the Absorber*

Examination of Table 5 shows that the numbers of  $\pi$ -mesons in the upward and downward streams are approximately of equal magnitude, at least in the lower half of the absorber when the transition effects of the downward stream are in equilibrium. This forms the experimental justification of the assumption made in § 4 that the lower energy  $\pi$ -mesons are emitted isotropically from 'stars' (cf. Franzinetti 1950). The number upward is a little lower than the number downward, but this is to be expected since the frequency of stars below a given point in the absorber is lower than that occurring above. By carrying through a calculation similar to that of Harding and Perkins (1949), but including the upward as well as the downward stream of  $\pi$ -mesons, it is found that the number of  $\pi$ -mesons emitted isotropically, and with energies less than 270 mev., and which come to rest in the emulsion, is 0.15 per star. This figure is to be compared with the total number of mesons emitted, viz. 0.27 per star, mentioned in § 4 (i). The difference accounts for the  $\pi$ -mesons producing stars already discussed in § 4 (i). We now show that the same assumptions and method of calculation which we used in § 4 (i) will also account for the observed frequencies of mesons stopping in the emulsions.

(a) *Contribution from collimated mesons.*

The differential range spectrum  $n(R)$  corresponding to equation (11) is for this group

$$\left. \begin{aligned} n(R)dR &= 0 && \text{for } R \leq R_0 \\ &= \frac{2b^2 dR}{(b+R)^3} && \text{for } R > R_0. \end{aligned} \right\} \dots\dots(17)$$

The frequency of  $\pi$ -mesons from this group stopping in  $dx$  at  $x$  is given by

$$\left. \begin{aligned} N_C(\pi) &= ae^{-x} dx \int_0^{x-R_0} \frac{2b^2}{(b+x-x')^3} dx' \\ &= ae^{-x} dx [0.5 - \{b/(b+x)\}^2] && x \geq R_0 \\ &= 0 && x < R_0. \end{aligned} \right\} \dots\dots(18)$$

The number of stars starting in  $dx$  is  $e^{-x}dx$  and the ratio is

$$a[0.5 - \{b/(b+x)\}^2]. \dots\dots(19)$$

Hence to obtain the frequency relating to our conditions we multiply the observed frequency of stars at  $x$ ,  $S(x)$ , by (19) and by a factor  $D$  expressing the probability of surviving decay

$$N_C(\pi) = DS(x)a[0.5 - \{b/(b+x)\}^2] \text{ per cm}^3 \text{ per day.} \dots\dots(20)$$

These mesons will all be observed in a downward stream. Numerical values will be inserted after we have evaluated the other contributions.

(b) *Contribution from isotropic mesons.*

The frequency of mesons stopping per cm<sup>3</sup> per day arising from the isotropic group is :

Down :

$$N_I(\pi_D) = DaS(x) \int_0^x e^{-R} \frac{b^2}{(b+R)^3} dR \int_0^{\pi/2} e^{R \cos \theta} \sin \theta d\theta \\ + DaS(x) \int_x^{R_0} e^{-R} \frac{b^2}{(b+R)^3} dR \int_{\varphi}^{\pi/2} e^{R \cos \theta} \sin \theta d\theta \quad \text{for } x \leq R_0 \quad \dots\dots (20a)$$

( $\cos \phi = x/R_0$ ) and

$$N_I(\pi_D) = DaS(x) \int_0^{R_0} e^{-R} \frac{b^2}{(b+R)^3} dR \int_0^{\pi/2} e^{R \cos \theta} d\theta \quad \text{for } x > R_0 \quad \dots\dots (20b)$$

Up :

$$N_I(\pi_U) = DaS(x) \int_0^{R_0} e^{-R} \frac{b^2}{(b+R)^3} dR \int_{\pi/2}^{\pi} e^{R \cos \theta} \sin \theta d\theta \\ = DaS(x) \times 0.19. \quad \dots\dots (20c)$$

The integration over  $\theta$  is straightforward and the remaining integration over  $R$  has been performed by numerical methods to give the results in Table 7.

Table 7

$T$ (gm/cm <sup>2</sup> C)	$N_0(\pi_D)/\text{cm}^3/\text{day}$	$N_I(\pi_D)$	$N_I(\pi_U)$	$N_0(\pi_D) + N_I(\pi_D)$
0	0	0	0.86	0
14	0	0.47	0.77	0.47
28	0	0.61	0.72	0.61
55	0	0.75	0.62	0.75
110	0	0.68	0.45	0.68
165	0.16	0.49	0.33	0.65
220	0.20	0.33	0.24	0.53
220 C + 85 Pb	0.28	0.22	0.21	0.50

The value of  $D$  has been determined from the mean measured lifetime of the  $\pi$ -mesons,  $\tau = 1.5 \times 10^{-8}$  sec. (Richardson 1948, Martinelli and Panofsky 1950), and a mean value of  $D = 0.9$  was used in evaluating the results in Table 7.

The results in the last two columns of Table 7 are plotted as the dotted lines in Figures 5(a) and (b), and it is seen that the agreement between the calculated and observed values is reasonable.

We must assume that on account of the low density of the atmosphere, and consequently the small value of  $D$ , the frequency of downward  $\pi$ -mesons arriving from the atmosphere must be negligibly small. Thus the expected frequency of downward mesons is zero at  $T=0$ , whereas the frequency observed was  $0.36 \pm 0.05/\text{cm}^3/\text{day}$ . The increase in downward mesons with thickness  $T$  is however very rapid, and at  $T=14 \text{ gm/cm}^2$  the expected number is 0.47. The plates used were 3 in.  $\times$  4 in., standing on their longer sides, and in actual fact the absorber thickness at the nominal value  $T=0$  should be taken as approximately 10 gm/cm<sup>2</sup>, made up of the light covering over the plates, and of the glass and emulsion of the plates themselves. The observed frequency at the nominal value of  $T=0$  can therefore be understood as being due to mesons generated in the local material, and not necessarily due to mesons arriving from the air.

The calculated value of downward  $\pi$ -mesons is a little too high and that of the upward  $\pi$ -mesons is a little too low. This is probably due to the curved

shape of the top of the carbon absorber, and better agreement could be obtained by taking into account the geometry of the pile, but we have not thought it worth while to push our calculations to this degree of refinement. An approximate estimate shows that the remaining discrepancy can be removed by these considerations.

Thus our crude model concerning the angular distribution of the  $\pi$ -mesons is perhaps not too far fetched, in so far as, at one and the same time, it shows the expected number of slow  $\pi$ -mesons to be in agreement with the observed upward and downward streams, and serves to explain the small difference in the observed absorption lengths for the N-radiation in air and in dense material of comparable atomic weight.

### (ii) *The Upward Stream of $\rho$ -Mesons*

There are four possible sources contributing to the upward stream of  $\rho$ -mesons : (a) 29% of the upward stream of  $\pi^-$ -particles do not give rise to stars, and hence will be recorded as  $\rho$ -mesons ; (b) about 10% of the upward stream of  $\pi^+$ - and  $\pi^-$ -particles will decay in flight, giving  $\mu$ -mesons ; (c) both downward and upward  $\pi^-$ -particles coming to rest in the glass backing of the emulsion will give rise to  $\mu$ -mesons ; these  $\mu$ -mesons are emitted isotropically and hence 50% will come to rest in the emulsion travelling in an upward direction ; (d) back-scattered  $\mu$ -mesons originally moving downward.

The contribution from (d) is uncertain, but it must be small, since the sum of the contributions (a), (b) and (c) is sufficient to account for the greater part of the observed frequency of upward  $\rho$ -mesons, as will be seen from Table 8 where the individual contributions are tabulated.

Table 8

$T$ (gm/cm <sup>2</sup> ) C	(a) 0.29 $N(\pi^-)$	(b) 0.1 $N(\pi^0)$	(c) 0.5 $N(\pi^+)$	(a)+(b)+(c)	Observed frequency of up $\rho$ -mesons
0	0.19	0.09	0.15	0.43	0.53 $\pm$ 0.09
55	0.18	0.08	0.20	0.46	0.46 $\pm$ 0.13
110	0.12	0.05	0.13	0.30	0.32 $\pm$ 0.07
165	0.12	0.05	0.15	0.32	0.46 $\pm$ 0.14
220	0.09	0.04	0.15	0.28	0.34 $\pm$ 0.06
220 C + 85 Pb	0.05	0.02	0.08	0.15	0.26 $\pm$ 0.06

Values are in number/cm<sup>2</sup>/day.

### (iii) *The Ratio of Negative to Positive $\pi$ -Mesons*

It was found that there was a negative excess in the  $\pi$ -mesons stopping in the emulsion at all depths in the absorber, the mean ratio of negative to positive mesons being  $3.1 \pm 0.25$ .

A negative excess in the mesons which are ejected from stars and come to the end of their range in the same piece of nuclear emulsion has been noted by C. F. Powell (1949). The mean energy of this group of mesons is 1.6 mev., and this negative excess has been attributed to the effect of the nuclear Coulomb field. An explanation along similar lines would hardly hold in the case of our mesons since their mean energy is much higher, of the order of 100 mev.

A more likely explanation seems to be the following: The ratio of negative to positive 50 mev. mesons produced by 345 mev. protons in various elements has been studied at Berkeley by Bradner and Jones (1950) and by Richman and



Wilcox (1950). For carbon the ratio is  $4.8 \pm 0.5$  positive mesons to one negative. For incident neutrons, one would expect from the charge symmetry of nuclear forces that the situation would be completely reversed, since in the carbon nucleus there are equal numbers of protons and neutrons, i.e. one would expect 4.8 negative mesons for 1 positive meson. Thus if  $\alpha$  is the proportion of cosmic-ray 'stars' produced by protons, the expected ratio of negative to positive  $\pi$ -mesons stopping in the emulsion would be

$$\frac{N(\pi^-)}{N(\pi^+)} = \frac{4.8 - 3.8\alpha}{1 + 3.8\alpha} \quad \dots\dots(21)$$

The observed ratio of  $3.1 \pm 0.25$  corresponds to a value for  $\alpha$  of  $0.11 \pm 0.04$ . This is similar to the proportion of charged particles in the N-radiation at the Jungfraujoch. Page (1950) gives  $\alpha = 0.17$ , and Barton (1950) finds 0.16. These experimental figures are upper limits, since not all the charged particles in the N-radiation are protons:  $\pi$ -mesons are probably also included in these observed values of  $\alpha$ . In any case they are not inconsistent with the value  $\alpha = 0.11 \pm 0.04$  required above.

One consequence of the above interpretation is that as the depth is increased the negative/positive ratio should decrease steadily from the value 3.1. This is due to the increasing proportion contributed by the more energetic collimated mesons to the total number stopping (cf. Table 7). The value of  $\alpha$  for the energetic events is close to 0.5 (Brown *et al.* 1949), which from equation (21) is seen to result in a lower value of the charge asymmetry of the  $\pi$ -mesons produced in carbon.

#### § 7. CONCLUSIONS

The conclusions at which we have arrived, based on measurements at the Jungfraujoch, are as follows :

- (i) The measured value of the absorption length in carbon for the radiation producing 'stars' is  $L_A = 166 \pm 8 \text{ gm/cm}^2$ , using absorbers up to  $250 \text{ gm/cm}^2$  in thickness.
- (ii) In dense absorbers, the N-radiation is composed partly of  $\pi$ -mesons, whereas in air the  $\pi$ -mesons are absent, due to the high probability of  $\pi$ - $\mu$  decay.
- (iii) The presence of these  $\pi$ -mesons, generated in the absorber, gives rise to an increase in the apparent absorption length of the N-radiation of about 14% in carbon, for the absorber thickness used in our experiments.
- (iv) The absorption length of the N-radiation in carbon, when corrected for the presence of these secondary stars due to  $\pi$ -mesons, is  $143 \pm 10 \text{ gm cm}^2$ , which is close to the value expected from the known absorption of the N-radiation in air.
- (v) From the size distribution of 'stars' we conclude that their distribution in energy is of the form  $dE/E^\gamma$  with  $\gamma = 2.6 \pm 0.1$ , in the range of  $E = 300$  to  $6,000 \text{ mev}$ .
- (vi) The differential range spectrum of the downward stream of  $\mu$ -mesons at the Jungfraujoch is constant up to  $265 \text{ gm/cm}^2$ .
- (vii) The mean ratio of negative to positive  $\pi$ -mesons with energies between 0 and  $450 \text{ mev}$ , produced in carbon by the cosmic radiation at the Jungfraujoch is  $3.1 \pm 0.25$ .

- (viii) About one-third of the upward stream of  $\rho$ -mesons at the Jungfraujoch is composed of  $\pi^-$ -mesons that do not give rise to 'stars'. Most of the remainder is due to the decay of  $\pi^+$ -mesons in the glass backing of the emulsions.

## ACKNOWLEDGMENTS

We are grateful to Professor J. D. Bernal for providing us with facilities to carry out this work and for his interest in its progress. We would like to thank Mrs. M. H. George for much assistance with the work of searching the emulsions. We express our thanks to Director Frei of the Jungfraujoch Railway for the loan of 15 tons of coal for the absorber. We are grateful to Professor von Muralt for the excellent arrangements made at the Scientific Station and to Hans Wiederkehr for carrying them out. Assistance at the Jungfraujoch from J. Gay and D. Tresise is also gratefully acknowledged.

The investigation was made possible by a grant from the Department of Scientific and Industrial Research.

## APPENDIX

*The Relation between Energy and Size of 'Stars' observed in C2 Emulsions*

The following relation has been given by Brown *et al.* (1949b) for 'electron sensitive' nuclear emulsions:

$$E(\text{MeV.}) = 37n + 4n^2. \quad \dots\dots(22)$$

$E$  is the energy released among the nucleons, and  $n$  is the number of branches in 'stars' with a grain density greater than  $1.5 g_{\min}$ . We require the corresponding relation for C2 emulsions for the total energy released. This may be done by using the data in Table IV, given by Brown *et al.*, and taking into account (i) the limited sensitivity of the C2 emulsions, (ii) the energy released in the form of fast particles with grain density less than  $1.5 g_{\min}$ .

(i) *Limited sensitivity of C2 emulsions.*

Brown *et al.* divide the heavy tracks into three groups: (a) short black tracks  $< 70\mu$ , (b) long black tracks  $> 70\mu$ , (c) grey tracks with grain density  $> 1.5 g_{\min}$  and  $< 5 g_{\min}$ .

In C2 emulsions all the tracks in groups (a) and (b) would be detected, but a fraction of group (c) would not. Taking the upper energy limit for protons of the C2 emulsion as 100 MeV. (Page 1950), we may determine the fraction of the (c) tracks lost from Figure 14 of Brown *et al.* as a function of the size of 'star' as observed in 'electron sensitive' emulsions, and hence obtain the mean number of branches that the 'stars' considered by Brown *et al.* would have had in C2 emulsions.

Table 9

Number of heavy branches in 'electron sensitive' emulsions	4, 5	7, 8	12-15	16-24
Fraction of grey tracks recorded in C2 emulsions	0.86	0.73	0.62	0.63
Mean number of branches ob- served in C2 emulsions	4.03	7.1	11.9	16.4

(ii) *Shower particles.*

From Table III of Brown *et al.*, we may determine the mean number of shower particles,  $\bar{n}_s$ , as a function of star size (Table 10).

Table 10

Number of heavy branches $\bar{n}_s$	4, 5	7, 8	12-15	16-24
	0.12	0.31	0.9	2.1

Most of the 'shower' particles are  $\pi$ -mesons, and from the results of Camerini *et al.*, we find the mean value of the total energy of these shower particles is 640 mev. According to Hooper (private communication), the energy released in the form of neutral particles other than neutrons is approximately one-half of that released in the form of shower particles. Hence the mean energy per shower particle may be taken as :

$$E = 960 \text{ mev.} \quad \dots\dots (23)$$

From Tables 9 and 10 and equation (23), we may now construct the following Table expressing the relation between the number of tracks and total energy released in nuclear disintegrations observed in C2 emulsions:

Table 11

Mean number of branches $n$	4.03	7.1	11.9	16.4
Energy in emitted nucleons (mev.)	211	507	1183	2035
Energy in shower particles (mev.)	112	295	864	1980
Total energy released $E$ (mev.)	323	802	2047	4015

The relation between the values of  $E$  and  $n$  given in Table 11 may be represented approximately by  $E(\text{mev.}) = 26n + 12.8n^2$ .

## REFERENCES

- ADELMAN, F. L., and JONES, S. B., 1949, *Phys. Rev.*, **75**, 1468.  
 BARTON, J. C., 1950, *Ph.D. Thesis*, London.  
 BELOVITSKI, G. E., MASLENNIKOVA, N. V., SMIRNOV, V. F., and SUCHOV, L. V., 1949, *Doklady Akad. Nauk. U.S.S.R.*, **69**, 321.  
 BERNARDINI, G., CORTINI, G., and MANFREDINI, M., 1949, *Phys. Rev.*, **76**, 1792.  
 BRADNER, H., and JONES, S. B., 1950, *Phys. Rev.*, **78**, 90 (A).  
 BROWN, R. H., *et al.*, 1949a, *Nature, Lond.*, **163**, 47, 82; 1949b, *Phil. Mag.*, **40**, 862.  
 CAMERINI, U., FOWLER, P. H., LOCK, W. O., and MUIRHEAD, H., 1950, *Phil. Mag.*, **41**, 413.  
 CAMERINI, U., MUIRHEAD, H., POWELL, C. F., and RITSON, D. M., 1948, *Nature, Lond.*, **162**, 433.  
 CLEMENTEL, E., 1950, *Nuovo Cim.*, **7**, 109.  
 CORTINI, G., and MANFREDINI, M., 1949, *Nature, Lond.*, **163**, 991.  
 DALLAPORTA, N., MERLIN, M., and PUPPI, G., 1950, *Nuovo Cim.*, **7**, 99.  
 FOWLER, P. H., 1950, *Phil. Mag.*, **41**, 169.  
 FRANZINETTI, C., 1950, *Phil. Mag.*, **41**, 86.  
 GEORGE, E. P., and EVANS, J., 1950, *Proc. Phys. Soc. A*, **63**, 1248.  
 GEORGE, E. P., and JASON, A. C., 1949 a, *Proc. Phys. Soc. A*, **62**, 243; 1949 b, *Cosmic Radiation* (London: Butterworth's Scientific Publications).  
 HARDING, J. B., and PERKINS, D. H., 1949, *Nature, Lond.*, **164**, 285.  
 HEITLER, W., and JÁNOSSY, L., 1949 a, *Proc. Phys. Soc. A*, **62**, 374; 1949 b, *Ibid.*, **62**, 669.  
 KRAUSHAAR, W. L., 1949, *Phys. Rev.*, **76**, 1045.  
 LATTES, C. M., OCCHIALINI, G. P. S., and POWELL, C. F., 1947, *Nature, Lond.*, **160**, 486.  
 MALASPINA, L., MERLIN, M., PIERUCCI, O., and ROSTAGNI, A., 1950, *Nuovo Cim.*, **7**, 145.



- MARTINELLI, E. A., and PANOFKY, W. K. H., 1950, *Phys. Rev.*, **77**, 465.  
 PAGE, N., 1950, *Proc. Phys. Soc. A*, **63**, 250.  
 PERKINS, D. H., 1947, *Nature, Lond.*, **160**, 707.  
 POWELL, C. F., 1949, *Cosmic Radiation* (London: Butterworth's Scientific Publications).  
 RICHARDSON, J. R., 1948, *Phys. Rev.*, **74**, 1720.  
 RICHMAN, C., and WILCOX, H. A., 1950, *Phys. Rev.*, **78**, 496.  
 ROSSI, B., 1948, *Rev. Mod. Phys.*, **20**, 537.  
 ROSSI, B., HILBERRY, N., and HOAG, J. B., 1940, *Phys. Rev.*, **57**, 461.  
 ROSSI, B., SANDS, M., and SARD, R., 1947, *Phys. Rev.*, **72**, 120.  
 SANDS, M., 1950, *Phys. Rev.*, **77**, 180.  
 WILSON, J. G., 1950, Oxford Conference on Cosmic Rays.

## Disintegrations produced by the Nuclear Capture of Slow Negative $\mu$ -Mesons

BY E. P. GEORGE AND J. EVANS

Birkbeck College, University of London

*MS. received 20th October 1950*

**ABSTRACT.** The 'prong distribution' for the disintegrations produced by the  $\sigma$ -mesons of the cosmic radiation in photographic emulsions exposed below ground is found to be different from that observed in emulsions exposed above ground. The underground distribution contains relatively more 'stars' consisting of one prong. The observations are consistent with the hypothesis that most of the  $\sigma$ -mesons below ground are in fact negative  $\mu$ -mesons and not negative  $\pi$ -mesons. It is concluded that  $8.7 \pm 1.7\%$  of the negative  $\mu$ -mesons captured in the emulsion lead to disintegrations accompanied by the emission of charged particles. The average number of prongs per disintegration produced by the capture of negative  $\mu$ -mesons is  $0.10 \pm 0.02$ . The mean number of prongs and the associated prong distribution suggest that a nuclear excitation of about 15 mev. is produced by the capture of a  $\mu$ -meson.

### § 1. INTRODUCTION

THE disintegration of nuclei following the capture of slow mesons in photographic emulsions exposed to the cosmic radiation was first reported by Perkins (1947). It was shown by observations carried out at Bristol that most of the disintegrations of this type are produced by negative  $\pi$ -mesons. Conversi, Pancini and Piccioni (1945, 1947) showed that the interaction between  $\mu$ -mesons and atomic nuclei is very weak, and this was confirmed by Camerini *et al.* (1948), who found that few, possibly none ( $9.5 \pm 9\%$ ), of the negative  $\mu$ -mesons stopping in silver bromide produced observable disintegrations.

On the other hand, Sard and collaborators (1948, 1950) have observed the production of neutrons by charged particles arrested in lead absorbers, and it is likely that several of the stopped charged particles were negative  $\mu$ -mesons. Further, Groetzing and McClure (1948, 1949) concentrated negative mesons by means of a magnetic focusing arrangement into an absorber, selecting those which stopped in it. The long path length in the iron cores discriminated in favour of  $\mu$ -mesons, and they confirmed the production of neutrons by meson capture. From these two counter investigations it may be concluded that something like three neutrons are emitted when a negative  $\mu$ -meson is absorbed by a lead nucleus.

A question of some interest is whether the capture of  $\mu$ -mesons may sometimes lead to nuclear disintegrations with the emission of charged particles. Several attempts to investigate this have been made at sea level or mountain altitudes, using either cloud chambers (Wang and Jones 1948, Chang 1949, Cool *et al.* 1949) or nuclear emulsions (Perkins 1949), but the results have not been conclusive. These investigations are all faced with the following difficulty: the slow mesons of the cosmic radiation which are arrested in absorbers or emulsions consist of a mixture of  $\pi$ - and  $\mu$ -mesons. The negative  $\pi$ -mesons are very efficient in producing nuclear disintegrations containing charged particles, and even at sea level most of the  $\sigma$ -meson 'stars' must be ascribed to  $\pi$ -mesons. Hence, in those few cloud-chamber pictures which show heavy tracks associated with stopping mesons it is not clear which type of meson is involved.

We have been able to overcome this difficulty by working underground at various depths up to a maximum of the equivalent of 60 metres of water. Under these conditions, the ratio of  $\pi$ - to  $\mu$ -mesons is reduced by a factor which may be as great as 20, depending on the depth, and we have been able to isolate the disintegrations produced by the capture of slow  $\mu$ -mesons from the small background of stars contributed by  $\pi$ -meson capture.

In order to avoid confusion we retain the phenomenological description ' $\sigma$ -meson' for those slow mesons which, when captured by a nucleus, produce nuclear disintegration 'stars', since we believe that only a small proportion of the  $\sigma$ -mesons observed below ground are in fact  $\pi$ -mesons.

## § 2. EXPERIMENTAL ARRANGEMENTS

The observations were made with Ilford Nuclear Research emulsions, Type G5, 200 microns in thickness. They were coated, stored and developed underground, using stations on the underground railway in London at depths equivalent to 20, 34 and 60 metres of water, in a manner described previously (George and Evans 1950). The plates were only brought to the surface for examination after fixing. The possibility of confusion due to pre- or post-exposures of the plates was thus completely eliminated.

## § 3. EXPERIMENTAL RESULTS

In the examination of 250 cubic centimetres of emulsion, 30  $\sigma$ -mesons, 5 positive  $\pi$ -mesons showing  $\pi$ - $\mu$  decay, and 1,014  $\mu$ -mesons have been observed to come to rest in the emulsion. The features of the disintegrations due to  $\sigma$ -mesons will first be discussed in detail.

### (i) *The Distribution in 'Prong' Number of the $\sigma$ -Stars produced Underground*

The distribution in prong number of all the underground  $\sigma$ -stars is given in Table 1. In this Table the expected distribution for an equal number of  $\sigma$ -mesons of the cosmic radiation at mountain and balloon altitudes in the atmosphere is given for comparison (Menon *et al.* 1950).

Table 1

No. of prongs	1	2	3	4	5
Underground $\sigma$ -mesons	23	5	2	0	0
$\sigma$ -mesons observed at altitude	10	8	7	4	1

The  $\sigma$ -mesons at altitude are known to consist almost exclusively of negative  $\pi$ -mesons, and hence the discrepancy between the prong distributions given in Table 1 strongly suggests that the majority of the underground  $\sigma$ -mesons are not  $\pi$ -mesons. Since they are obviously mesons, and since  $\mu$ -mesons are observed in large numbers, we make the tentative suggestion that most of these underground  $\sigma$ -mesons are, in fact, negative  $\mu$ -mesons, and that they produce nuclear disintegrations substantially different in character from those due to negative  $\pi$ -mesons.

(ii) *The Directions of Motion of the Underground Mesons*

The mesons were divided into two classes, according to whether they entered the emulsion from above or below the horizontal. The results are given in Table 2.

The  $\mu$ -mesons show a marked collimation in the vertical direction, as also do the  $\sigma$ -mesons, while such  $\pi^+$ -mesons as have been observed appear to be distributed nearly isotropically. The directions of motion of the slow  $\pi$ -mesons, of both signs, observed under thick absorbers at the Jungfraujoch have been

Table 2

	Total no. of mesons observed		Up (% of whole)
	Down	Up	
$\mu$ -mesons	988	26	$2.6 \pm 0.3$
$\sigma$ -mesons	27	3	$10 \pm 6$
$\pi^+$ -mesons (showing $\pi$ - $\mu$ decay)	2	3	$\sim 60$

Table 3

Depth below ground (metres water)	Frequency per cm <sup>3</sup> per day		
	$\sigma$ -mesons	$\mu$ -mesons	Stars
20	$0.0032 \pm 0.0007$	$0.098 \pm 0.005$	$0.0062 \pm 0.0012$
34	$0.0011 \pm 0.0005$	$0.058 \pm 0.004$	$0.0056 \pm 0.001$
60	$0.0005 \pm 0.0003$	$0.017 \pm 0.002$	$0.0047 \pm 0.0009$

shown by Barton *et al.* (1951) to be distributed almost isotropically, and the  $\pi$ -mesons produced by the  $\gamma$ -rays from the 350 mev. electron synchrotron at Berkeley have been shown to be distributed isotropically also (McMillan *et al.* 1949). The low energy  $\pi$ -mesons observed in the present investigation are probably produced following electromagnetic excitation of nuclei by the fast  $\mu$ -mesons of the penetrating component (George and Evans 1950), and we should therefore expect the underground  $\pi$ -mesons to be isotropic also. It is seen from the Table that this is consistent with the observations for the positive  $\pi$ -mesons, but is certainly not so for the  $\sigma$ -mesons. The distribution of the latter resembles more closely that of the  $\mu$ -mesons, and appears to be consistent with the hypothesis that many of the  $\sigma$ -mesons are  $\mu$ -mesons.

(iii) *The Frequency of Occurrence of  $\sigma$ -Mesons at different Depths below Ground*

The results are given in the second column of Table 3, and the figures for stars and slow  $\mu$ -mesons are also given for comparison.

Under thick absorbers, the frequency of  $\pi$ -mesons is known to be proportional to that of the stars (Harding and Perkins 1949, Barton *et al.* 1951). Between the



extreme levels of observation the frequency of stars, and hence, presumably, of  $\pi$ -mesons, only varies by a factor of at the most 1.5, whereas the frequency of  $\sigma$ -mesons is seen to vary by a factor of about 6. This last figure is in agreement with the figure for slow  $\mu$ -mesons, which again supports the idea that at least the greater part of the underground  $\sigma$ -mesons are  $\mu$ - and not  $\pi$ -mesons.

#### § 4. DISCUSSION

The distribution in prong number, the angular distribution of the  $\sigma$ -mesons, and the depth variation of the  $\sigma$ -stars all point to the suggested interpretation of the  $\sigma$ -mesons. This is further supported by the negative/positive ratio the  $\pi$ -mesons would have if the  $\sigma$ -mesons were  $\pi$ -mesons. Thus, assume that the  $\sigma$ -stars are all produced by negative  $\pi$ -mesons. Then from the observed number, 30, we may deduce that 41 negative  $\pi$ -mesons came to rest in our plates, since 28% do not produce a visible star (Adelman and Jones 1949). In the same volume, five positive  $\pi$ -mesons were observed, and this would therefore correspond to a negative, positive ratio of 8:1. On account of the probable electromagnetic origin of the underground  $\pi$ -mesons (George and Evans 1950) the value of the negative/positive ratio would be expected to be about 1.7:1, found for the production of  $\pi$ -mesons by energetic photons. In fact, assuming 1.7 negative  $\pi$ -mesons for every positive one, and bearing in mind the proportion of 'star-less' negative  $\pi$ -mesons, we are led to expect that the number of negative  $\pi$ -mesons giving rise to  $\sigma$ -stars would be approximately equal to the number of positive  $\pi$ -mesons. Since we have seen five examples of  $\pi$ - $\mu$  decay we may expect that something like five of the 30  $\sigma$ -mesons are, in fact, negative  $\pi$ -mesons.

We have examined the  $\sigma$ -stars to see whether, using the criteria laid down by Menon *et al.* (1950), we could identify stars characteristic of  $\pi$ -mesons. We find that the two stars with 3 prongs and one of the 2-pronged stars are characteristic of  $\pi$ -meson disintegrations in light elements, and are therefore unlikely to be produced by  $\mu$ -mesons on account of the small probability of capture of the  $\mu$ -mesons by the atoms of the gelatine. Two examples of the stars ascribed to  $\pi$ -mesons are shown in Figure 1 (Plate\*). In both cases the mesons were travelling upwards, and this further supports their classification as  $\pi$ -mesons. In addition we have classified one other 2-pronged star as a  $\pi$ -meson disintegration. From the known prong distribution of the  $\pi$ -meson stars we should also ascribe at least one of the 1-pronged stars to the  $\pi$ -meson group, though in this case we do not know, of course, which one.

By the above analysis we have selected from the 30  $\sigma$ -mesons five cases which we ascribe to  $\pi$ -meson disintegrations, the prong distribution being one 1-pronged, two 2-pronged and two 3-pronged stars, a result in reasonable accord with the detailed studies made in other laboratories on negative  $\pi$ -mesons (Menon *et al.* 1950). The distribution in the directions of motion of these particles is two down and three up, which again appears to be in reasonable accord with the assumption of a strictly local production of  $\pi$ -mesons. The plates were standing on the floor of a large platform tunnel, and assuming an original isotropic distribution in  $\pi$ -mesons, the upward direction would be favoured for those seen in the plates, on account of the opportunity for decay in transit for the downward travelling mesons in the air-space over the plates.

This leaves three 2-pronged stars and twenty-two 1-pronged stars which are ascribed to disintegrations produced by  $\mu$ -mesons. The three 2-pronged stars are

\* For Plates see end of issue.

shown in Figure 2, and are seen to be very untypical of disintegrations produced by  $\pi$ -mesons, on account of the extremely low energy, of the order of 1 to 2 mev., of the emitted charged particles.

In nineteen out of the twenty-two 1-pronged stars the single heavy track escaped, while in three cases it ended in the emulsion. Photo-micrographs of one of these three examples are shown in Figure 3. We may conclude that the mean range of the charged particles is greater than 300 microns, corresponding to an energy of 7 mev. for protons.

From the measured value, 1.27, of the ratio of positive to negative particles with momentum  $10^{10}$  ev/c. at sea level determined by Owen and Wilson (1949) we may assume that 458 out of the total of 1,039  $\mu$ -mesons were negative. Of these, 54% will be captured in Ag and Br (Menon *et al.* 1950) and 20% of the remainder will be captured in gelatine. This gives a total of 290 negative  $\mu$ -mesons which experienced nuclear absorption. This now leads to the distribution in the number of prongs for the disintegrations produced by negative  $\mu$ -mesons, given in the second row of Table 4.

Table 4

No. of prongs	0	1	2	>2
No. of cases observed	265	22	3	0
Calculated, assuming Poisson distribution	262	26	1.3	0.5

From the observations of Sard *et al.* (1948, 1950) and Groetzing and McClure (1948, 1949) we may take it that the neutral particles emitted in the first category are neutrons, and further, that on the average two to three neutrons are emitted. The average number of prongs per disintegration is  $0.10 \pm 0.02$ , and this corresponds to an average excitation of about 15 mev. (Fujimoto and Yamaguchi 1949). The calculated prong distribution assuming the numbers of charged particles to follow Poisson's law is given in the third row of Table 4, and is seen to be in reasonable agreement with observation.

The excitation of nuclei by  $\mu$ -meson capture has been discussed by Tiomno and Wheeler (1949), assuming a reaction of the form  $\mu^- + P \rightarrow N + \mu_0$ , where  $\mu_0$  is a neutral particle, possibly a neutrino. The nuclear excitation caused by the recoil momentum of the neutron is considered under various models. For the limiting cases in which the nucleus is assumed to follow the Hartree model or the Fermi gas model, the calculated values of the mean energy of nuclear excitation are 18.5 mev. and 12.6 mev. respectively, corresponding to mean prong numbers of 0.14 and 0.09. Our observed values lie between these two limits.

With such an excitation, in the case of the 2-pronged stars most of the energy is lost as binding energy, leaving only 1 or 2 mev. available for kinetic energy. The 2-pronged stars would therefore be expected to have very short tracks, as is in fact found (Figure 2). Further, at this excitation, the nuclear potential barrier favours neutron emission, the theoretical number of neutrons corresponding to our observed prong distribution is about two, which agrees with results of the counter investigations discussed earlier.

## § 5. CONCLUSIONS

From the observations reported in this paper, we have drawn the following conclusions:

(i) Under absorbers of thickness greater than 2,000 gm/cm<sup>2</sup> most of the  $\sigma$ -stars are produced by negative  $\mu$ -mesons.

(ii)  $2.5 \pm 0.5\%$  of all the slow  $\mu$ -mesons of the cosmic radiation, or  $8.7 \pm 1.7\%$  of all the negative  $\mu$ -mesons captured in the emulsion, give visible stars (cf. Camerini *et al.* 1948).

(iii) 90% of the stars produced by  $\mu$ -mesons have one prong and 10% two prongs.

(iv) The nuclear excitation corresponding to the observed prong distribution of the  $\sigma$ -stars due to  $\mu$ -mesons is about 15 mev., in agreement with calculations based on the reaction  $\mu^- + \text{P} \rightarrow \text{N} + \mu_0$ .

#### ACKNOWLEDGMENTS

We would like to express our thanks to Messrs. Waller and Vincent of Ilford Limited for help in coating the plates, and to Mrs. M. H. George and Mr. R. H. Creamer for assistance in searching them. We are grateful to Mrs. E. B. Evans for the photographs and to Dr. K. J. Le Couteur for helpful discussion. We thank the London Transport Executive for permission to work underground, and the Central Research Fund, London University, and the Department of Scientific and Industrial Research for research grants.

#### REFERENCES

- ADELMAN, F. L., and JONES, S. B., 1949, *Phys. Rev.*, **75**, 1468 (A).  
 BARTON, J. C., GEORGE, E. P., and JASON, A. C., 1951, *Proc. Phys. Soc. A*, **64**, 175.  
 CAMERINI, U., MUIRHEAD, H., POWELL, C. F., and RITSON, D. M., 1948, *Nature, Lond.*, **162**, 433.  
 CHANG, W. Y., 1949, *Rev. Mod. Phys.*, **21**, 166.  
 CONVERSI, M., PANCINI, E., and PICCIONI, O., 1945, *Phys. Rev.*, **68**, 232; 1947, *Ibid.*, **71**, 209.  
 COOL, R. L., FOWLER, E. C., STREET, J. C., FOWLER, W. B., and SARD, R. D., 1949, *Phys. Rev.*, **75**, 1275.  
 FUJIMOTO, Y., and YAMAGUCHI, Y., 1949, *Progr. Theor. Phys.*, **4**, 468.  
 GEORGE, E. P., and EVANS, J., 1950, *Proc. Phys. Soc. A*, **63**, 1248.  
 GROETZINGER, G., and MCCLURE, G. W., 1948, *Phys. Rev.*, **74**, 341; 1949, *Ibid.*, **75**, 340.  
 HARDING, J. B., and PERKINS, D. H., 1949, *Nature, Lond.*, **164**, 285.  
 LE COUTEUR, K. J., 1950, *Proc. Phys. Soc. A*, **63**, 259.  
 McMILLAN, E. M., PETERSON, J. M., and WHITE, R. D., 1949, *Science*, **110**, 579.  
 MENON, M. H. K., MUIRHEAD, H., and ROCHAT, O., 1950, *Phil. Mag.*, **41**, 583.  
 OWEN, B. G., and WILSON, J. G., 1949, *Proc. Phys. Soc. A*, **62**, 601.  
 PERKINS, D. H., 1947, *Nature, Lond.*, **159**, 126; 1949, *Ibid.*, **163**, 682.  
 SARD, R. D., ITTNER, W. B., CONFORTO, A. M., and CROUCH, M. F., 1948, *Phys. Rev.*, **74**, 97; 1949, *Ibid.*, **76**, 1134; 1950, *Ibid.*, **79**, 179.  
 TIOMNO, J., and WHEELER, J. A., 1949, *Rev. Mod. Phys.*, **21**, 153.  
 WANG, K. C., and JONES, S. B., 1948, *Phys. Rev.*, **74**, 1547.



## Some Gamma-Rays from Light Elements under Proton Bombardment

By J. H. CARVER AND D. H. WILKINSON,

Cavendish Laboratory, Cambridge

*MS. received 29th September 1950*

**ABSTRACT.** The energy of the photo-protons from deuterium, measured in an ionization chamber, has been used to determine the energy of gamma-rays produced by the proton bombardment of several light elements. The results are expressed in the following Table :

Isotope	Target thickness (kev.)	Proton energy (kev.)	Gamma-ray energy (mev.)
$^9\text{Be}$	2	1000	$7.39 \pm 0.15$
$^{11}\text{B}$	200	950	$12.50 \pm 0.21$
$^{13}\text{C}$	20	570	$\left\{ \begin{array}{l} 8.14 \pm 0.08 \\ 5.81 \pm 0.25 \end{array} \right.$
$^{19}\text{F}$	thick	740	$12.09 \pm 0.28$
$^7\text{Li}$	thick	500	$14.4 \pm 0.4$
$^{15}\text{N}$	unknown	900	$4.45 \pm 0.04$

The absence of certain well-known lines from the above table merely means that their energy was not determined in this investigation.

IN the course of a series of measurements of the photo-disintegration cross section of the deuteron we have determined the energy of several gamma-rays. Photo-protons spent their energy in deuterium or a mixture of deuterium and argon. It was assumed, for the gases individually, that the ionization produced was proportional to the energy of the proton. Such assumptions are always questionable, but in this case may be well justified by three remarks. Firstly, the smallest proton energy involved was 1.1 mev. and the dependence of  $W$ , the energy loss per ion pair, on particle energy is always weak at such particle velocities. Secondly, hydrogen and argon are both well known for their constancy of  $W$ , even at low energies. Thirdly, Bakker \* has reported values of  $W$  for protons of 340 mev. which differ by but 3 or 4% from those obtaining at low energies.

Our measurements consist essentially in the comparison of the energies of the photo-protons produced by the gamma-ray in question with those of the photo-protons produced by the gamma-ray resulting from the proton bombardment of fluorine. These latter have been extensively investigated (see Chao, Tollestrup, Fowler and Lauritsen 1950 for references), and it is known that a thick target bombarded by protons of about 500 kev. results in the almost pure radiation of  $6.14 \pm 0.03$  mev. which has been taken as standard in this work. For the reduction of photo-proton to gamma-ray energy the value of 2.230 mev. given by Bell and Elliott (1950) for the deuteron binding energy was used.

The photo-proton pulses were amplified and analysed by the ninety-nine channel kick-sorter described by one of us (Wilkinson 1950). Owing to the

\* Report to the 1950 Harwell Conference.

momentum of the gamma-ray there exists a natural spread in the energy of the photo-protons. The magnitude of this spread is often found surprising: it has a minimum value of 0.196 in terms of the mean photo-proton energy. This sets an unfortunate limit to the precision of this method of measuring gamma-ray energies. The method possesses, however, some notable advantages of which the principal is the fact that its efficiency increases with decreasing gamma-ray energy—down to 4.5 mev. at any rate—whereas that of the pair spectrometer decreases very rapidly with decreasing gamma-ray energy. The relatively constant efficiency of the method from 3 to 15 mev. or so makes it well worthy of consideration in those studies where the relative intensities of gamma-rays, as well as their energies, must be known accurately. The efficiency need not be so low as is commonly supposed: with the deuterium-filled chamber used in this work, a counting rate of about 4,000 per minute is given by 1 millicurie of 6-mev. gamma-rays at a distance of 10 cm. The greatest disadvantage of the method is that it is very sensitive to fast neutrons whose flux must be less than 0.001 of that of the gamma-rays for clean results to be obtained.

The gamma-rays on which we report all derive from the proton bombardment of light isotopes and are due to radiative capture with the exception of those from  $^{15}\text{N}$ . The bombarded isotopes are:

$^9\text{Be}$ : A thin target and a proton energy of 1,000 kev. were used. The measured gamma-ray energy was  $7.39 \pm 0.15$  mev. Measurements by Fowler, Lauritsen and Lauritsen (1948) had given  $7.4 \pm 0.2$  mev., and by Walker (1950),  $7.37 \pm 0.07$  mev.

$^{11}\text{B}$ : Protons of 950 kev. were used with a natural boron target of thickness 200 kev. Gamma-rays of 16.6, 11.8 and 4.3 mev. are known from this reaction for a thick target and a proton energy of 900 kev. (Fowler, Gaertner and Lauritsen 1938). Only the middle gamma-ray was measured here and found to be of  $12.50 \pm 0.21$  mev. The most accurate measurements are those of Walker (1950), who finds  $11.76 \pm 0.18$  and  $12.12 \pm 0.12$  mev. for protons of energy 510 and 1,200 kev. and thick targets.

$^{13}\text{C}$ : Protons of 570 kev. were used with a target of the separated isotope of stopping power about 20 kev. Lauritsen, Lauritsen and Fowler (1941) have reported 8.1 and 5.8 mev. gamma-rays of equal intensity from this resonance. We found a strong gamma-ray of  $8.14 \pm 0.08$  mev., but only a weak radiation of energy  $5.81 \pm 0.25$  mev. whose intensity was estimated as about 0.07 of that of the stronger line. It is possible, but not, we believe, likely, that this weaker line is due to fluorine contamination (6.1 mev.). The measurements were carried out at  $0^\circ$  to the proton beam.

$^{19}\text{F}$ : The radiative transition from the 669 kev. resonance discovered by Devons and Hereward (1948) was measured and found to be of  $12.09 \pm 0.28$  mev. and to possess an intensity  $1.72 \pm 0.25\%$  of that of the combined 6- and 7-mev. lines from this resonance. This energy is in accord with the  $12.0 \pm 0.2$  mev. reported by Rae, Rutherglen and Smith (1950) and confirms their remark that the transition takes place not to the ground state of  $^{20}\text{Ne}$  but rather to the excited state at about 1.5 mev. known from other measurements. These two determinations of the gamma-ray energy locate this state at  $1.50 \pm 0.2$  mev.

$^7\text{Li}$ : Protons of 500 kev. bombarded a thick target of metallic lithium. Gamma-rays of  $14.8 \pm 0.3$  and  $17.6 \pm 0.2$  mev. at the 440-kev. resonance are known from the work of Walker and McDaniel (1948). We measured the softer gamma-ray only, finding an energy of  $14.4 \pm 0.4$  mev.

$^{15}\text{N}$ : The gamma-ray in this case comes from  $^{12}\text{C}$  which results from alpha-particle emission following proton capture at about 900 kev. An excited state of  $^{12}\text{C}$ , formed in the  $^9\text{Be}(\alpha n)^{12}\text{C}$  reaction, at  $4.40 \pm 0.05$  mev. has been reported by Pringle, Roulston and Standil (1950), and at 4.45 mev. by Bradford and Bennett (1950). Walker (1950) finds  $4.43 \pm 0.15$  from the reaction  $^{11}\text{B}(\text{p}\gamma)^{12}\text{C}$ . T. Lauritsen\* has reported gamma-rays of energy 4.47 mev. from the reaction here studied; we find an energy of  $4.45 \pm 0.04$  mev. The gamma-rays are markedly anisotropic at 900 kev., having a distribution of the order  $1 + 0.3 \cos^2 \theta$ , though interference terms are probably present and the distribution depends somewhat on the proton energy. A target of  $^{15}\text{N}$  on molybdenum was used.

## ACKNOWLEDGMENTS

The authors would like to thank Sir John Cockcroft and Dr. W. D. Allen of the Atomic Energy Research Establishment, Harwell, who supplied the separated isotopes. One of us (J. H. C.) wishes to thank the Australian National University for the award of a travelling scholarship.

## REFERENCES

- BELL, R. E., and ELLIOTT, L. G., 1950, *Phys. Rev.*, **79**, 282.  
 BRADFORD, C. E., and BENNETT, W. E., 1950, *Phys. Rev.*, **78**, 302.  
 CHAO, C. Y., TOLLESTRUP, A. V., FOWLER, W. A., and LAURITSEN, C. C., 1950, *Phys. Rev.*, **79**, 108.  
 DEVONS, S., and HEReward, H. G., 1948, *Nature, Lond.*, **162**, 331.  
 FOWLER, W. A., GAERTTNER, E. R., and LAURITSEN, C. C., 1938, *Phys. Rev.*, **53**, 628.  
 FOWLER, W. A., LAURITSEN, C. C., and LAURITSEN, T., 1948, *Rev. Mod. Phys.*, **20**, 236.  
 LAURITSEN, T., LAURITSEN, C. C., and FOWLER, W. A., 1941, *Phys. Rev.*, **59**, 241.  
 PRINGLE, R. W., ROULSTON, K. I., and STANDIL, S., 1950, *Phys. Rev.*, **78**, 627.  
 RAE, E. R., RUTHERGLEN, J. G., and SMITH, R. D., 1950, *Proc. Phys. Soc. A*, **63**, 775.  
 WALKER, R. L., 1950, *Phys. Rev.*, **79**, 172.  
 WALKER, R. L., and MCDANIEL, B. D., 1948, *Phys. Rev.*, **74**, 315.  
 WILKINSON, D. H., 1950, *Proc. Camb. Phil. Soc.*, **46**, 508.

## LETTERS TO THE EDITOR

Fall and Re-increase of the  $^{12}\text{C}(\gamma, 3^4\text{He})$  Cross Section

Some preliminary results of an investigation of the photo-disintegration  $^{12}\text{C}(\gamma, 3^4\text{He})$ , using nuclear emulsions irradiated by gamma-rays from the A.E.R.E. synchrotron, have already been reported (Goward, Telegdi and Wilkins 1950). This investigation has been continued, with peak gamma-ray energies of up to 25.5 mev., and analysis of about 600 stars confirms and extends some interesting trends shown by the earlier results.

Figure 1 shows a histogram of the total energy release  $E_T$  of all the stars observed whose measurements indicated satisfactory momentum balance as carbon disintegrations ( $|\Delta| < 0.8$  in the notation of Goward and Wilkins (1950)). The superposed cross section  $\sigma$  curve was calculated by assuming a theoretical gamma-ray spectrum (Rossi and Greisen 1941), and is corrected for the appreciable influence of random errors in  $E_T$ . These errors are not closely known, but a reasonable assumption is a gaussian curve of total width 1.2 mev. at half amplitude. The cross-section curve then shows a considerable and effectively vertical drop at  $E_T \simeq 12$  mev., or  $E_\gamma$  (gamma-ray energy)  $\simeq 19.3$  mev. The subsequent re-increase in cross section is now firmly established by the observation of some

\* Report to the 1950 Harwell Conference.



80 stars with  $E_T > 14$  mev. The absolute cross-section values are considerably higher than the earlier estimate, mainly because of more experienced and thorough emulsion searching and more adequate correction for escape factors and overlooked stars. A reasonable estimate of the maximum cross section is  $2.4 \times 10^{-28}$  but this may easily still be an underestimate by about 50%.

In considering possible explanations of the cross-section curve shape, it must be remembered that most of the Figure 1 histogram was obtained by using the range-energy data of Lattes, Fowler and Cuer (1947); the more recent data of Rotblat, corrected to normal atmospheric conditions, would give  $E_T$  (and  $E_\gamma$ ) values some 0.5 mev. lower. Thus the main cross section fall may well occur near  $E_\gamma = 18.7$  mev., at which energy McElhinney *et al.* (1949) found evidence for a rapid rise in the  $^{13}\text{C}(\gamma, n)^{11}\text{C}$  cross section from zero to a value of the order of  $10^{-27}$  cm<sup>2</sup>.

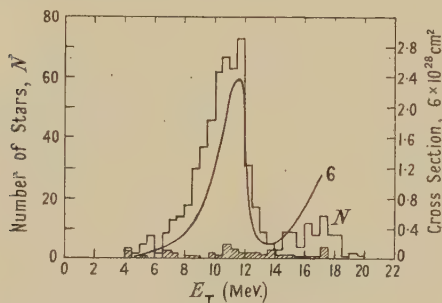


Figure 1.

Histogram,  $N$ , of total energy ( $E_T$ ) released in 597 carbon stars, with the corresponding cross section curve,  $\sigma$ . Events involving ground state  $^8\text{Be}$  are shown by shading.

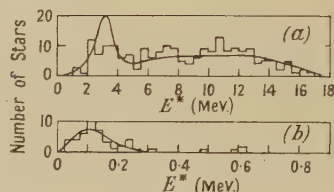


Figure 2.

- (a)  $E^*$  histogram for stars with  $E_T > 14$  mev., omitting stars involving ground state  $^8\text{Be}$ . The fitted curve shows the result expected if all stars involve a 3 mev. level of  $^8\text{Be}$  of experimental width  $\Gamma = 1.5$  mev.
- (b) Low energy part of  $E^*$  histogram for all  $E_T$  values with stars involving ground state  $^8\text{Be}$  included.

The re-increase of cross section at higher gamma-ray energies might suggest some alternative mode of disintegration to that already established for stars with  $E_T < 14$  mev., where the predominant mode of disintegration was via the 3 mev. excited level of  $^8\text{Be}$ . Analysis does not give significant support to this suggestion, however, as is shown by comparison of the experimental  $E^*$  histogram and calculated curve in Figure 2 (a).

A significantly increased proportion of stars is now found to involve ground state  $^8\text{Be}$  nuclei; the true overall proportion with correction for searching losses appears to be in excess of 10% in the present experiments. Such stars are indicated by shading in Figure 1, the proportion apparently increasing with energy. The considerable certainty with which these stars are identifiable is shown by Figure 2 (b). The fitted curve indicates the histogram shape expected if 43 stars involve ground state  $^8\text{Be}$ , with a disintegration energy of 0.1 mev. and negligible real level-width.

Atomic Energy Research Establishment,  
Harwell, Didcot, Berks.  
17th October 1950.

J. J. WILKINS.  
F. K. GOWARD.

GOWARD, F. K., TELEGDY, V. L., and WILKINS, J. J., 1950, *Proc. Phys. Soc. A*, **63**, 402.

GOWARD, F. K., and WILKINS, J. J., 1950, *Proc. Phys. Soc. A*, **63**, 662.

LATTES, C. M. G., FOWLER, P. H., and CUER, P., 1947, *Proc. Phys. Soc.*, **59**, 883.

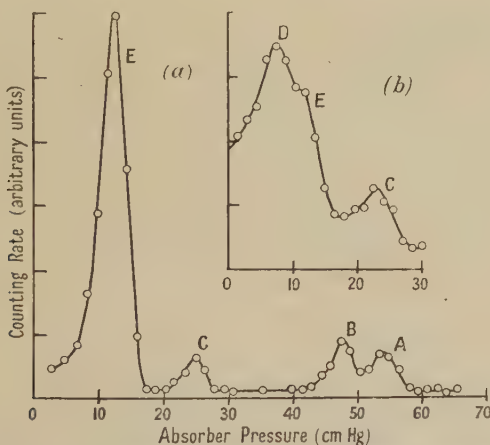
McELHINNEY, J., HANSON, A. O., BECKER, R. A., DUFFIELD, R. B., and DIVEN, B. C., 1949, *Phys. Rev.*, **75**, 542.

ROSSI, B., and GREISEN, K., 1941, *Rev. Mod. Phys.*, **13**, 240.

## The Reaction $^{23}\text{Na}(\text{d}, \alpha)^{21}\text{Ne}$

Some recent measurements on the reaction  $^{20}\text{Ne}(\text{d}, \text{p})^{21}\text{Ne}$  have pointed to the existence of levels in  $^{21}\text{Ne}$  with excitation energies of about 0.35, 1.8 and 2.8 mev. (Elder, Motz and Davison 1947, Zucker and Watson 1950, Ambrosen and Bisgaard 1950). The reaction  $^{23}\text{Na}(\text{d}, \alpha)^{21}\text{Ne}$  might be expected to lead to the same states, but earlier measurements by Murrell and Smith (1939) had revealed only the transitions to the ground state and to the 1.8 mev. level of  $^{21}\text{Ne}$ . A new study of this process therefore seemed to be of interest.

The energy distribution of alpha-particles from the reaction  $^{23}\text{Na}(\text{d}, \alpha)$  was studied with the aid of a differential ionization chamber and an air absorption cell. This technique has been described in an earlier letter (French and Treacy 1950). Thin targets of  $\text{Na}_2\text{SO}_4$  or  $\text{NaCl}$  were used, with deuteron bombarding energies between 0.83 and 0.93 mev. In addition to the alpha-particles from the process  $^{13}\text{C}(\text{d}, \alpha)$  in a carbon contamination layer on the target surface, four groups of alpha-particles from the disintegration of sodium were detected. With the  $\text{Na}_2\text{SO}_4$  targets, protons from the reaction  $^{16}\text{O}(\text{d}, \text{p})^{17}\text{O}^*$  were also observed. The Figure contains the results of typical measurements made at 0.83 mev. deuteron energy with a target of  $\text{NaCl}$ , about 0.4 mm. air equivalent evaporated on brass. In curve (a) only three of the sodium groups can be seen, the fourth being masked by the strong peak from carbon. The chief object of this particular run was to demonstrate the doublet structure at the high energy end of the spectrum; in other runs, with fresh targets of about twice the thickness, the fourth group was clearly resolved from the carbon peak (see curve (b) inset).



Alpha-particle groups (A, B, C, D) from deuteron bombardment of sodium at 0.83 mev. Group D masked by the carbon group E in the main figure, appears clearly (inset) when a fresh target is used.

Five separate determinations were made of the energy of each of the four groups from sodium. For calibration of the range scale, the following were taken as standards: (a) alpha-particles from  $\text{ThC}$ , mean range 4.70 cm.; (b) alpha-particles from  $^{13}\text{C}(\text{d}, \alpha)$ , a  $Q$  value of  $5.20 \pm 0.05$  mev. was assumed, after consideration of all the available data (Hornyak *et al.* 1950); (c) alpha-particles from  $^{18}\text{O}(\text{p}, \alpha)$ ,  $Q = 3.97 \pm 0.05$  mev. (Freeman 1950); (d) protons from  $^{18}\text{O}(\text{d}, \text{p})^{17}\text{O}^*$ ,  $Q = 1.049$  mev. (Buechner *et al.* 1949).

The new range-energy curves of Bethe (1950) were used in the analysis, although we have been forced to conclude from the accompanying text that his curve for protons refers to standard air, not to air at N.T.P. as stated on the graph.†

In the Table below are given the  $Q$  values with their probable errors for the different groups and the corresponding excitation energies in  $^{21}\text{Ne}$ . The values suggested by Hornyak *et al.* (1950) on the basis of the  $^{20}\text{Ne}(\text{d}, \text{p})$  experiments are given for comparison.

Our value of  $0.38 \pm 0.02$  mev. for the excitation of the first level in  $^{21}\text{Ne}$  agrees well with the figure of 0.39 mev. found by Ambrosen and Bisgaard (1950). The smaller splitting (0.31 mev.) found by Elder, Motz and Davison (1947) and by Zucker and Watson

† Professor Bethe has since confirmed our conclusion in a private communication.

Group	This work		Hornyak <i>et al.</i>	
	$Q$ (mev.)	Excitation (mev.)	$Q$ (mev.)	Excitation (mev.)
A	$6.84 \pm 0.05$	0	6.86	0
B	$6.46 \pm 0.04$	$0.38 \pm 0.02$	6.52	0.34
C	$5.09 \pm 0.04$	$1.75 \pm 0.04$	5.06	1.80
D	$4.08 \pm 0.06$	$2.76 \pm 0.05$	4.02	2.84

(1950) may be due to the less complete resolution of the two groups in their experiments. For the higher levels our results show satisfactory agreement with the values chosen by Hornyak *et al.* (1950).

Our figure of  $6.84 \pm 0.05$  mev. for the energy release of the ground state transition in  $^{23}\text{Na}(d, \alpha)^{21}\text{Ne}$  agrees well with that computed from the values  $2.35 \pm 0.04$  mev. in the process  $^{23}\text{Na}(p, \alpha)^{20}\text{Ne}$  (Freeman 1950) and  $4.51 \pm 0.07$  mev. in  $^{20}\text{Ne}(d, p)^{21}\text{Ne}$  (Hornyak *et al.* 1950).

We are grateful to Dr. W. E. Burcham for pointing out that a new study of the reaction  $^{23}\text{Na}(d, \alpha)$  was desirable. One of us (D. M. T.) is indebted to the Department of Scientific and Industrial Research for a maintenance grant.

Cavendish Laboratory,  
Cambridge.

28th October 1950.

A. P. FRENCH.

D. M. THOMSON.

AMBROSEN, J., and BISGAARD, K. M., 1950, *Nature, Lond.*, **165**, 888.

BETHE, H. A., 1950, *Rev. Mod. Phys.*, **22**, 213.

BUECHNER, W. W., STRAIT, E. N., SPERDUTO, S., and MALM, R., 1949, *Phys. Rev.*, **76**, 1543.

ELDER, F. K., MOTZ, H. T., and DAVISON, P. W., 1947, *Phys. Rev.*, **71**, 917.

FREEMAN, J. M., 1950, *Proc. Phys. Soc. A*, **63**, 668.

FRENCH, A. P., and TREACY, P. B., 1950, *Proc. Phys. Soc. A*, **63**, 665.

HORNYAK, W. F., LAURITSEN, T., MORRISON, P., and FOWLER, W. A., 1950, *Rev. Mod. Phys.*, **22**, 291.

MURRELL, E. B. M., and SMITH, C. L., 1939, *Proc. Roy. Soc. A*, **173**, 410.

ZUCKER, A., and WATSON, W. W., 1950, *Phys. Rev.*, **78**, 14.

## Nuclear Spin of Erbium-167

The paramagnetic resonance spectrum of a single crystal of erbium ethyl sulphate, diluted with lanthanum ethyl sulphate, has been observed at 1.2 cm. wavelength. For all directions of the external magnetic field a single strong line is found; centred on this is a set of eight almost equally spaced weak lines. The relative intensity of these lines, and their variation with angle, is consistent with their assignment to the hyperfine structure of the single odd isotope of mass 167 (natural abundance = 22.8% (Leland 1950)). It follows that the nuclear spin of this isotope is 7/2. This is the same as that of neodymium 143 and 145 (Bleaney and Scovil 1950), and these three isotopes are the first odd-neutron nuclei to have been discovered with spin 7/2.

The spectrum has been analysed in terms of the usual Hamiltonian,

$$\mathcal{H} = \beta\{g_{\parallel}H_zS_z + g_{\perp}(H_xS_x + H_yS_y)\} + AS_zI_z + B(S_xI_x + S_yI_y) + Q\{I_z^2 - \frac{1}{3}I(I+1)\},$$

and the following values are found for the parameters (the effective value of  $S$  is taken as  $\frac{1}{2}$ , since only one electronic transition is observed):

$$g_{\parallel} \text{ (parallel to axis)} = 1.47 \pm 0.03; \quad g_{\perp} \text{ (perpendicular to axis)} = 8.85 \pm 0.2;$$

$$A = 0.0059 \text{ cm}^{-1} \pm 0.0002; \quad B = 0.0307 \text{ cm}^{-1} \pm 0.0005; \quad Q < 0.005 \text{ cm}^{-1}.$$

The anisotropy in the  $g$ -values is by far the largest yet discovered. Susceptibility measurements of van den Handel (1940) reveal very little anisotropy at temperatures down to 15° K.; this result can only be reconciled with ours if there are other very low-lying levels besides those giving rise to the transition observed by us. This is also suggested by the very short spin-lattice relaxation time (see below).



The ratio  $A:B$  is nearly the same as the ratio  $g_{\parallel}:g_{\perp}$ , as was also the case with neodymium. As a result, the width of the hyperfine structure in gauss as observed at constant frequency is almost the same in all directions. The theoretical work of Elliott and Stevens (1951) is in accordance with this, and shows also that no effect due to a quadrupole moment should be detectable. Our upper limit for  $Q$  is based on the absence of observable deviations from the normal spacing of the hyperfine structure, which would be of the order of  $Q^2/B$ .

The line-width showed an interesting effect, being dependent on the direction of the external magnetic field, and varying inversely as the  $g$ -value. This behaviour is to be expected if the dominant broadening is due to spin-lattice relaxation, and the relaxation time  $\tau$  is independent of the orientation of the magnetic field. We have

$$\tau = \frac{1}{2\pi c\Delta\bar{\nu}} = \frac{\hbar}{2\pi g\beta\Delta H} = \frac{1.14 \times 10^{-7}}{g\Delta H},$$

where  $\Delta\bar{\nu}$ ,  $\Delta H$  refer to the half-width at half intensity in wave numbers and gauss respectively. At  $\bar{\nu}=0.845 \text{ cm}^{-1}$  the values of  $\Delta H$  parallel and perpendicular to the axis respectively were  $81 \pm 5$  and  $14 \pm 1$  gauss, giving  $\tau=0.95 \pm 0.05 \times 10^{-9}$  second at the lowest temperature, estimated to be  $13 \pm 1^\circ \text{ K.}$  from the vapour pressure of the liquid hydrogen. At  $20^\circ \text{ K.}$  the lines were about ten times broader, showing that  $\tau$  varies roughly as the inverse seventh power of the temperature. It should be noted that as the orientation of the crystal is changed, the magnetic field changes, but the frequency of the transition remains constant. The measurements show that  $\tau$  also remains constant under these conditions. The theory of Van Vleck (1940) for caesium titanium alum shows that in strong fields the relaxation time should be isotropic and independent of the external field, if the 'Raman processes' predominate in the relaxation mechanism, as is certainly the case in our experiment.

No absorption lines could be obtained in the ethyl sulphates of cerium, samarium, dysprosium and ytterbium at  $1.2 \text{ cm.}$  wavelength,  $20^\circ \text{ K.}$  and fields up to  $12 \text{ kg.}$  Measurements are now in progress on the bromates of these elements. Work is also planned to observe the hyperfine lines at zero magnetic field, by which means a value of  $Q$  of  $1/100$  of that given above should be detectable.

Our thanks are due to Mr. J. K. Marsh for the generous gift of the samples of erbium and other rare earths.

Clarendon Laboratory,  
Oxford.

B. BLEANEY.  
H. E. D. SCOVIL.

14th November 1950.

BLEANEY, B., and SCOVIL, H. E. D., 1950, *Proc. Phys. Soc. A*, **63**, 1369.

ELLIOTT, R. J., and STEVENS, K. W. H., 1951, *Proc. Phys. Soc. A*, **64**, 205.

VAN DEN HANDEL, J., 1940, *Thesis* (Leiden University).

LELAND, W. T., 1950, *Phys. Rev.*, **77**, 634.

VAN VLECK, J. H., 1940, *Phys. Rev.*, **57**, 426.

## A Preliminary Survey of the Paramagnetic Resonance Phenomena observed in Rare Earth Ethyl Sulphates

In recent letters Bleaney and Scovil (1950, 1951) have reported the results of their experimental work on the rare earth ethyl sulphates of the form  $M(\text{C}_2\text{H}_5\text{SO}_4)_3 \cdot 9\text{H}_2\text{O}$ . Here we report the results of some preliminary theoretical investigations using a crystalline electric field hypothesis to account for the magnetic properties at low temperatures. In most of our work so far we have used only first-order perturbation theory, with the result that we have only sought approximate agreement with experiment.

From the crystal structure of cerium ethyl sulphate (Ketelaar 1937) it seems reasonable to assume that the ion is embedded in a crystal field possessing  $D_{3h}$  symmetry. Using potential terms up to the sixth degree and neglecting terms of odd parity (which give no contribution in first order) our potential takes the form

$$V = A_0 + A_2(3z^2 - r^2) + A_4(35z^4 - 30r^2z^2 + 3r^4) + A_6^0(231z^6 - 315r^2z^4 + 105r^4z^2 - 5r^6) \\ + A_6^6(x^6 - 15x^4y^2 + 15x^2y^4 - y^6).$$

The coefficients  $A$  can be estimated for cerium, and we take slightly different values for the other ions.

Assuming that  $V < \text{spin-orbit coupling}$ , we can treat it as a perturbation on the lowest  $J$  manifold, and our results for the ions with an odd number of electrons are as follows:

$\text{Ce}^{+++} 4f^1 {}^2F_{5/2}$ . The sixth-order terms have no matrix elements inside  $J=5/2$  so the states are eigenstates of  $J_z$ . We find the doublet spanned by  $J_z = \pm 5/2$  lies lowest, which accounts for the absence of a resonance.

$\text{Nd}^{+++} 4f^3 {}^4I_{9/2}$ . Neglecting  $A_6^6$ , we find  $J_z = \pm 7/2$  is lowest with  $J_z = \pm 5/2$  near. The effect of  $A_6^6$  will be to mix these states and change the lowest states to

$$a|\frac{7}{2}\rangle + b|-\frac{5}{2}\rangle \quad \text{and} \quad a|-\frac{7}{2}\rangle + b|\frac{5}{2}\rangle.$$

Taking  $|a|=0.9$  and  $|b|=0.4$  gives  $g_{\parallel}=3.54$  and  $g_{\perp}=2.0$ , whereas experiment gives  $g_{\parallel}=3.61$  and  $g_{\perp}=2.05$ . The only other states for which transitions are allowed are  $J_z = \pm 1/2$ , which yield  $g_{\parallel}=8/11$  and  $g_{\perp}=40/11$ .

$\text{Sm}^{+++} 4f^5 {}^6H_{5/2}$ . The sixth-order terms have no matrix elements and  $V$  gives  $J_z = \pm 1/2$  lowest. The corresponding  $g$ -values are  $g_{\parallel}=2/7$  and  $g_{\perp}=6/7$ . No transitions have been observed as these values lie outside the range of observation.

$\text{Gd}^{+++} 4f^7 {}^8S$ . Since this ion is in an orbital S-state, to our approximation the crystalline field gives no splitting, and other effects become important (Pryce 1950).  $g$  is isotropic and closely equal to 2.

$\text{Dy}^{+++} 4f^9 {}^6H_{15/2}$ . Our potential field gives the ground states as approximately  $J_z = \pm 15/2$ , to which are admixed  $J_z = \pm 3/2$ , and there will be no transitions. If our estimates of the crystalline fields are slightly inaccurate ( $A_n \bar{r}^n$  varies from ion to ion) it may happen that  $J_z = \pm 13/2$  is lowest, and to this are admixed small amounts of  $J_z = \pm 1/2$  and  $J_z = \pm 11/2$ . This would lead to small  $g$ -values which would not have been observed and which would appear to be in disagreement with susceptibility measurements of van den Handel (1940).

$\text{Er}^{+++} 4f^{11} {}^4I_{15/2}$ . The crystalline field without  $A_6^6$  gives  $J_z = \pm 5/2$  and  $J_z = \pm 7/2$  close together at the bottom. When these are admixed we get the states  $a|\frac{7}{2}\rangle + b|-\frac{5}{2}\rangle$  and  $a|-\frac{7}{2}\rangle + b|\frac{5}{2}\rangle$  with  $|a| \simeq |b| \simeq 1/\sqrt{2}$ . The corresponding  $g$ -values are  $g_{\parallel}=1.2$  and  $g_{\perp}=8.9$ . On the other hand small changes in the crystalline field may give  $J_z = \pm 1/2$  lowest, to which are admixed small amounts of  $J_z = \pm 11/2$  and  $\pm 13/2$ . The corresponding  $g$ 's are approximately  $g_{\parallel}=1.2$  and  $g_{\perp}=9.6$ , and with the experimental  $g$ 's of  $g_{\parallel}=1.47$  and  $g_{\perp}=8.85$  we cannot, at present, decide which levels are actually lowest.

$\text{Yb}^{+++} 4f^{13} {}^2F_{7/2}$ . Here we find  $J_z = \pm 3/2$  is the lowest level, and there will be no transitions in agreement with experiment.

We now turn to the consideration of the nuclear hyperfine structure. The absence of hyperfine structure in gadolinium points to the fact that the admixture of states containing unpaired s-electrons (Abragam 1950) is small, and this will probably be true for the other ions also. With our approximate electronic states the hyperfine structure arising from magnetic interactions should show the same anisotropy as the  $g$ 's, as is approximately correct. The deviations are probably due to admixtures of states in other  $J$  manifolds (particularly  $J'=J \pm 1$ ) to the ground states, and show that second-order effects are not negligible. Using the values given by Bleaney and Scovil for the constants in their Hamiltonian, we can estimate the magnitudes of the nuclear magnetic moments and set upper limits to the nuclear electric quadrupole moments. These values are liable to considerable error as it is necessary to estimate  $1/r^3$  (Sternheimer 1950). The accompanying Table gives our results. In particular the upper limit set to the quadrupole moments is found to be large.

	$A$	$Q$	$\mu(1/r^3)$	$Q(1/r^3)$	$(1/r^3)$	$\mu$	$Q'$
$^{143}\text{Nd}$	0.040	$<0.002$	47	$<870$	34	1.4	$<25$
$^{145}\text{Nd}$	0.025	$<0.002$	29	$<870$	34	0.85	$<25$
$^{167}\text{Er}$	0.0059	$<0.005$	45	$\left. \begin{array}{l} <740 \\ <1300 \end{array} \right\}$	75	0.6	$\left\{ \begin{array}{l} <10 \\ <17 \end{array} \right.$

This work is continuing and will be reported more fully in due course.

$A$  and  $Q$  are as defined by Bleaney and Scovil and are in  $\text{cm}^{-1}$ ;  $\overline{1/r^3}$  is given in units of  $10^{24} \text{ cm}^{-3}$ ;  $\mu$  is given in nuclear magnetons;  $Q'$  is the quadrupole moment in units of  $e \times 10^{-24} \text{ cm}^2$  and is defined (Mack 1950) by  $Q' = \int \rho_I (3z^2 - r^2) d\tau$ , where  $\rho_I$  denotes the charge density for  $m_I = I$ . The two upper limits of  $Q$  for erbium arise from the uncertainty in the ground state. The smaller value is due to  $|\pm \frac{1}{2}\rangle$ .

Clarendon Laboratory,  
Oxford.

14th November 1950.

R. J. ELLIOTT.

K. W. H. STEVENS.

ABRAGAM, A., 1950, *Phys. Rev.*, **79**, 534.

BLEANEY, B., and SCOVIL, D., 1950, *Proc. Phys. Soc. A*, **63**, 1369; 1951, *Ibid.*, **64**, 204.

VAN DEN HANDEL, J., 1940, *Thesis* (Leiden).

KETELAAR, J. A. A., 1937, *Physica*, **4**, 619.

MACK, J. E., 1950, *Rev. Mod. Phys.*, **22**, 64.

PRYCE, M. H. L., 1950, *Phys. Rev.*, in the press.

STERNHEIMER, R., 1950, *Phys. Rev.*, **80**, 102.

## Scattering of Neutrons by Ferromagnetic Crystals

Consider neutrons with wavelength greater than the Bragg reflection wavelength scattered by a ferromagnetic crystal. Then inelastic magnetic scattering in which the neutrons lose energy by disorienting atomic magnetic moments within a domain would be expected to be small from energetic reasons. J. M. Cassels has suggested to the author that at temperatures not too far below the Curie point where there are an appreciable number of disoriented atomic moments within a domain, some of the disoriented electron spins may be reoriented during scattering into the direction of magnetization. This would result in loss of exchange energy by the scatterer, and consequent gain in energy by the neutrons.

The purpose of this note is to report the result of an investigation of this effect using Bloch spin wave functions to provide a simple model of a ferromagnetic, with just one magnetic electron per atom. The approximate theory of Bloch spin waves (Seitz 1940) in which the waves are assumed to be non-interacting, is probably good up to room temperatures in iron. Using this theory the total cross section for inelastic magnetic scattering of monochromatic neutrons, with wavelength greater than the Bragg reflection wavelength, by a single crystal can be written  $\sigma = \sum \sigma(\mathbf{n})$ .  $(2\pi/a)\mathbf{n}$  is a vector in the reciprocal lattice,  $a$  being the constant for a cubic lattice. We take the lattice constant and the Curie temperature and the body-centred cubic structure for iron, but just one magnetic electron per atom.

In the scattering process discussed here, the neutron receives two contributions to its momentum. One is from the spin wave which in practice is always small, due to the energy relation. The other is from the periodic field and corresponds to the momentum, though not, of course, the energy, relation appropriate to a Bragg scattering. Each  $\sigma(\mathbf{n})$  is then the cross section corresponding to such a momentum relation. The first term, with  $\mathbf{n}=0$ , is small angle scattering, where the energy transfer is small. For  $\mathbf{n}$  not equal to 0,  $\sigma(\mathbf{n})$  represents a scattering into a small solid angle of the order  $\frac{1}{2\pi}$  steradian round the direction of the vector  $\mathbf{p} - (2\pi/a)\mathbf{n}$  where  $\mathbf{p}$  is the wave number of the incoming neutrons. (In fact the momentum equation is  $\mathbf{p}' = \mathbf{p} - (2\pi/a)\mathbf{n} + \mathbf{k}$ , where  $\mathbf{p}'$  is the wave number of the scattered neutron, and  $\mathbf{k}$  is the wave number of the annihilated spin wave and is very small.) Since  $|\mathbf{p}| < \frac{1}{2}(2\pi/a)|\mathbf{n}|$ , scattering occurs in directions near the directions of the reciprocal lattice vectors. It is found that only the terms for  $\mathbf{n}^2=2$  are important, due largely to the decrease of the atomic form factor for large  $|\mathbf{n}|$ .

As an example, for a crystal temperature of  $400^\circ \text{K}$ . for  $\mathbf{n}=(1,1,0)$ ,  $\mathbf{p}=(2\pi/a)(\frac{1}{2},0,0)$  and for an unmagnetized crystal and unpolarized neutrons, it is found that  $\sigma(\mathbf{n})$  is about  $\frac{1}{50}$ . This corresponds to a differential cross section of  $\frac{1}{2}$  barn per steradian.

If this effect were to be observed it would provide a test of the Bloch model. The possibility of observing it depends on the large differential cross section for wavelengths at which the nuclear scattering is isotropic, and of the order of magnitude of about 8 barns. Moreover, the energy of the scattered neutrons will be greater than that of the incoming



neutrons, the final wave number corresponding to  $\sigma(\mathbf{n})$  being given approximately by  $|\mathbf{p}'| = |\mathbf{p} - (2\pi/a)\mathbf{n}|$ . As the direction of scattering corresponding to  $\sigma(\mathbf{n})$  does not depend on  $|\mathbf{p}|$ , for  $\mathbf{p}$  in the direction of  $\mathbf{n}$ , such neutrons need not be monochromatic, provided the wavelength is greater than the Bragg reflection wavelength.

In real iron, instead of just one spin per atom there are approximately two. The likely effect of this would be to broaden somewhat the angular range of the scattering corresponding to each  $\sigma(\mathbf{n})$ . Such a change would probably not, however, invalidate the qualitative conclusions of this work.

Department of Mathematical Physics,  
University of Birmingham.  
4th November 1950.

R. G. MOORHOUSE.

SEITZ, F., 1940, *The Modern Theory of Solids* (London and New York: McGraw-Hill), pp. 617 ff.

### A Note on the Radially Symmetrical Phase Growth Controlled by Heat Conduction

In a recent paper Frank (1950) gave a function for the space-time dependence of the temperature in radially symmetrical heat conduction problems, when a sphere of new phase is growing. His function is

$$U(s) = U_{\infty} + A[s^{-1}\exp(-\frac{1}{2}s^2) - \frac{1}{2}\pi^{1/2}\{1 - \operatorname{erf}(\frac{1}{2}s)\}]. \quad \dots\dots(1)$$

The temperature is dependent upon the only variable  $s$ , which is a combination of the space- and time-coordinates  $r$  and  $t$ :

$$s = ra^{-1}t^{-1/2}. \quad \dots\dots(2)$$

The temperature of the boundary is always  $U_S(S) = \text{const.}$  (equilibrium temperature between the two phases) and its velocity of propagation is ( $S$  marks the boundary)

$$v = dr/dt = \frac{1}{2}Sat^{-1/2} \quad \dots\dots(3)$$

There is another means of describing the temperature around a growing sphere of new phase. The source function for a point heat source is, in  $n$ -dimensional space

$$U(r, t) = Q(2^n \pi^{n/2} c \gamma a^n t^{n/2})^{-1} \exp(-r^2/4a^2 t). \quad \dots\dots(4)$$

The heat is generated on the surface of the growing sphere and the corresponding temperature distribution is given by an integral over the surface having the value

$$U(r, t) = \frac{Q}{2^n \pi^{n/2} c \gamma a^n t^{n/2}} \exp\left(-\frac{r^2 + \rho^2}{4a^2 t}\right) \left\{ \left(\frac{i\rho r}{4a^2 t}\right)^{1-\frac{1}{2}n} \Gamma\left(\frac{1}{2}n - 1\right) J_{\frac{1}{2}n-1}\left(i\frac{2\rho r}{4a^2 t}\right) \right\} \dots\dots(5)$$

where  $Q$  is the quantity of heat,  $c$  the specific heat,  $\gamma$  the density,  $a^2$  the thermal conductivity and  $J$  the Bessel function of the first kind. One has also to integrate over all the time that heat is generated and this gives (for  $n=3$ )

$$U(r, t) = \int_{\tau=0}^t \frac{Q_0 \rho(\tau) v(\tau) d\tau}{2\pi^{1/2} c \gamma a r (t-\tau)^{1/2}} \left\{ \exp\left(-\frac{[r-\rho(\tau)]^2}{4a^2(t-\tau)}\right) - \exp\left(-\frac{[r+\rho(\tau)]^2}{4a^2(t-\tau)}\right) \right\}, \dots\dots(6)$$

$Q_0$  is the quantity of heat for unit volume.  $\rho = \int v(\eta) d\eta$  and  $v$  are the position and velocity of boundary between the two phases.

In the above-mentioned case  $\rho$  and  $v$  are determined by equations (2) and (3). Then equation (6) becomes

$$U = -\frac{Q_0 s}{\pi^{1/2} c \gamma} \int_{Z=0}^{\infty} \frac{Z^2 - 1}{(Z^2 + 1)^2} \exp(-\frac{1}{2}s^2 Z^2) dZ \quad \dots\dots(7)$$

where  $Z^2 = (t^{1/2} + \tau^{1/2})/(t^{1/2} - \tau^{1/2})$ . Integration with known formulae (see, for example, Magnus and Oberhettinger 1948) gives the function of equation (1) as it must be.

The advantage of the integral (6) lies in the possibility of choosing any function for  $v$  (and  $p$ ) which may be desirable for any problem suggested by theoretical consideration or by experience.

A one-dimensional case of phase growth, in which the velocity  $v$  is assumed proportional to the difference between the equilibrium temperature  $U_S$  and the temperature of the boundary  $U$ ,  $v = C(U_S - U)$ , was treated by Geist und Dehlinger (1949). The temperature of the boundary  $U$  lies beneath  $U_S$  on account of supercooling. To use the one-dimensional analogue to equation (6), (6'), in this case, obviously one must first determine  $v$  as a function of  $t$  from an integral equation resulting from the velocity law inserted into equation (6').

Nürnberg,  
Germany.

D. GEIST.

1st November 1950.

FRANK, F. C., 1950, *Proc. Roy. Soc. A*, **201**, 586.

GEIST, D., and DEHLINGER, U., 1949, *Z. Naturforsch.*, **4 a**, 415.

MAGNUS, W., and OBERHETTINGER, F., 1948, *Formeln und Sätze für die speziellen Funktionen der mathematischen Physik* (Berlin: Springer-Verlag.) p. 126.

## Calculation of Relative Transition Probabilities for First Negative Bands of $N_2^+$

The relative transition probabilities between the lower vibrational levels of the two electronic states corresponding to the transition  $x^2\Sigma_g^+ - B^2\Sigma_u^+$  in  $N_2^+$  have been calculated here using the simple harmonic wave functions. These normalized wave functions are well known and take the form

$$S_v = d^{-1/2} (2^v v! \sqrt{\pi})^{-1/2} H_v(x/d) \exp \{-\frac{1}{2}(x/d)^2\}, \quad \dots \dots (1)$$

where  $x = r - r_e$  ( $r_e$  being the equilibrium internuclear distance) and  $v$  is the vibrational quantum number. Further  $d^2 = \hbar / 4\pi^2 \mu \omega_e$ , where  $\mu$  is the reduced mass of the system and  $\omega_e$  is the usual quantity occurring in the expression for the vibrational energy. The relative transition probabilities depend on the expression

$$p(n', v'; n'', v'') = \left| \int_0^\infty S(n', v' | r) S(n'', v'' | r) dr \right|^2 \quad \dots \dots (2)$$

where  $n'$  and  $n''$  refer to the quantum numbers of the upper and lower electronic states. The  $p$  values for various  $(v', v'')$  numbers were calculated using the wave functions given in equation (1), the integration over the internuclear distance  $r$  being carried out graphically.

The values of the constants for the two electronic states, together with the reduced mass of the system, are given in Table 1 (see Herzberg 1950).

Table 1

	$\mu = 1.162 \times 10^{-23}$ gm.		
	$r_e$ ( $10^{-8}$ cm.)	$\omega_e$ ( $\text{cm}^{-1}$ )	$d$ ( $10^{-10}$ cm.)
$x^2\Sigma_g^+$	1.116	2207	4.67
$B^2\Sigma_u^+$	1.075	2420	4.46

Table 2 gives the final  $p$  values, together with the values (in brackets) obtained by Bates (1949) using the Morse potential function. The experimental values obtained by Herzberg (1928) are given in square brackets.

Table 2

$v' \setminus v''$	0	1	2
0	0.69 (0.65) [0.69]	0.34 (0.26) [0.26]	—
1	0.29 (0.30) [0.23]	0.26 (0.22) [0.27]	—
2	0.02 (0.05) [0.07]	—	—
3	0.00 (0.00) [0.00]	—	0.29 (0.41) [0.36]

It appears that good agreement with experiment is obtained by using simple harmonic oscillator wave functions and the use of complicated Morse wave functions hardly seems justified in the view of the accuracy. For higher ( $v'$ ,  $v''$ ) numbers, however, where increased cancellation of the wave functions occurs the simple harmonic wave functions will certainly be useless and, although the Morse functions should give fairly accurate results, the calculations become extremely lengthy.

It would be of interest to apply the method of distorted wave functions (as adopted by Pillow 1949, 1950) to the transitions considered above.

Department of Physics,  
Imperial College, London, S.W.7.  
23rd November 1950.

G. STEPHENSON.

BATES, D. R., 1949, *Proc. Roy. Soc. A*, **196**, 217.

HERZBERG, G., 1928, *Z. Phys.*, **49**, 761; 1950, *Molecular Spectra and Molecular Structure* (New York: Van Nostrand).

PILLOW, M. E., 1949, *Proc. Phys. Soc. A*, **62**, 237; 1950, *Ibid.*, **63**, 940.

### $C_2$ (Swan) Bands in Krypton

Swan bands are known to be excited, among other methods, by inert gases. Among the gases that have so far been used are helium, neon and argon. While studying the selective efficiency of the production of these bands at various pressures of the above three gases in a discharge tube having carbon electrodes, some connection was noticed between the efficiency of the bands and the excitation potentials of the gases. Thus the bands were much more efficient and purer in argon than in neon, and better in neon than in helium. The order of efficiency was observed to be generally in inverse proportion to the excitation potentials of the gases; krypton, having less excitation potential than argon, was expected to act as a still better exciter of Swan bands. This suggestion has led us to investigate these bands in krypton.

The discharge tube was of the H-type fitted with carbon electrodes. It was filled with mercury-free krypton gas, at successive pressures in the range 5 mm. to 50 mm. Hg, and the discharge was excited by a neon sign transformer, with its primary fed from 230 v. A.C. mains through a variac. The best conditions of gas pressure and current density were established to obtain bands as intense and pure as possible. As expected, the bands came out with comparative ease, as in argon, and probably a little better. The relative intensities, from visual estimates, for the different composite sequences of the bands for equivalent pressure and current density conditions are given below together with the impurity spectra. The figures are based upon 100 for the (0, 0) band in every case.

	Helium	Neon	Argon	Krypton
1st excitation potential	19.77	16.58	11.57	9.98
$C_2$ (Swan) sequences				
$\Delta v = +2$	40	30 ?	120	50
+1	200	300	380	310
0	160	200	210	230
-1	330	300	350	430
-2	320	{overlapped by Ne lines}	360	470
Comet tail ( $CO^+$ )	prominent	weaker than in He	absent	absent
Triplet ( $CO$ )	weak	absent	absent	absent
CH (4315)	strong	weak	prominent	weak
Atomic lines	H and He lines fair in intensity	H feeble Ne strong	A lines very feeble, if any	a few prominent Kr lines

It appears from these observations that, among the inert gases investigated, krypton acts as a more efficient source than helium or neon for excitation of Swan bands, and is more



or less comparable with argon, if not a little better. Xenon ( $V_e=8.39$ ), which is expected to be still better, is under investigation in this laboratory. In this connection it may be noted that there is evidence of selective excitation of the bands at a definite region of pressure characteristic of each gas. It appears that this excitation is a consequence of the energy of electrons in the discharge (depending on the excitation and ionization potentials of the gases), metastable states and the probability of the collisions of the second kind; this is discussed in a paper to be published in *Current Science*. A more detailed paper giving quantitative estimates with relevant aspects is under preparation.

The authors are indebted to Dr. N. R. Tawde for his helpful guidance and discussion.

Spectroscopic Laboratories,  
The Institute of Science,  
Bombay, India.  
24th November 1950.

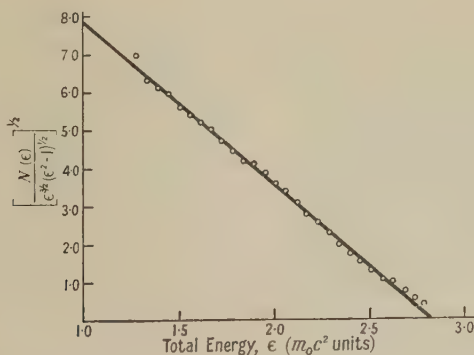
G. K. MEHTA.  
V. RAJESWARI.

### The $^{12}\text{C}(n, 2n)^{11}\text{C}$ Reaction in an Anthracene Crystal

When the 110-inch cyclotron at the Atomic Energy Research Establishment, Harwell, began operating recently, it was necessary to check that in those parts of the building which were occupied for any length of time the neutron flux (of maximum energy 175 mev.) was less than the specified biological tolerance level.

For neutrons of energy greater than 20.4 mev. this has been carried out satisfactorily by the use of the  $^{12}\text{C}(n, 2n)^{11}\text{C}$  reaction, the threshold for which occurs at the above neutron energy (Sherr 1945). The  $^{11}\text{C}$  decays with a half-life of  $20.35 \pm 0.08$  minutes, emitting a positron of maximum energy 0.97 mev. (Mattauch and Flammersfeld 1949). The cross section for the reaction has been calculated theoretically by Heckrotte and Wolff (1948). It is, to a rough approximation, constant, and the calculated value at 90 mev. (0.012 barn) is in substantial agreement with the value obtained experimentally by McMillan and York (1948) at 90 mev. ( $0.022 \pm 0.004$  barn).

The maximum permissible flux of fast neutrons of energy greater than 5 mev. has been calculated by Neary and by Tait (A.E.R.E. private communication) as  $30 \text{ neutrons cm}^{-2} \text{ sec}^{-1}$ . It is desirable to be able to measure a fraction of a tolerance dose, and so a sensitive method of detection is necessary.



High sensitivity has been achieved by irradiating an anthracene crystal (mass 4.48 gm.) and counting, with an E.M.I. photomultiplier tube, the scintillations produced in the crystal itself by the positrons from the decaying  $^{11}\text{C}$  nuclei. It is possible to detect a neutron flux of  $15 \text{ neutrons cm}^{-2} \text{ sec}^{-1}$  by this method. It involves an irradiation time of 30 minutes and a similar counting time. The method is not affected by the presence of gamma radiation.

The technique also provides an interesting example of the use of a scintillation counter for the study of a beta-ray spectrum. After the crystal had been irradiated for 30.5 minutes in a flux of  $2 \times 10^6$  neutrons  $\text{cm}^{-2} \text{sec}^{-1}$ , a pulse-size distribution was obtained using a single-channel 'kick-sorter'. The 'Fermi diagram' derived from this distribution is illustrated in the Figure. The results compare favourably with those obtained with magnetic beta-ray spectrographs (Siegbahn and Bohr 1944).

The scintillation counting apparatus and crystal were made available by Mr. R. B. Owen. The authors wish also to thank the Director, Atomic Energy Research Establishment, and the President, South African Council of Scientific and Industrial Research, for permission to publish this note.

Atomic Energy Research Establishment,  
Harwell, Didcot, Berks.  
27th November 1950.

J. SHARPE.  
G. H. STAFFORD.  
(of South African C.S.I.R.).

HECKROTTE, W., and WOLFF, P., 1948, *Phys. Rev.*, **73**, 265.

McMILLAN, E. M., and YORK, H. F., 1948, *Phys. Rev.*, **73**, 262.

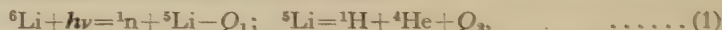
MATTAUCH and FLAMMERSFELD, 1949, *Isotopic Report*. (Special issue of *Z. Naturforsch.*)

SHERR, R., 1945, *Phys. Rev.*, **68**, 249.

SIEGBAHN, K., and BOHR, E., 1944, *Arkiv Mat. Astr. Fys.*, **30 B**, No. 3.

## The Reaction ${}^6\text{Li}(\gamma\text{n}){}^5\text{Li}$ and Energy Levels of the ${}^5\text{Li}$ Nucleus

In the course of photo-disintegration experiments using lithium loaded emulsions (Titterton 1950 a, b) evidence was sought for the reaction



and while some events were observed which were compatible with this disintegration scheme, they were too few to be sure of the assignment.

Recently Ilford E<sub>1</sub> emulsions loaded with the separated isotope  ${}^6\text{Li}$  have been irradiated with gamma-rays from the 440 kev.  ${}^7\text{Li}\gamma$  resonance and have yielded definite evidence for the reaction. The recoiling  ${}^5\text{Li}$  nucleus (having a lifetime of about  $10^{-21}$  second) breaks up into a proton and an alpha-particle to form a V-track in the emulsion. In some cases the discrimination is good enough to identify the proton, in others it is not. Three typical events are shown in Figure 1 (a) and (b), where two correspond to break-up from the ground state of  ${}^5\text{Li}$  and the third to break-up from an excited state.

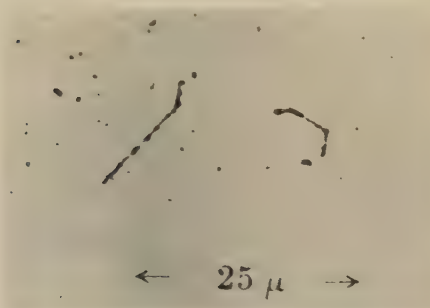


Figure 1 (a). V-tracks resulting from break-up of  ${}^5\text{Li}$  nuclei in ground state.

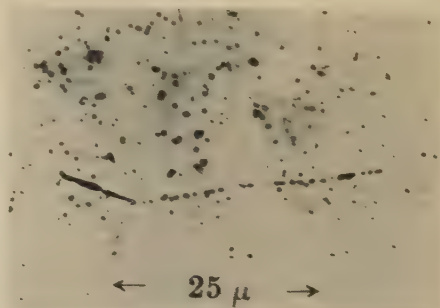


Figure 1 (b). V-track resulting from an excited state of  ${}^5\text{Li}$ .

The energy release  $Q$  on the break-up of a compound nucleus into fragments of mass  $m_1$  and  $m_2$  moving in paths diverging by  $\theta^\circ$  in the laboratory frame is given by

$$Q = \frac{1}{(m_1 + m_2)} \{m_1 E_2 + m_2 E_1 - 2(m_1 m_2 E_1 E_2)^{1/2} \cos \theta\}, \quad \dots\dots (2)$$

where  $E_1$  is the energy of the particle of mass  $m_1$  and  $E_2$  that of mass  $m_2$ . For the  ${}^5\text{Li}$  case this reduces to

$$Q = \frac{1}{5}(E_\alpha + 4E_p - 4(E_\alpha E_p)^{1/2} \cos \theta). \quad \dots\dots (3)$$

A second relation can be derived from the conservation conditions and, for the 17.6 Mev.  $\gamma$ -ray, is

$$(E_\alpha + E_p) = 5Q/6 + 2.3, \quad \dots\dots (4)$$

where all energies are measured in Mev., the  $\gamma$ -ray momentum being neglected.

Each event resulting from this  $\gamma$ -ray must then satisfy (3) and (4) simultaneously. Some events are due to  $\gamma$ -rays from the broad 14.8 Mev. group. However, as the  $\gamma$ -rays of this group have only half the intensity of those due to the sharp line at 17.6 Mev. (Walker and McDaniel 1948) and the energy resolution of the experiment is not better than 300 kv., it is reasonable to apply equation (4) to all events.

Seventy events have been observed, and in about 50% of the cases it is clear by inspection which track of the V is the proton. In these cases the appropriate values of  $(E_\alpha - E_p)$  and  $Q$  are calculated directly. For the remaining events each track is assumed to be first a proton and then an  $\alpha$ -particle and the two possible values of  $Q$  and  $(E_\alpha - E_p)$  calculated. The assignment giving values simultaneously satisfying equations (3) and (4) is accepted. The histograms of Figure 2 show (a) number of events plotted against measured energy release  $(E_\alpha + E_p)$ , (b) number of events plotted against  $Q$ .

In each case definite groups a and a' are found corresponding to break-up of  ${}^5\text{Li}$  from the ground state. A value for the instability of the state is found to be  $Q_2 = 1.6 \pm 0.2$  Mev., and from this  $Q_1$  can be derived and is  $5.4 \pm 0.2$  Mev.

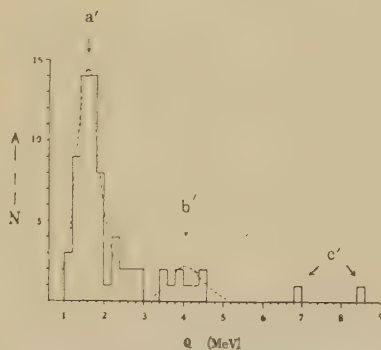
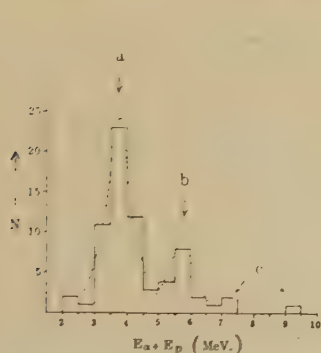
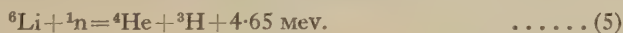


Figure 2 (a). Energy distribution of  $(E_\alpha + E_p)$ .

Figure 2 (b). Distribution of  $Q$  values

The group b of Figure 2 (a), if real, should lead to a group in position b' in Figure 2 (b), and, in fact, the corresponding  $Q$  values do fall within 0.5 Mev. of this expected position. While the evidence is by no means as strong as in the case of the ground state, it suggests a broad level in the  ${}^5\text{Li}$  nucleus at  $2.5 \pm 0.5$  Mev. The events marked c and c' satisfy equations (3) and (4) simultaneously and could possibly be due to still higher levels, but further evidence will be required to confirm this. It may be that higher levels will become so broad that there will be considerable overlapping. A continuum of  $Q$  values would then be expected.

The possibility that such V tracks should result from the reaction



has been considered.

It can be shown that the geometry of all except two of the events is incompatible with the dynamics of reaction (5) for any neutron energy. This is to be expected since, with such a low proton bombarding energy and an analysed beam, the neutron production will be by  $(\gamma n)$  reactions only.

A preliminary value for the mean cross section of the reaction  ${}^6\text{Li}(\gamma n)$  for the  ${}^7\text{Li}\gamma$  radiations can be calculated and is found to be  $(5 \pm 2) \times 10^{-28} \text{ cm}^2$ .



We are indebted to Miss Pauline Port for help with the microscope work, to Dr. W. D. Allen and his group for providing the  $^6\text{Li}$  isotope, to Mr. C. Waller of Ilford Limited, who prepared the special plates, and to Messrs. D. R. Chick and E. K. Inall of the A.E.I. Research Laboratory, Aldermaston, for the hospitality of their Laboratory and help in effecting the irradiation.

Research School of Physical Sciences,  
Australian National University,  
Canberra.

Atomic Energy Research Establishment,  
Harwell, Berks.

5th December 1950.

E. W. TITTERTON.

T. A. BRINKLEY.

TITTERTON, E. W., 1950 a, *Proc. Phys. Soc. A*, **63**, 915; 1950 b, *Ibid.*, **63**, 1297.  
WALKER, R. L., and McDANIEL, B. D., 1948, *Phys. Rev.*, **74**, 315.

## CONTENTS FOR SECTION B

	PAGE
Mr. H. BARRELL and Mr. J. S. PRESTON. An Improved Beam Divider for Fizeau Interferometers . . . . .	97
Dr. R. C. FAUST. Fresnel Diffraction at a Transparent Lamina . . . . .	105
Prof. W. GLASER. The Refractive Index of Electron Optics and its Connection with the Routhian Function . . . . .	114
Miss S. M. CRAWFORD and Dr. H. KOLSKY. Stress Birefringence in Polyethylene .	119
Dr. R. C. PARKER and Mr. E. J. W. WHITTAKER. The Friction and Mechanical Properties of Powders Bonded by Synthetic Resins . . . . .	126
Mr. J. T. KENDALL and Mr. D. YEO. Magnetic Susceptibility and Anisotropy of Mica . . . . .	135
Dr. W. DIEMINGER. The Scattering of Radio Waves . . . . .	142
Dr. S. W. COUSINS and Dr. A. A. WARE. Pinch Effect Oscillations in a High Current Toroidal Ring Discharge . . . . .	159
Prof. K. G. EMELÉUS. Turbulence in Gaseous Conductor . . . . .	166
Corrigenda . . . . .	169
Letters to the Editor :	
Mr. J. H. FRISBY and Dr. D. ROAF. Quantitative Measurement of Samples of Tritium . . . . .	169
Dr. MARY P. LORD. Binocular Eye Movements at High Convergence. .	171
Reviews of Books . . . . .	173
Contents for Section A . . . . .	174
Abstracts for Section A . . . . .	174

## ABSTRACTS FOR SECTION B

*An Improved Beam Divider for Fizeau Interferometers*, by H. BARRELL and J. S. PRESTON.

**ABSTRACT.** A transparent material, presumed to be titanium oxide, is suggested for replacing aluminium or silver as a coating for glass beam dividers in Fizeau interferometers, particularly those adapted for measuring length or displacement in the reflected fringe system. The method of depositing the films, and their optical properties, are described; the coatings are very resistant chemically and mechanically. Evidence produced in photographs and microphotometer records, supplemented by calculations of fringe intensity distributions, shows that the performance of the new material in the interferometer is superior to that of aluminium and of plain glass.

*Fresnel Diffraction at a Transparent Lamina*, by R. C. FAUST.

**ABSTRACT.** Fresnel diffraction at the edge of a transparent lamina has been studied and an analogy drawn between the observed phenomena and interference fringes of the Fizeau and Edser-Butler types. The variation of the diffraction pattern with changing wavelength has been employed to determine accurately both the thickness and the refractive index of thin transparent sheets. The refractive index was found by an immersion method, the accuracy of which is here discussed. The Becke line which is often observed during such measurements is shown to be a strongly asymmetrical diffraction pattern occurring when the thickness of a lamina changes over a small but finite distance.

*The Refractive Index of Electron Optics and its Connection with the Routhian Function*, by W. GLASER.

**ABSTRACT.** The derivation of the electron-optical refractive index from Hamilton's Principle is discussed. It is shown that the criticisms made by Ehrenberg and Siday of our method are invalid, and that our derivation made in 1933 is correct. To prove that our method is generally applicable, the isotropic refractive index of an axially symmetrical field is obtained.

*Stress Birefringence in Polyethylene*, S. M. CRAWFORD and H. KOLSKY.

**ABSTRACT.** The birefringence and strain produced in polyethylene by different stresses have been measured at temperatures between 20° and 90° C. It has been found that the relation between strain and birefringence is linear up to strains of 0.25 and for greater strains there is still no hysteresis. This indicates that no true flow occurs in this temperature range. The stress-birefringence relation, on the other hand, rapidly departs from linearity and shows large hysteresis, so that the nature of the birefringence effects is in direct contrast with that observed in rubber. An expression has been derived for the birefringence in terms of the orientation of rod-like crystallites embedded in an elastic matrix and this was found to be in qualitative agreement with the experimental results.

*The Friction and Mechanical Properties of Powders Bonded by Synthetic Resins*, by R. C. PARKER and E. J. W. WHITTAKER.

**ABSTRACT.** The coefficient of friction and mechanical properties have been determined for a series of non-metallic materials formed by bonding mineral powders with resins. The manner in which the coefficient of friction varies with particle size has been studied, and a tentative explanation has been advanced involving certain geometrical parameters. A correlation was observed between the coefficient of friction and the hardness of the mineral powders expressed on Moh's scale. Marked correlations were also obtained between compression strength, cross-breaking strength and the reciprocal of the particle size for most of the materials; consideration is given to the various mechanical and thermodynamical factors involved.

*Magnetic Susceptibility and Anisotropy of Mica*, by J. T. KENDALL and D. YEO.

**ABSTRACT.** The magnetic susceptibility and anisotropy of natural muscovite and synthetic fluorophlogopite have been measured. These minerals contain small quantities of iron which cause paramagnetic and ferromagnetic effects. To a fair approximation the mean susceptibility is found to vary linearly with the total iron content, and the paramagnetic anisotropy to be proportional to the ferrous iron content. At low field strengths ferromagnetic impurities (probably sub-microscopic inclusions of magnetite) cause anomalous results. It is shown that such inclusions are present in all the micas examined, and account for the apparent paramagnetism of synthetic mica. The inclusions are probably orientated with their magnetic axes in a preferred direction relative to the crystallographic axes of the mica.

*The Scattering of Radio Waves*, by W. DIEMINGER.

**ABSTRACT.** A review of the recent work on scattering draws attention to a number of discrepancies in the interpretation of the data. Most workers believe that the scattering is due to clouds in the E layer.

The experiments described in this paper indicate that there are several types of scattering phenomena. It is concluded that the most common source of scatter is the reflection of waves from irregularities on the surface of the earth. In this case the wave path is from the sender to F layer—earth—F layer and hence to receiver, i.e. is analogous to a  $2 \times F$  reflection. The characteristics of the different types of scattering and their effects on the propagation of short waves are discussed.

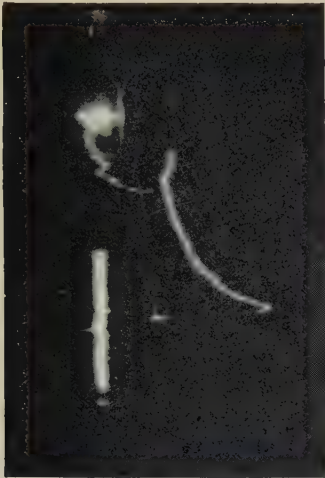
*Pinch Effect Oscillations in a High Current Toroidal Ring Discharge*, by S. W. COUSINS and A. A. WARE.

**ABSTRACT.** A toroidal ring discharge with currents greater than  $10^4$  amperes has been studied with a rotating mirror camera. The photographs show a lateral oscillation of the discharge, which consists of an alternate contraction and expansion of the current filament. The frequency of the oscillations increases with decrease in pressure or increase in voltage and is inversely proportional to the square root of the atomic weight of the gas. The oscillations are thought to be due to plasma ion waves, which are excited by the large 'pinch' effect forces.

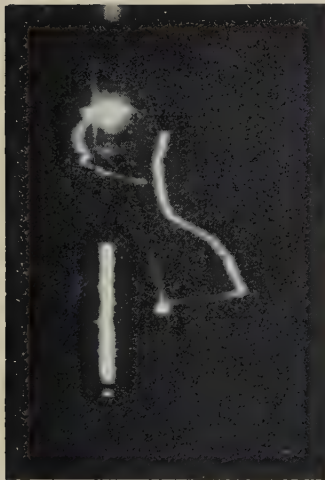
*Turbulence in Gaseous Conductors*, by K. G. EMELÉUS.

**ABSTRACT.** It is suggested that turbulent flow of electricity may occur under certain conditions in an ionized gas, even if the gas is not in a magnetic field. Examples are given of high and low frequency disturbances which may be of this character. The difficulties in the way of developing a quantitative theory, and the possibility of the coupling of electromagnetic and hydromechanical phenomena, are pointed out.





(a)

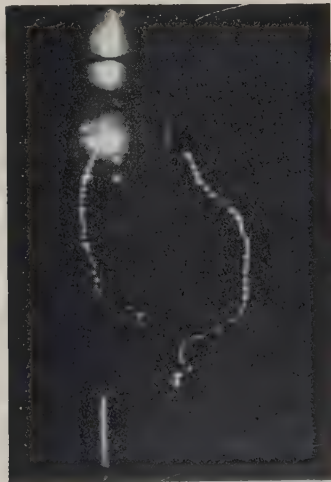


(b)

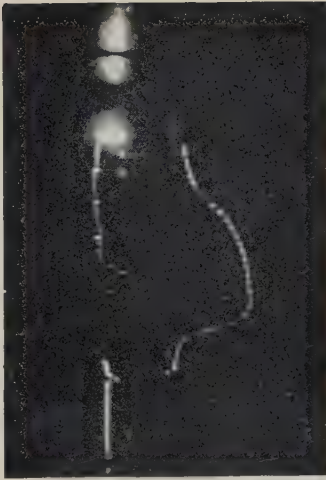


(c)

PLATE I. Variation of pulse shape with amplitude at 1.2° K.



(a)



(b)

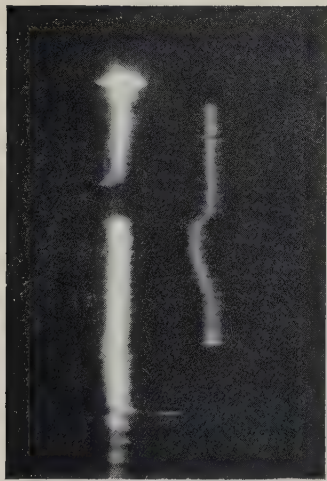


(c)

PLATE II. Variation of pulse shape with range at 1.2° K.



(a)



(b)

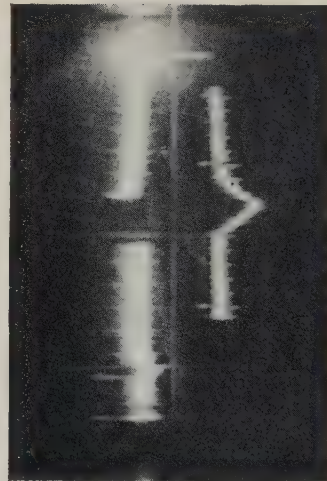


(c)

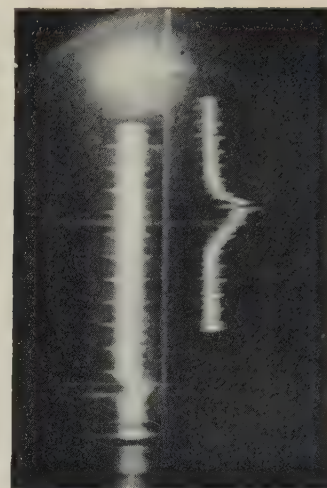
PLATE III. Variation of pulse shape with amplitude at 2.12° K.



(a)



(b)



(c)

PLATE IV. Variation of pulse shape with range at 2.12° K.

In Plates I, II and IV a positive temperature excursion is represented by a negative deflection; in Plate III by a positive deflection, i.e. the temperature excursion is positive in all cases.



Figure 1 (a).

Figure 1 (b).

Figure 1. Two examples of  $\sigma$ -stars showing at least one short-range proton (marked with an arrow) and other more energetic particles. According to Menon *et al.* (1950), these are typical of disintegrations produced by the capture of negative  $\pi$ -mesons in light elements. The mesons were travelling upwards, as shown. These events have therefore been classified as  $\pi$ -meson disintegrations.

Observers ; Mrs. M. H. George and J. Evans.



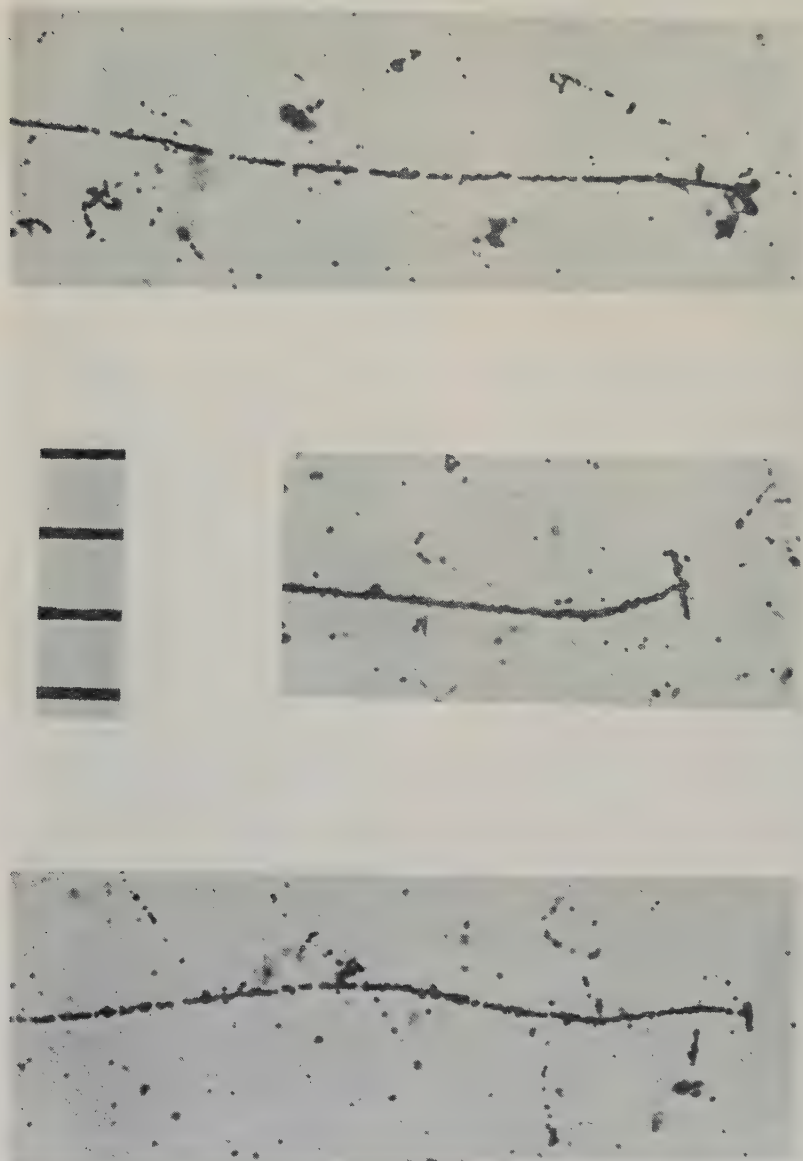


Figure 2. Three examples of 2-prong  $\sigma$ -stars in which the incident meson is assumed to be a negative  $\mu$ -meson. The scale is an image of the stage graticule showing steps of 10 microns, and it will be seen that the lengths of the prongs are very short, corresponding to kinetic energies of 1 or 2 Mev. for protons. These disintegrations are very dissimilar from those 2-prong stars produced by the capture of negative  $\pi$ -mesons.

Observer: E. P. George.

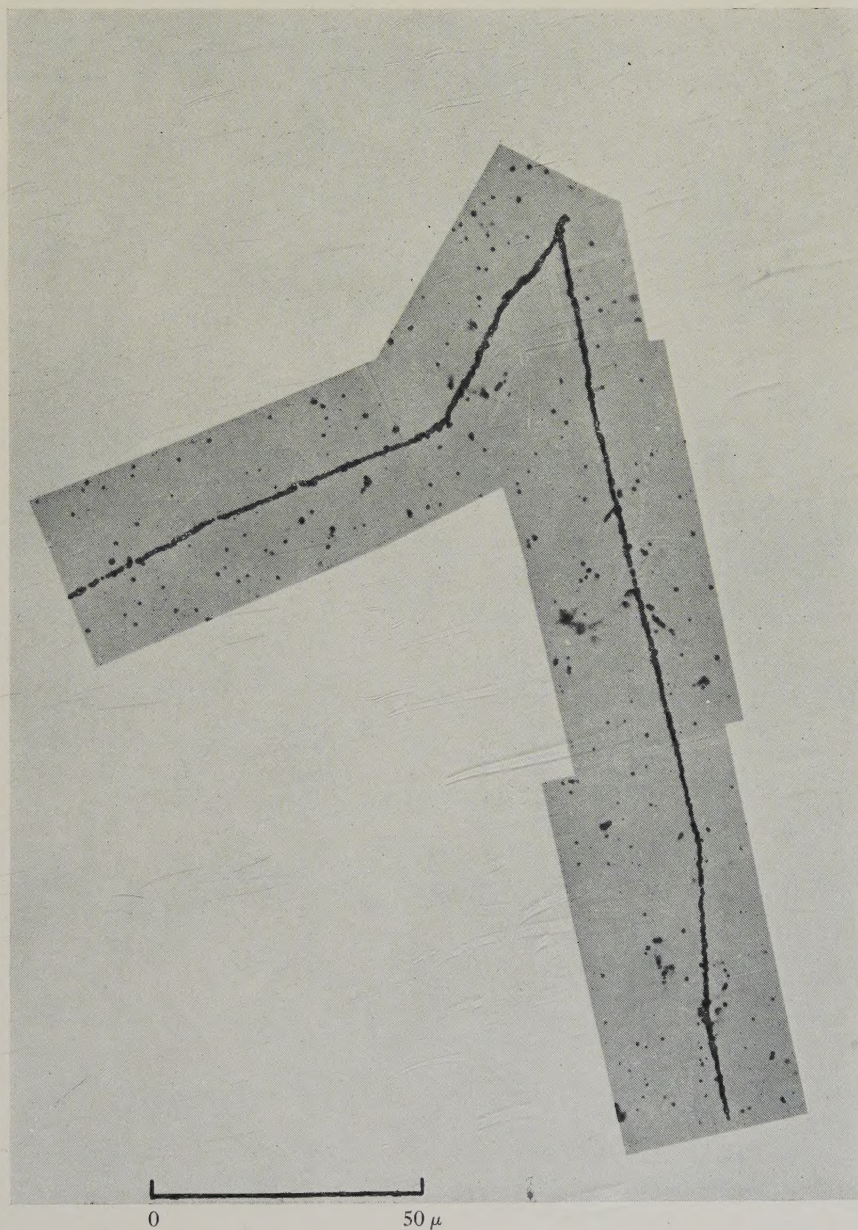


Figure 3. An example showing a 1-prong  $\sigma$ -star observed below ground. This class of  $\sigma$ -star is by far the most frequent. In most cases the single heavy particle leaves the emulsion. This is one of the three cases in which the heavy particle remains in the emulsion.

*Observer* : R. H. Creamer.





# A CRAFTSMANSHIP AND DRAUGHTSMANSHIP COMPETITION

is being held for Apprentices and Learners in  
the Instrument and Allied Trades to be held  
in connection with the Physical Society's

## 35th Annual Exhibition of Scientific Instruments and Apparatus

Prizes and Certificates will be awarded in  
different age groups and subject classes

1st Prize £10 10 0    2nd Prize £5 5 0    3rd Prize £2 12 6

---

**FINAL DATE OF ENTRY—21st FEBRUARY 1951**

---

Application forms and further particulars may  
be obtained from

**THE PHYSICAL SOCIETY**

**1 Lowther Gardens, Prince Consort Road, London S.W.7**



The  
**PHILOSOPHICAL  
MAGAZINE**

(First Published 1798)

*A Journal of  
Theoretical, Experimental  
and Applied Physics*

EDITOR:

**PROFESSOR N. F. MOTT**  
M.A., D.Sc., F.R.S.

EDITORIAL BOARD:

**SIR LAWRENCE BRAGG**  
O.B.E., M.C., M.A., D.Sc., F.R.S.

**ALLAN FERGUSON**  
M.A., D.Sc.

**SIR GEORGE THOMSON**  
M.A., D.Sc., F.R.S.

**PROFESSOR A. M. TYNDAL**  
C.B.E., D.Sc., F.R.S.



Established 150 Years

ANNUAL SUBSCRIPTION

**£6 0s. 0d.**

OR

**13s. 0d.**

**EACH MONTH  
POST-FREE**

*Contents for February 1951*

**P. W. A. BOWE** (Cavendish Laboratory, Cambridge). "The Waveforms of Atmospherics and the Propagation of very Low Frequency Radio Waves."

**R. S. LEIGH** (Mathematics Department, Imperial College, London). "A Calculation of the Elastic Constants of Aluminium."

**A. R. FRASER** (Royal Society Mond Laboratory, Cambridge). "The Condensation of a Perfect Bose-Einstein Gas—I."

**A. R. FRASER** (Royal Society Mond Laboratory, Cambridge). "The Condensation of a Perfect Bose-Einstein Gas—II."

**L. SOWERBY** (Department of Applied Mathematics, University of Liverpool). "The Unsteady Flow of Viscous Incompressible Fluid Inside an Infinite Channel."

**S. O. C. SØRENSEN** (The H. H. Wills Physical Laboratory, University of Bristol). "Emission of Energetic Helium and Lithium Fragments in Nuclear Explosions."

**KUN HUANG** (Department of Theoretical Physics, University of Liverpool). "A Note on Hildebrand's Approximation for Thermal Pressures in Solids."

**P. E. HODGSON** (Imperial College of Science and Technology, London). "The Emission of  $\text{Li}^{\beta}$  from Cosmic Ray induced Nuclear Disintegrations."

**F. R. N. NABARRO** (Department of Metallurgy, The University of Birmingham). "The Law of Constant Resolved Shear Stress in Crystal Plasticity."

**CORRESPONDENCE:**

**J. M. CASSELS, T. C. RANDLE, T. G. PICKAVANCE & A. E. TAYLOR** (Atomic Energy Research Establishment, Harwell). "The Production of Neutrons by High Energy Protons."

**D. K. C. MacDONALD** (Clarendon Laboratory, Oxford). "The Velocity Brownian Movement."

**BOOK REVIEWS.**

**TAYLOR & FRANCIS LTD., Red Lion Court, Fleet St., LONDON, E.C.4**